NASA Technical Memorandum 100459

Atomic Oxygen Effects Measurements for Shuttle Missions STS-8 and 41-G

Volume I

Compiled by James T. Visentine

FOREWORD

A variety of materials was exposed in the Orbiter cargo bay on Space Shuttle flights STS-8 and 41-G (STS-17) to develop a fundamental understanding of the deleterious effects which result from space flight exposure of thin, organic films, advanced composites, and metallized surfaces to atomic oxygen, the principal constituent of the low Earth orbit environment. These materials included polyimide films, fluorocarbons, polyurethanes, silicones, siloxanes, epoxies, carbon fibers and graphites, infrared optical materials, metallized optical films, Kevlar coverings, fiberglass fabric, and high-temperature reflective coatings. Effects measured post-flight included mass loss (surface recession), surface morphology changes, reflectance losses, chemical composition changes, and decreases in optical density of the metallized films.

To provide for controlled exposure during both missions, approximately 300 material specimens provided by the participating organizations (NASA, Canada, British Aerospace, TRW, Aerospace Corporation, Washington University and the University of Alabama) were exposed on an across-the-bay structure during STS-8 by flying the Orbiter with its payload bay into the velocity vector for 40 hours at an altitude of 222 km (120 nmi). During STS 41-G, material specimens attached to the lower arm boom of the Shuttle remote manipulator system were oriented toward the direction of flight for 34 hours at an altitude of 272 km. Given the differences in exposure time and solar activity conditions -- which influence the atomic oxygen number density in the neutral atmosphere -- that arose from different flight dates (September 1983 and October 1984), atomic oxygen fluences for STS-8 and 41-G were determined to be 3.5×10^{20} and 3.0×10^{20} atoms/cm^2, respectively. These exposures, in turn, produced surface recessions of 0.4 and 0.3 mil for highly reactive materials, such as the polyimide films, which ranged from 0.5 to 2.0 mils in thickness during both STS missions.

The results of these exposures together with the post-flight measurements are reviewed and summarized in 9 reports found in Volume I and 5 reports in Volume II of this technical memorandum. The reports were issued by the participating NASA centers and U. S. aerospace corporations, the Government of Canada, and university research centers.

James T. Visentine, Compiler
NASA Lyndon B. Johnson Space Center
Houston, Texas

ACKNOWLEDGMENT

Changes to the STS flight manifest during late 1983 provided an opportunity for the NASA materials science community to conduct an atomic oxygen effects experiment during the eighth Space Shuttle mission. This experiment was designed, developed, assembled, and integrated into the Orbiter within a 12-week period prior to flight, with special consideration given to flight safety, materials selection, and the post-flight analysis capabilities that were made available by the participating NASA Centers. Approximately 300 individual specimens were prepared by the participating organizations and analyzed prior to flight. After the mission was completed, these samples were returned to the co-investigators, who then completed their analyses and prepared these post-flight reports. We extend our special thanks to the following persons who contributed immensely to the successful completion of this experiment, and to their co-authors whose names are found in their respective documents: Dr. Lubert Leger of JSC, who served as principal investigator; Ms. Ann Whitaker and Ms. Sally Little of MSFC; Messrs. Wayne Slemp and George Sykes of the Langley Research Center; Dr. Bruce Banks and Mr. Mike Mirtich of the Lewis Research Center; Dr. John Park, Dr. Ted Gull, and Mr. Jack Triolo of GSFC; Drs. Ranty Liang and Dave Brinza of JPL; Drs. Wayne Stuckey and Graham Arnold of Aerospace Corporation; and Dr. John Gregory of the University of Alabama, Huntsville. Special recognition is also extended to Dr. Dave Zimcik of the Government of Canada, who later participated in the STS-41G experiment.

James T. Visentine

Contents

STS-8 MISSION SUMMARY - CHALLENGER

August 30 - September 5, 1983

COMMANDER:	**Richard H. Truly**
PILOT:	**Daniel C. Brandenstein**
MISSION SPECIALIST:	**Guion S. Bluford, Jr.**
MISSION SPECIALIST:	**Dale A. Gardner**
MISSION SPECIALIST:	**William E. Thornton**
MISSION DURATION:	**6 days, 1 hour, 9 minutes, 32 seconds**
MILES TRAVELED:	**2,184,983 nautical miles (2,514,478 statute miles)**
ORBITS OF EARTH:	**97**

First night launch and night landing

Challenger carried INSAT-1B, payload flight test article (PFTA), 2 Getaway Special canisters, and included the STS-8 (EOIM-2) atomic oxygen effects experiment

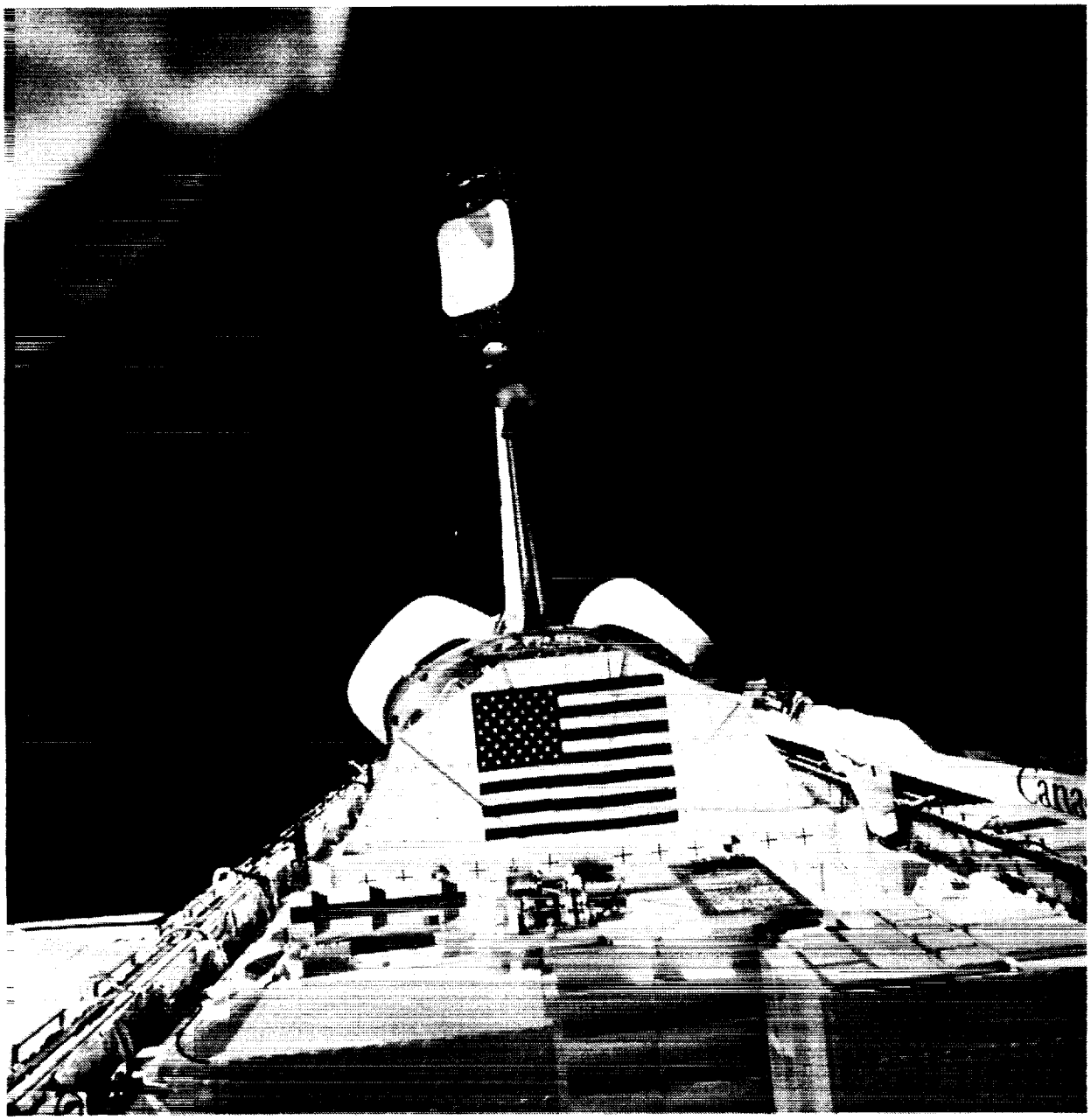

STS-8 Atomic Oxygen Effects Experiment. The STS-8 material science exposure trays are shown in the foreground during INSAT 1-B deployment (August 31, 1983).

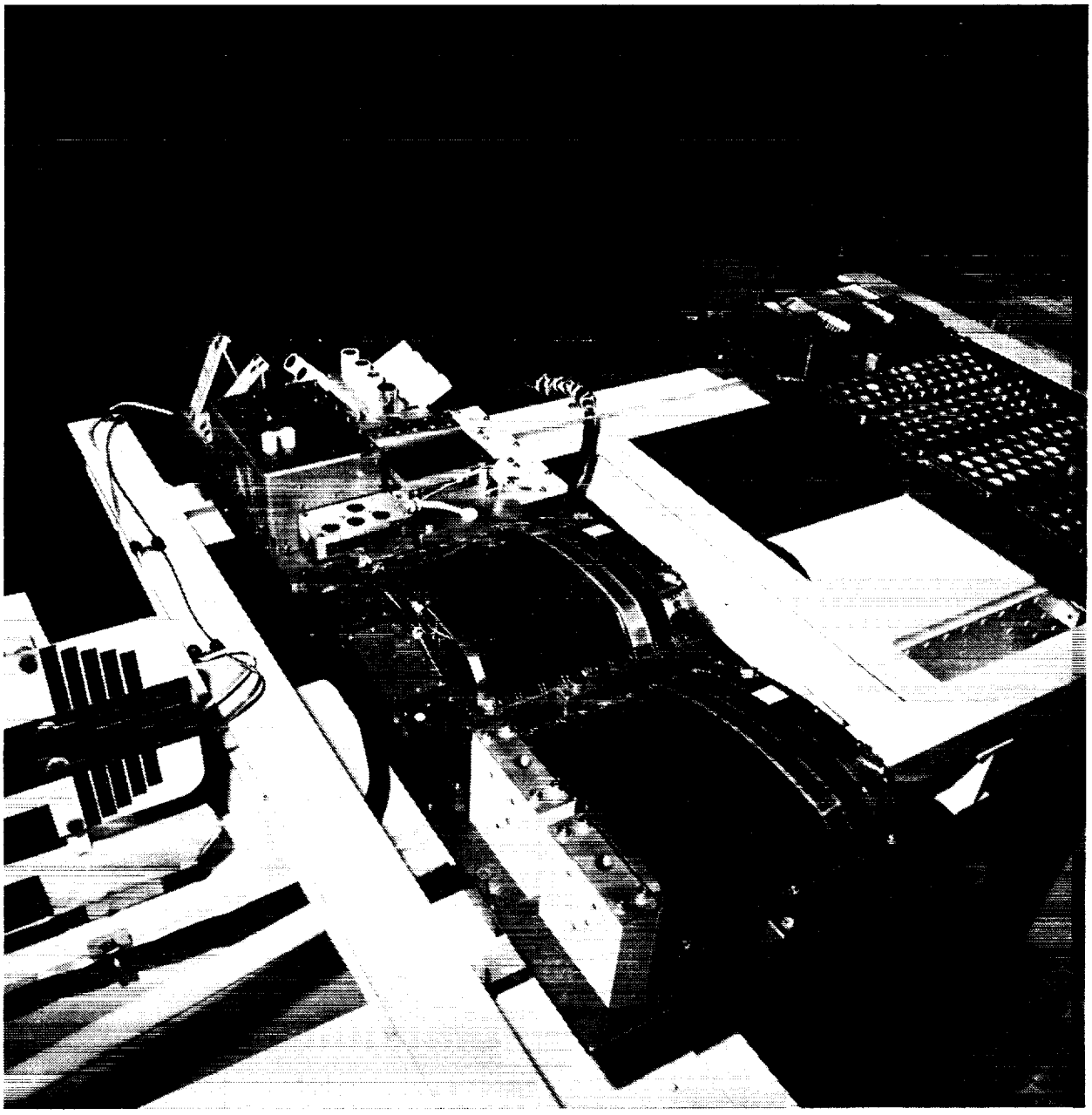

Closeup view of the STS-8 Atomic Oxygen Effects Experiment. The active and passive experiment trays are located on the left and right sides of the DFI pallet structure, respectively. These trays included approximately 300 material specimens, which were provided by the NASA Centers and aerospace contractors.

STS-8 POST-FLIGHT REPORT

The Atomic Oxygen Interaction Experiment (DSO 0301) conducted during STS-8 was successfully completed during the mission timeline. This experiment consisted of material specimens installed within passive exposure trays attached to an across-the-bay structure (DFI pallet) and active experiments to assess the effects of temperature, solar ultraviolet radiation, and charged particles (ions and electrons) on material interaction rates with atomic oxygen, the principal constituent of the LEO environment. These experiments were initiated during Flight Day 3 at 08:30 hours MET, and were concluded on Flight Day 5 at 1900 hours MET. A combination of three separate exposures (3/08:30-3/20:10; 4/07:30-4/19:30; and 5/00:55-5/19:00) resulted in a total exposure of 41.75 hours, which was accomplished by flying the Orbiter with its payload bay into the velocity vector. This attitude produced direct impingment of the oxygen atoms onto the material specimens. The flight specimens were exposed to an average atomic oxygen flux of 1.9×10^{15} atoms/S-cm^2, which produced a fluence of 2.9×10^{20} atoms/cm^2. This fluence, combined with fluences obtained during non-EOIM exposure periods during the time the Orbiter was oriented in different flight attitudes, produced a total fluence of 3.5×10^{20} atoms/cm^2.

Material specimens are being analyzed, and preliminary results indicate additional exposure will be required during future Space Shuttle flights to evaluate protective coating techniques and to further analyze atomic oxygen interactions with surfaces in more detail.

Submitted to the NSTS Integration Office, September 8, 1983.

41-G (STS-17) MISSION SUMMARY - CHALLENGER

October 5 - 13, 1984

COMMANDER:	**Robert Crippen**
PILOT:	**Jon McBride**
MISSION SPECIALIST:	**David Leestma**
MISSION SPECIALIST:	**Sally K. Ride**
MISSION SPECIALIST:	**Kathryn Sullivan**
PAYLOAD SPECIALIST:	**Paul Scully-Power**
PAYLOAD SPECIALIST:	**Marc Garneau**
MISSION DURATION:	**8 days, 5 hours, 24 minutes, 32 seconds**
MILES TRAVELED:	**2,984,397 nautical miles (3,434,684 statute miles)**
INCLINATION:	**57°**
ORBITS OF EARTH:	**132**

Extravehicular Activity (EVA):	Kathryn Sullivan and David Leestma
EVA Duration:	3 hr, 29 min

Challenger carried 4 payloads, 8 Getaway Special canisters, 4 middeck experiments and included the Canadian ACOMEX Atomic Oxygen Effects Experiment

Exposure of material samples on the Shuttle RMS, during the STS 41-G flight.

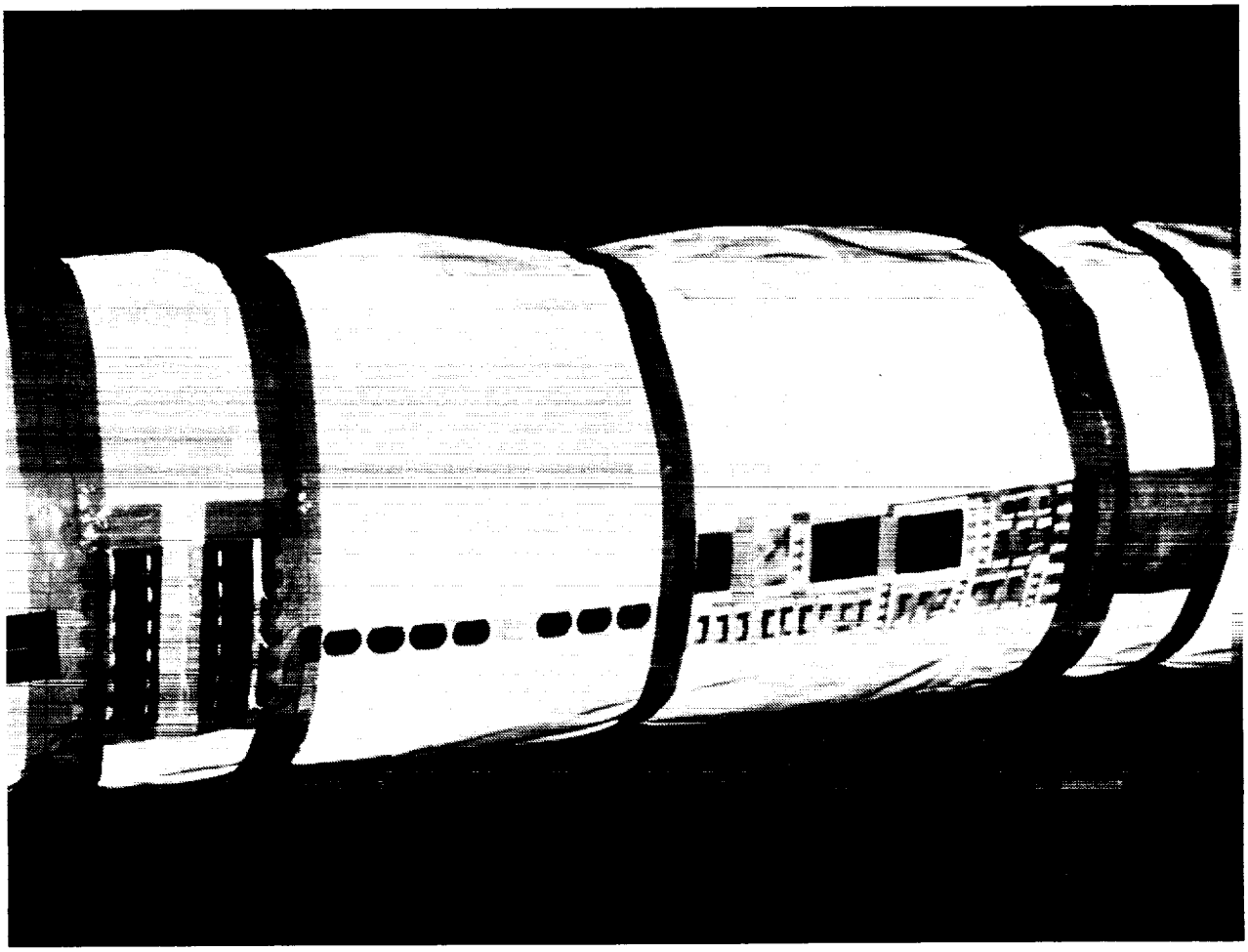

Closeup view of the STS 41-G material specimens, shown tape-attached to the thermal blanket. Nylon cord tethers used to secure the exposure trays are visible underneath the circumferential bands of Kapton tape.

STS 41-G POST-FLIGHT REPORT

The Atomic Oxygen Interaction Experiment (DSO 0308) conducted during STS 41-G was successfully completed per the mission timeline. This experiment consisted of material specimens and subassembly components provided by MSFC and Canada's Communication Research Center taped-attached (see figure 1) to the RMS to expose space telescope solar cells and coated discs (MSFC experiment) and composite specimens of different configurations of graphite and Kevlar (Acomex Experiment) to the ambient density environment. These experiments were initiated on Flight Day 3 at 2200 hours GMT and completed during Flight Day 5 at 15:22 hours GMT, for a total exposure period of 34.08 hours. Specimens were exposed to an atomic oxygen flux of 2.0×10^{15} atoms/cm^2 sec, which produced a total fluence of 2.45×10^{20} atoms/cm^2.

At other times during the mission, the RMS was positioned to observe ice buildup on the Orbiter side water dump valve during venting operations. This activity was performed for about 30 minutes twice daily and resulted in non-normal (oblique) impingement of oxygen atoms onto the material specimens. Given these exposure conditions, the total fluence (normal and oblique) experienced during the STS 41-G exposure period is estimated to be 3.0×10^{20} atoms/cm^2.

Material specimens are being analyzed, and preliminary results indicate additional exposure will be required during future Space Shuttle flights to evaluate protective coating techniques and further analyze atomic oxygen interactions with surfaces in more detail.

Submitted to the NSTS Integration Office,
October 21, 1984

ACRONYMS

AES	auger electron spectroscopy
BRDF	bidirectional reflection distribution function
CMP	contamination monitor package
ELL	elipsometry
EOIM	Effects of oxygen interactions with materials
ESCA	electron spectroscopy for chemical analysis
ESD	electrostatic discharge
FGS	fine guidance system
GAS	Get Away Special
GSFC	Goddard Space Flight Center
INSAT	Indian National Satellite
ITO	indium tin oxide
LEO	low Earth orbit
MSFC	Marshall Space Flight Center
MSIS	mass spectrometer and incoherent scatter
PBI	polybenzimidazole
PFTA	payload flight test article
PIXE	proton induced x-ray emission
PMMA	polymethyl methacrylate
QCM	quartz crystal microbalances
RBS	Rutherford backscattering
RE	reaction efficiency
RMS	remote manipulator system
RTG	radioisotope thermoelectric generators
SEM	scanning electron microscope
SIMS	secondary ion mass spectroscopy
ST	space telescope
STS	Space Transportation System
TDS	total diffuse scatter
TQCM	temperature controlled quarts crystal microbalances
TS	tethered satellite
UV	ultraviolet
WDX	wavelength dispersive x-ray

1.0 INTRODUCTION

This technical memorandum represents a compilation of 15 technical papers and is organized by subject matter into three separate volumes. Volume 1 of this document summarizes the effects of atomic oxygen exposure upon typical spacecraft materials, such as polyimide films, thermal control paints, epoxies, silicones, and fluorocarbons. Volume 2 summarizes the effects of these interactions upon optical coatings, thin metallized films, and advanced spacecraft materials, such as high-temperature coatings and new coatings for infrared optical systems. In addition to these results, Volume 2 includes a description of a generic model proposed by the NASA Jet Propulsion Laboratory, which may explain the atomic oxygen interaction mechanisms that lead to surface recession and weight loss. Volume 3 presents a futuristic look into the atomic oxygen program and outlines requirements for follow-on studies to produce an accurate reaction rate data base for Space Station design. It also identifies Shuttle flight experiments and on-going activities underway at research laboratories in the United States to evaluate materials in a neutral, 5 eV O-atom environment and to develop a more thorough understanding of the chemical mechanisms leading to surface recession and space glow. This volume, entitled *Atomic Oxygen Effects Experiments: Current Status and Future Directions* includes a detailed discussion of atomic oxygen simulation techniques now under development in the United States. In light of these discussions, it is limited in its distribution to U. S. Government agencies and contractors only.

2.0 STS-8 ATOMIC OXYGEN EFFECTS EXPERIMENT*

James T. Visentine, Lubert J. Leger,
Jerome F. Kuminecz, and Ivan K. Spiker

NASA Lyndon B. Johnson Space Center
Houston, Texas 77058

Abstract

A flight experiment was performed on the eighth Space Shuttle mission to measure reaction of surfaces with atomic oxygen in the low Earth orbital environment. More than 300 individual samples were exposed to ram (normal to surface) conditions for 41.75 hours leading to a total atomic oxygen fluence of 3.5×10^{20} atoms/cm^2. Reaction rates for surface recession measured primarily by mass change of several organic films were in the range of 3.0×10^{-24} cm^3/atom, and $< 5 \times 10^{-26}$ cm^3/atom for Teflon. Effects of parameters such as temperature and solar radiation were assessed, as was the importance of atmospheric ionic species on surface recession. In an experiment performed on the fifth Space Shuttle flight, no temperature dependence of reaction rate for the organic films studied was found in the temperature range of 25° to 125° C. Preliminary findings indicate that the reactivity of organic films is not affected by temperature (in the range of 65° to 125° C), solar radiation, or ionic species. Significant surface morphology changes led to a carpetlike appearance also consistent with previous findings.

2.1 Introduction

Measurement of significant surface changes of materials exposed to the low Earth orbit (LEO) environment during the early Space Shuttle flights has renewed interest in materials compatibility in space. Generally, these changes were manifested as mass loss of organic films,[1,2] carbon, and osmium[3] and oxidation of silver.[3] Only ram-facing surfaces were affected, and, generally, the changes were proportional to exposure time. It has been proposed[1] that these effects are due to oxidation of the surfaces caused by impinging atomic oxygen, the major constituent of the Earth's atmosphere at low orbital altitudes (<300 km). In addition to being highly chemically reactive, the atomic oxygen atoms have high kinetic energy (>5 eV) relative to spacecraft surfaces. The impinging flux is dependent on many parameters such as altitude, attitude, and solar activity but can range as high as 10^{15} atoms/cm^2-sec and can result in surface thickness loss for organic compounds of as much as 6 μm/day during solar maximum activity at moderate (300 km) altitudes. Obviously, effects of this magnitude have significant implications on spacecraft system performance.

The first dedicated experiment developed to study LEO atomic oxygen effects on materials, referred to as the Effects of Oxygen Interactions with Materials (EOIM) experiment, was flown on the fifth Space Shuttle flight (STS-5). Results[4-9] from this experiment support an atomic oxygen-based mechanism and provide quantitative reaction rates for some organic materials. Reaction rates for unfilled organic compounds were in the range of 1.3×10^{-24} to 2.8×10^{-24} cm^3/atom.

Subsequent to the completion of the STS experiment, another opportunity for experimentatic was presented as a result of Space Shuttle flig manifest changes. Unfortunately, as in the STS-5 case, only 2 months were available for experiment development and manufacture. Using the STS-5 experience base, an experiment was formulated and performed on the STS-8 mission with the objectives of (1) obtaining a larger quantitative reaction rate data base, (2) confirming reaction rate temperature dependence, (3) determining whether mass transfer from surface to surface occurs as a result of the interaction, (4) evaluating solar radiation effects on

* AIAA Paper 85-0415 Presented at the 23rd Aerospace Sciences Meeting, January 14-17, 1985.

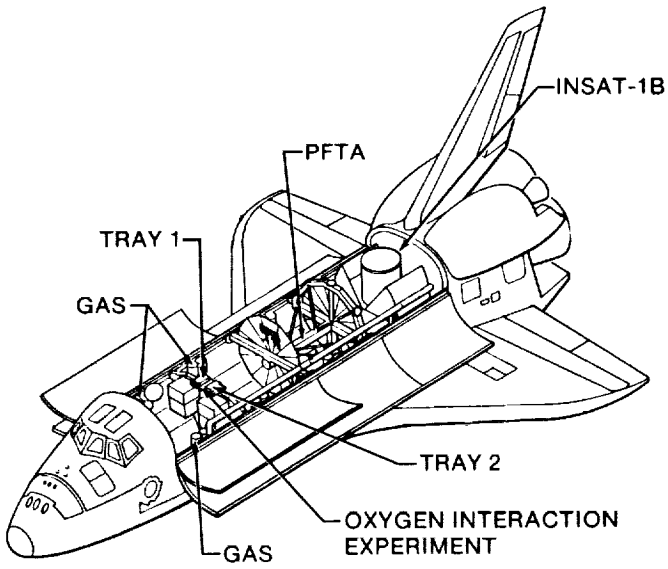

Fig. 1 STS-8 atomic oxygen flight experiment configuration.

reaction rate, and (5) determining the importance of atmospheric electrically charged species on reaction rate. Fifteen organizations participated in the experiment. The experimental approach and hardware, the exposure conditions, and the results obtained for a group of organic films commonly used on spacecraft are described herein. Other papers in this technical memorandum also provide results from the STS-8 Atomic Oxygen Effects Experiment.[10-15]

2.2 Experiment Description

The basic experimental approach consisted of exposing samples to the LEO environment and then returning them for ground-based laboratory analysis. More than 360 samples were supplied and analyzed by the participating organizations. A summary identification of these samples is provided in Table 1. Most of these samples were exposed in disc form (2.54 cm diameter); however, film strips, woven cables, and fabrics were also used.

All the samples and the special fixtures which supported them were attached to two trays, which were mounted on a support structure located in the forward region of the Orbiter payload bay as shown in Figure 1. This arrangement resulted in locating the samples above the payload bay hinge line to minimize reflection of the incoming flux and provide an unobscured view for direct impingement.

Tray 1 (Fig. 2) was located on the starboard side of the vehicle and included experiments which were active during flight. The active experiments were operated only during the three 14-hour exposures described later. Active hardware consisted of two heater plates, an electronically controlled cover which provided selected day-night exposure of certain samples, and three grid assemblies which were used to determine the effects of the plasma environment on material interaction rates. The heater plates were controlled to temperatures of 65° C and 121° C and provided an assessment of the effect of sample temperature on reaction rate. Reaction rate

Table 1 Partial Listing of STS-8 Sample Types

Coatings[a]	Polymeric films
Black and white paints	Kapton
Anodized coatings	Mylar
Conductive coatings	Teflon TFE and FEP
Silicone	Tedlar
Polyurethane	Polyethylene
Epoxy	Polyester
Indium tin oxide	Polyimide
Silicon oxide	Polysiloxane/ polyimide
Aluminum oxide	
Titanium oxide	Polymethyl meth- acrylate (PMMA)
Carbon	
Molybdenum	Polybenzimidazole (PBI)
Tungsten	
Nickel	Polystyrene
Copper	Polysulfone
Aluminum	
Chromium	Composites
Gold	Graphite/aluminum
Platinum	Graphite/magnesium
Iridium	Graphite/epoxy
Osmium	Polyimide composite
Magnesium	Polysulfone composite
Lead	Magnesium metal matrix
Tantalum	
Niobium	Kevlar cable
	Other
	Silver discs
	Reflectors
	Silver interconnects
	Solar cells

[a]Includes base metal specimens as well as metal coatings.

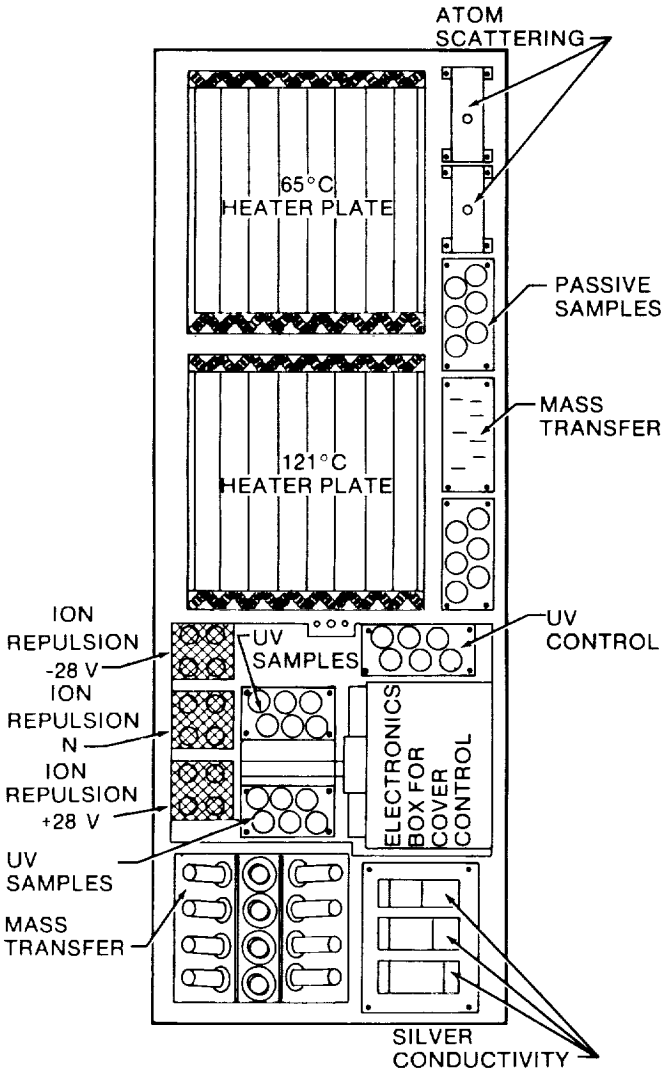

Fig. 2 Exposure tray 1.

dependence on impinging angle (cosine flux reduction) was also evaluated from heater plate data by arranging the heater surfaces to hold the samples at various angles (42°, 22°, 17°, and 6°) relative to the impinging flux. To maintain contact with the heater surfaces, film strip samples were attached to the heater plates using springs on both ends.

The solar ultraviolet (UV) experiment was designed to evaluate the effects of solar radiation on reaction rates by exposing one set of samples to impinging flux during the day pass and another set of identical samples to impinging flux during the night pass. Controlled exposure was provided by an electromechanically driven cover which was actuated at the terminator by a photocell. By comparing the surface recession for these two sample sets with a fully exposed identical sample set and knowing the exposure time, a preliminary evaluation of solar UV radiation on reaction rate was obtained.

Effects of electrically charged atmospheric constituents on surface change were evaluated using the charged grid assemblies. Four electrically grounded samples were placed under each of three gold grids (50 lines/mm, 73 percent transparent) held at ground potential, at +28 V, and at −28 V relative to ground. The +28-V grid repelled incoming positively charged ions and accelerated incoming electrons. The −28-V grid did just the opposite; i.e., it repelled electrons and accelerated incoming ions. This arrangement of grids is not the optimum arrangement for the experiment objective (i.e., stacked grids are better); nevertheless, as discussed later, useful results were obtained.

Passive experiments on tray 1 addressed mass transfer, silver oxidation and resultant electrical conductivity change, and oxygen atom scattering effects, and included a limited number of exposed disc samples. Mass transfer resulting from atmospheric-surface interactions was evaluated using small tubes (see Fig. 2) in combination with glass discs coated with various optical coatings. The walls of each tube contained surfaces reactive with the atomic oxygen, and the coated discs acted as collectors for condensable reaction byproducts. Several different tube coatings and disc samples were used. A similar mass transfer experiment (see Fig. 2) consisted of reactive surfaces which generate byproducts of reaction that were collected on KRS-5 crystals for subsequent multiple internal reflectance infrared spectral analysis. The results of both experiments are provided in other sections[10-11] of this document.

Scattering of the atomic oxygen beam by vitreous carbon surfaces was measured using a third experiment, which included two uniquely designed passive reflectometers that incorporated a silver film detecting surface. Additional details of this experiment are also provided in another section[12] of this report.

Tray 2 (Fig. 3), located on the port side of the vehicle, was primarily dedicated to passive exposure of disc samples (2.54 cm diameter). These samples were mounted on six discholders each holding 46 samples as thick as 0.6 cm Samples were held in place by a combination of Belleville springs on the back side and a top cover which allowed only 3.2 cm^2 of the surface of the samples to be exposed. Each sample discholder was shared by several organizations.

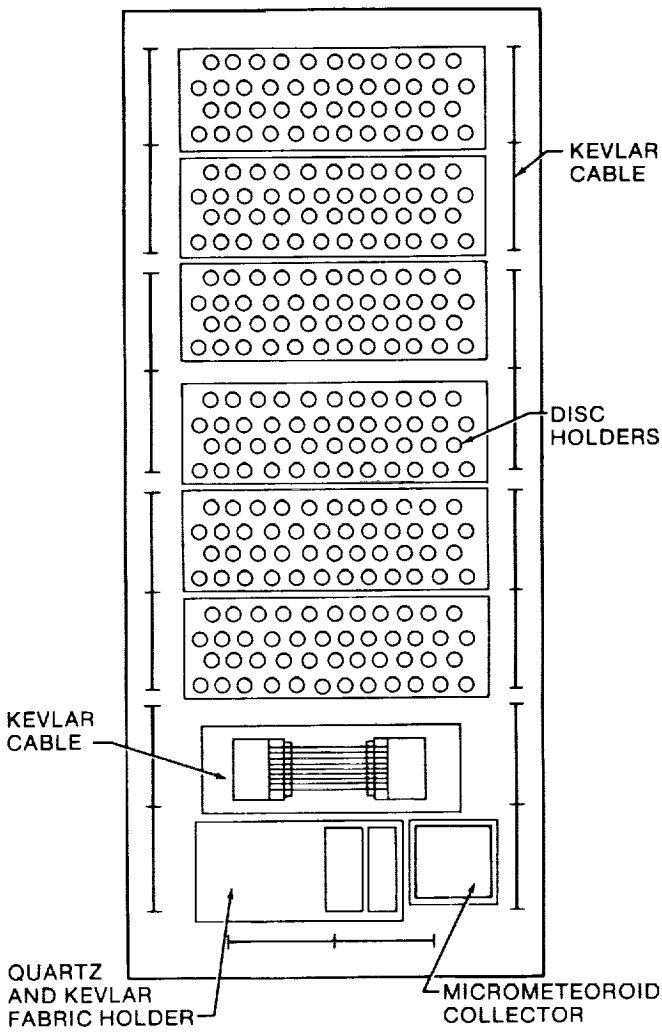

Fig. 3 Exposure tray 2.

Other samples on tray 2 consisted of Kevlar cable samples mounted on the peripheral edges of the trays, samples of Kevlar and quartz fabric mounted on one tray end, and a special holder with additional Kevlar cable samples intended for tensile tests and larger samples than those which were edge-mounted.

During the STS-5 atomic oxygen experiment, protective techniques for Mylar windows currently used on Long Duration Exposure Facility micrometeoroid collectors were evaluated. From these data, a technique was selected and verified during the STS-8 experiment on tray 2 by exposing a full collector cell with an improved protective overcoat.

As previously mentioned, samples mounted on the heaters were thermally controlled. All other specimens, including those on tray 2, floated at the overall equilibrium tray temperature, which is estimated to have been $-15°$ C. Certain specimens with absorptance to emittance (α/ε) ratios considerably greater than 1 may have been at higher temperatures during the day portion of each orbital pass.

2.3 Sample Description

Discussions in this paper will address certain organic film strips and disc samples located during the exposure on tray 1 and disc samples located on tray 2. Three identical sample sets, one control and one each for the two exposure conditions, were used on both the solar radiation and the charged grid experiments. Four samples, Kapton, carbon (amorphous), osmium (200 Å vapor deposited), and iridium (200 Å vapor deposited), were located under the charged grids and the control grid. Six solar radiation samples included polyethylene, Kapton, Mylar A, Kapton overcoated with Teflon (Kapton F), Kapton overcoated with T-650 silicone, and graphite. In consideration of brevity, only the Kapton results will be reported quantitatively in this paper.

In addition to the evaluation of temperature effects using the heater plates, effects of sample thickness and manufacturing variations were also assessed using the following sample set on each heater: Kapton, 12.7, 25.4, and 50.8 μm (manufacturing roll side exposed); Kapton, 12.7, 25.4, and 50.8 μm (side opposite to roll exposed); Mylar D, 50.8 μm (roll side and side opposite to roll exposed); Mylar A, 12.7 and 40.6 μm (side opposite roll exposed); Tedlar, 12.7 μm (side opposite roll exposed); and Kapton F (Teflon side exposed). Each of these samples was approximately 10 cm by 2.54 cm and, therefore, provided sufficient material for several measurements. Control samples mounted under the exposed samples were exposed to the same payload bay environment except for atmospheric impingement.

2.4 Exposure Fluence

The STS-8 exposure provided the largest atomic oxygen fluence of any experiment to date. The high fluence was achieved by lowering the vehicle altitude to 225 km and maintaining the payload bay pointing into the velocity vector, nose to the Earth, for a total of 41.75 hr during three exposure periods of approximately 14 hr each. This attitude provided 86 percent of all the mission atomic oxygen fluence; therefore, essentially all of the impingement was normal to the exposure surfaces for the first time. It can be assumed that the remaining fluence

(14 percent) was provided under conditions which resulted in an atomic oxygen beam sweeping relative to the sample surface. Using atmospheric density as derived from the mass spectrometer and incoherent scatter (MSIS) model[16] for the specific mission flight period, (see Fig. 4) total exposure fluence was 3.5×10^{20} atoms/cm2.

2.5 Analysis Techniques

Postflight laboratory analysis techniques consisted primarily of mass loss determinations and scanning electron microscope (SEM) evaluations. For mass loss determinations of thin film samples (65° and 121° C), specimens were prepared by cutting 5-cm^2 strips of material with a die from both the control samples and the exposed samples. Three samples were prepared from each strip. Samples had been vacuum baked before flight to remove volatile products and were again vacuum baked after flight to remove water vapor. Mass loss determinations were made by comparing control and exposed sample weights. Since the 5-cm^2 disc samples were cut before flight, postflight weights were compared to the preflight weights after vacuum baking. These weight changes were converted to thickness loss, which is independent of film thickness.

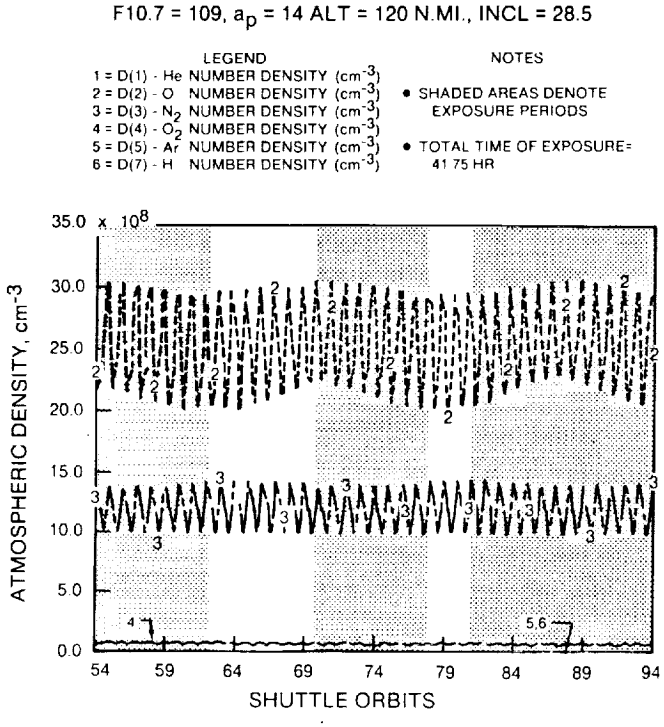

Fig. 4 MSIS atmospheric density estimations.

2.6 Results and Discussion

2.6.1 Recession Rates and Material-Peculiar Effects

Recession data from the film strips mounted on the heater plates and from the disc samples mounted on tray 2 will be discussed first because these data provide the largest sample base and also address material parameters such as thickness and manufacturing peculiarities. These data will be used as a point of departure for discussion of solar radiation and charged species effects.

Average thickness loss for the strip and disc samples is shown in Table 2. As mentioned previously, the notations "air" and "roll" under the "exposed side" column refer to the manufacturing process for the films. "Roll" is the film side in contact with the manufacturing rolls, and "air" refers to the opposite side. Both sides of the film were exposed to determine reaction rate dependency on manufacturing details. Since the heater plates supported the samples at off-normal angles to the incoming oxygen beam, the recession data have been corrected (cos θ) for flux reductions. Each strip data point represents three individual specimens (5 cm^2 in size) with a standard deviation of 0.6 μm. Minimum detection of mass and corresponding thickness change, considering errors associated with sample preparation, is 0.2 μm. In general, the data for a given material are in good agreement considering all the variables involved in the measurements. For example, Kapton and Mylar recession varies by only ±5 to 10 percent.

Temperature effects on recession rates can be assessed by comparing the 121° C, 65° C, and, in several cases, the disc samples, which, as mentioned earlier, had an estimated equilibrium temperature of −15° C. As can be seen in Table 2, no recession rate temperature dependency is evident for any of the films over the temperature range involved. This finding is in agreement with the organic film data obtained on the STS-5[4] mission and ground simulation results[17] and is not unexpected since the incoming atoms have >5.0 eV of kinetic energy, which appear, based on scattering measurements made by Gregory,[12] to be totally transferred to the surface.

Because of an apparent dependence of recession rate on film thickness as indicated by the STS-5 results, samples for the STS-8 experiment were carefully selected to further study this effect. Since the thickness dependence might arise from

Table 2 Recession and reaction efficiency for organic films

Material	Thickness, μm (mils)	Exposed side[a]	Surface recession,[b] μm				Reaction efficiency $cm^3/atom \times 10^{-24}$
			Strip samples		Disc samples	Average[c]	
			121° C	65° C			
Kapton	12.7 (0.5)	air	9.5	10.5	11.1		
		roll	11.8	10.3			
Kapton	25.4 (1..0)	air	9.8	10.7			
		roll	9.9	9.0		10.5	3.0
Kapton	50.8 (2.0)	air	11.1	10.6			
		roll	11.1	11.1			
Mylar A	12.7 (0.5)	air	12.7	12.3	12.7	12.6	3.6
Mylar A	40.6 (1.6)	air	12.1	11.9		12.0	3.4
Mylar D	50.8 (2.0)	air	9.9	10.2		10.4	3.0
		roll	11.0	10.4			
Clear Tedlar	12.7 (0.5)	air	10.9	11.5		11.2	3.2
Polyethylene	20.3 (0.8)	n/a			11.5	11.5	3.3
Teflon TFE	12.7 (0.5)	air			<0.2	<0.2	<0.05
Kapton F	30.5 (1.2)	n/a	<0.2	<0.2	<0.2	<0.2	<0.05

[a]Refers to manufacturing process.
[b]Corrected for flux reduction due to nonnormal impingement (cosθ).
[c]Strip samples and disc samples.

minor surface density variations introduced in the manufacturing process, reactivity of both sides (roll and air) of the films was examined and the data are included in Table 2. No differences in recession rates for roll and air sides are evident for Kapton and Mylar D.

Since the recession rates are not affected by either temperature or the specific side exposed, these data points were combined (average recession for temperature, air and roll) and examined for thickness dependency. There is no apparent recession rate dependence on sample thickness for Kapton, whereas the Mylar recession rate decreases slightly with increase in film thickness. (See Mylar data for 12.7, 40.6, and 50.8 μm thickness.) Whereas the Kapton behavior is in disagreement with the STS-5 results which show an increased recession rate with increasing film thickness, the Mylar thickness dependency is in general agreement with the STS-5 results. Because Mylar has similar recession dependency on thickness for considerably different total recession levels (STS-5 and STS-8), thickness effects seem to be a characteristic of bulk properties. On the other hand, thickness dependency for Kapton may be surface-property controlled.

As mentioned in previous papers, a reaction efficiency can be computed by normalizing the total surface recession by mission atomic oxygen fluence. The last column in Table 2 shows the reaction efficiencies derived for the STS-8 experiment using a total fluence of 3.5×10^{20} atoms/cm^2. All of these reaction efficiencies are higher than the efficiencies measured for the same materials on STS-5 by approximately a factor of 2. There are three significant differences, all related to exposure conditions, which could affect reaction rates. These are, for STS-8 and STS-5 respectively, incident flux, 2.3×10^{15} atoms/cm^2-sec versus 3.8×10^{14} atoms/cm^2-sec; total fluence, 3.5×10^{20} atoms/cm^2 versus 9.9×10^{19} atoms/cm^2; and sample orientation relative to ram, or normal versus sweeping impingement.

Flux differences do not appear to be a significant factor in influencing reaction rates. In fact, one would expect lower flux to result in higher reaction

efficiencies since atom to atom recombinations or other competing reactions should be less favored at lower flux as a result of lower atomic oxygen surface densities.

Reaction rates may have been affected by total fluence differences in that low fluence results in small surface recession which could be dominated by surface effects or minor amounts of contamination. High fluence results in rates representative of bulk properties. Aside from fluence considerations, if contaminants were present on the sample surfaces, the STS-5 recession rates should have been lower than the STS-8 rates. It should be noted that the STS-5 strip samples were attached with silicone-based adhesive tape, and although the samples were outgassed prior to flight, some silicone contaminant may have been transferred by migration to the sample surfaces. It has been shown previously[5] that silicones are considerably less reactive than non-silicon-containing organics. To preclude similar problems, tape with acrylic-based adhesive was used exclusively on the STS-8 samples.

Finally, the capture probability for the impinging atoms by the surface may be dependent on impingement angle. If such dependence exists, it might be expected that low impingement angles, as result from the sweeping-beam case of STS-5, may lead to lower capture probability and lower reaction efficiency. Although data from the inclined samples, to be discussed later, support this hypothesis, additional data on impingment angle effects are needed to completely define reaction rate dependency. Thus, differences in the reaction rates determined on the two experiments were most likely due to either minor contaminants or atom impingement angle.

2.6.2 Impingment Angle

Eleven samples consisting of Kapton (12.7 and 50.8 μm), Mylar (12.7 and 40.6 μm), and Tedlar were mounted on the inclined portion of both heater plates, positioned 42° off the main beam axis, and were exposed to only 74 percent of the normal impingement flux. When the recession data gathered from the samples inclined at 42° are combined and divided by the respective normal impingement recession, the result is a ratio of 0.64 ± 0.03 rather than 0.74, which indicates that recession at low impingement angles is less than would be expected, as it would be if it were simply due to flux reduction. This finding is in qualitative agreement with the STS-5 results and is also supported by data from other positions on the

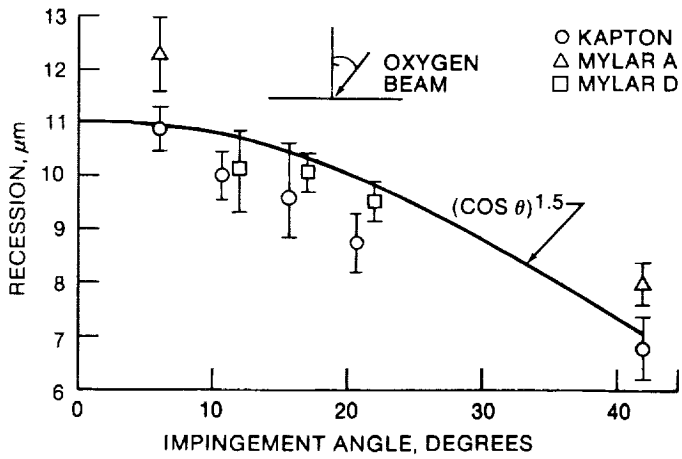

Fig. 5 Surface recession as a function of atomic oxygen impingement angle.

plates where samples were at various angles to the impinging beams. The data fit a $(\cos \theta)^{1.5}$ function better than $\cos \theta$, as can be seen by comparing the curves in Figure 5. It appears, at least for Kapton and Mylar, that as the impinging angle increases, reaction probability dcreases.

2.6.3 Solar Radiation

As mentioned earlier, a preliminary assessment of the effect of solar radiation on reaction efficiencies was made using three sets of six samples each with one control set exposed to the total fluence (3.5×10^{20} atoms/cm^2), one exposed during day only, and one exposed during night only. By comparing the total recession expected from integrated exposures to the measured recession, solar effects can be assessed. In recognition that exposure times in the two positions were necessary to properly assess fluence, two timers were operated in conjunction with the electronically actuated (photocell driven) covers. Unfortunately, the timers did not operate properly; therefore, fluence estimates for each position had to be made based on the assumption (since light-level variations in photocell operation were not known) that the cover actuated at the umbra to penumbra position in the orbital pass.

Data for the film samples used in the solar radiation effects experiment are shown in Table 3. Although Kapton overcoated with T-650 silicone was exposed, it is not included in the table since the T-650 coating quality varied considerably. Additional discussion of the T-650-coated samples is included in

Table 3 Solar radiation effects on surface recession

Material	Thickness loss, μm		Night recession / Day recession	Expected[a] night fluence / Day fluence
	Shuttered (day only)	Shuttered (night only)		
Polyethylene, 20.3 μm (0.8 mil)	5.4	5.0	0.93	
Kapton, 12.7 μm (0.5 mil), air side	5.9	4.8	0.81	0.85 to 1.2
Mylar A, 12.7 μm (0.5 mil), air side	7.0	5.7	0.81	
Kapton F, 30.5 μm (1.2 mil)	<0.2	<0.2	--	

[a]Takes into account night/day atmospheric density variations.

a following section addressing surface morphology. For actuation of the sample cover between umbra and penumbra, a night/day fluence ratio of 0.85 to 1.2 can be expected. As can be seen in the table, the night/day recession ratios are in the same range as the fluence ratios and thus indicate no effect of solar radiation on recession rate. The graphite data reported in Reference 12 show a night/day ratio of 0.71. If it is assumed that graphite reactivity is independent of solar radiation effects, the graphite data can be used as a measure of fluence. Therefore, the use of the ratio of 0.71 indicates that the reactivities of Kapton and Mylar are greater during the night exposure. Considering the available data limitations, the only conclusion which can be drawn is that solar radiation does not appear to have any major effect on the reactivities of Kapton and Mylar.

Kapton, 12.7 μm, was exposed under all three grid positions. Recession for these samples, after correction for 73 percent transmission efficiency of the gold grids, is 11.6 μm for neutral grid, 11.4 μm for +28-V grid, and 11.4 μm for −28-V grid. When measurement errors of ±0.6 μm inferred from the other samples were considered, there was no effect of the charged grids on recession rate, as expected, since ion and electron densities at the STS-8 altitude are approximately a factor of 10^4 lower than the neutral species.

2.6.4 Conductive Coatings

Three electrically conductive coatings were also exposed within the discholders. These coatings were Electrodag 401 (silver in a silicone binder), Electrodag 106 (graphite in an epoxy binder), and Aquadag E (graphite in an aqueous binder). As expected, the Electrodag 106 and the Aquadag E both had large surface recessions of 4.1 and 4.3 μm, respectively. These recessions represent 68 percent of the Electrodag 106 coating thickness and 100 percent of the Aquadag thickness. The Electrodag 402 coating had good stability, showing a recession of 0.2 μm.

2.6.5 Surface Morphology

Some differences from previous flights in sample surface morphology were expected for the STS-8 samples because of predominantly normal impingement. This is not the case, however, as is indicated in Figure 6, which shows a Kapton surface for exposed and control conditions at 10 000× magnification. The carpetlike appearance of the exposed sample is very similar to that of earlier STS-5 samples.

The T-650-coated Kapton referred to earlier was prepared to evaluate thin coatings for protection

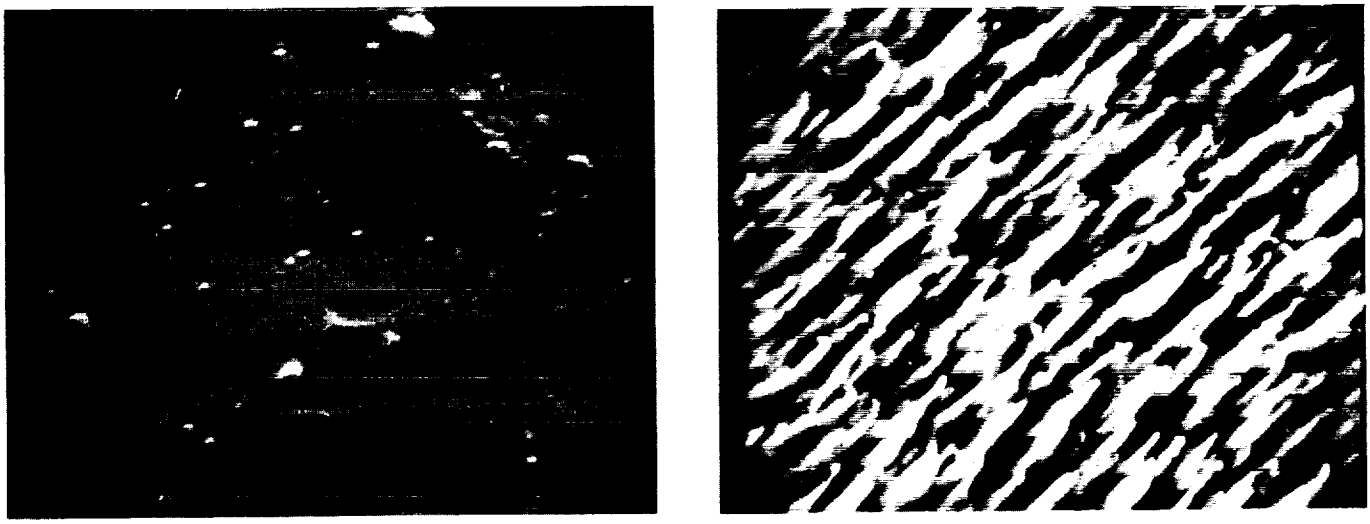

(a) Before exposure.

(b) After atomic oxygen exposure.

Fig.6 SEM photographs (10 000×) of 25.4-μm Kapton film specimens exposed during STS-8.

of previously manufactured flight hardware. These samples were prepared by spraying a 5-percent solution of T-650 onto the Kapton film surface. This technique did not produce uniform coatings, but the samples were exposed anyway to determine whether surface migration of the silicone would provide some protection. It is obvious from Figure 7, which shows this sample after exposure at 10 000× magnification, that this coating technique did not provide complete protection. Postflight measurements indicated the surface receded an average of 2.1 μm.

2.7 Concluding Remarks

A significant expansion of the data base for interaction of materials with atomic oxygen in the low Earth orbital environment was provided by the STS-8 experiment. Quantitative reaction rates for more than 50 materials have been established, although these rates need verification by combined recession rate and ambient density measurement made simultaneously. In addition, the rates for many of these materials are based on limited samples, and exposure of more samples is needed for verification of previous results.

It has been shown that the reaction between the environment and surfaces, as a first approximation, is not dependent on temperature, solar radiation, or electrically charged species. Additional measurements are needed both to confirm these findings and to study the effects of mechanical stress and other parameters on reaction rate.

Almost all of the data which have been generated to date address only the engineering aspects of atomic oxygen surface interactions.

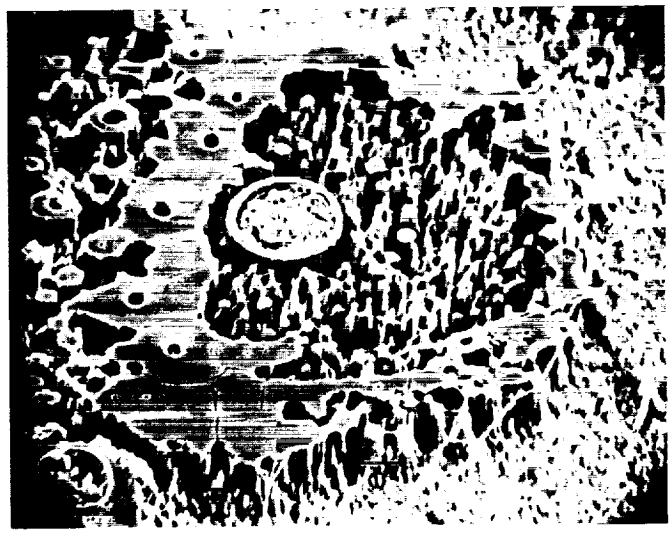

Fig. 7 SEM photograph (10 000×) of 12.7-μm Kapton film specimen coated with T-650 silicone and exposed during STS-8. Protected and unprotected areas of Kapton are due to nonuniform application of coating.

Studies which address the basic interaction mechanism will be performed on an upcoming Space Shuttle flight experiment now that the significance of LEO effects has been established. It appears that ground-based mechanistic studies may soon be possible at atom flux and energy levels characteristic of the natural environment.

References

1. Leger, L. J., "Oxygen Atom Reaction With Shuttle Materials at Orbital Altitudes," NASA TM-58246, May 1982.

2. Leger, L. J., "Oxygen Atom Reaction With Shuttle Materials at Orbital Altitudes – Data and Experiment Status," *AIAA 21st Aerospace Sciences Meeting*, Jan. 1983.

3. Peters, P. N., Linton, R. C., and Miller, E. R., "Results of Apparent Atomic Oxygen Reaction on Ag, C, and Os Exposed During the Shuttle STS-4 Orbits," *Journal of Geophysical Research*, Vol. 10, July 1983, pp. 569-571.

4. Leger, L. J., Spiker, I. K., Kuminecz, J. F., Ballentine, T. J., and Visentine, J. T., "STS Flight 5 LEO Effects Experiment – Background Description and Thin Film Results," AIAA Paper 83-2631-CP, Oct. 1983.

5. Whitaker, A. F., "LEO Atomic Oxygen Effects on Spacecraft Materials," AIAA Paper 83-2632-CP, Oct. 1983.

6. Park, J. J., Gull, T. R., Herzig, H., and Toft, A. R., "Effects of Atomic Oxygen on Paint and Optical Coatings," AIAA Paper 83-2634-CP, Oct. 1983.

7. Zinner, E., Fraundorf, P., Lindstron, D., Sandford, S., Swan, P., and Walker, R., "Erosion of Mylar and Protection by Thin Metal Films," AIAA Paper 83-2636-CP, Oct. 1983.

8. Banks, B., Mirtich, M., Rutledge, S., and Swel, D., "Sputtered Coatings for Protection of Spacecraft Polymers," NASA TM-83706, Apr. 1984.

9. Liang, R. and Gupta, A., "Mechanistic Studies of Kapton Degradation in Shuttle Environment," AIAA Paper 83-2656-CP, Oct. 1983.

10. Gull, T. R., Herzig, H., Toft, A. R., Park, J., and Triolo, J., "Effects on Optical Surfaces at Shuttle Altitudes," AIAA Paper 85-0418, Jan 1985.

11. Stuckey, W., et al., "Effects on Advanced Materials: Results of the STS-8 EOIM Experiment," AIAA Paper 85-0419, Jan. 1985.

12. Gregory, J. C. and Peters, P. N., "Measurement of Reaction Rates and Activation Energies of 5 eV Oxygen Atoms With Graphite and Other Solid Surfaces," AIAA Paper 85-0417, Jan. 1985.

13. Whitaker, A. F., Little, S. A., Harwell, R. J., Griner, D. B., and DeHaye, R. F., "Orbital Atomic Oxygen Effects on Thermal Control and Optical Materials, STS-8 Results," AIAA Paper 85-0416, Jan. 1985.

14. Banks, B. A., Mirtich, M. J., Rutledge, S. K., Swec, D. M., and Nahra, H. K., "Ion Beam Sputter-Deposited Thin Film Coatings for Protection of Spacecraft Polymers in Low Earth Orbit," AIAA Paper 85-0420, Jan. 1985.

15. Liang, R. H. and Gupta, A., "Mechanistic Studies of Interactions of Materials With Energetic Oxygen Atoms in Low Earth Orbit," AIAA Paper 85-0422, Jan. 1985.

16. Hedin, A. E., Reber, C. A., Newton, G. P., Spencer, N. W., Brinton, H. C., Mayer, H. G., and Pottes, W. E., "A Global Thermospheric Model Based on Mass Spectrometer and Incoherent Scatter Data: MSIS 2 Composition," *Journal of Geophysical Research*, Vol. 10, 1977, p. 2139.

17. Arnold, G. S. and Peplinski, D. R., "Reaction of Atomic Oxygen With Polyimide Films," submitted to *AIAA Journal*, June 11, 1984.

3.0 RESULTS FROM CONTAMINATION MONITOR PACKAGE ON THE STS-8 MISSION *

J. J. Triolo, R. Kruger, and R. McIntosh

NASA/Goddard Space Flight Center
Greenbelt, Maryland 20771

Abstract

Modification to the contamination monitor package which had been flown on STS-3 involved coating the quartz crystal microbalances (QCM's) with carbon and osmium. During the STS-8 exposure to the velocity vector at Space Shuttle attitudes, the reaction rates with ambient atomic oxygen for carbon and osmium were determined by QCM measurements of mass loss. Mass loss rates of 7.23×10^{13} atoms s^{-1} for carbon and 3.90×10^{12} atoms s^{-1} for osmium were found during these attitudes for averaged day-night fluxes of 2.06×10^{15} atoms $s^{-1}\,cm^{-2}$.

3.1 Introduction

In view of the effects of atmospheric atomic oxygen seen previously on materials at Space Shuttle altitudes, an experiment was devised to obtain information on the effects of the atmosphere on two materials, carbon and osmium. These elements were selected as the test materials because previously they had been observed to react [1,2] and because osmium was being considered for use on the optical elements of space-borne telescopes. The instrument for making the necessary measurements was a modified version of the contamination monitor package (CMP) flown on STS-3.[3] The instrument package was capable of measuring very small changes in mass loss as a function of time.

3.2 Description of Instrument

A number of modifications were made to the CMP for the STS-8 mission. The four temperature-controlled quartz crystal microbalances (TQCM's) were relocated as shown in Figure 1. TQCM's 1 and 2 were coated with carbon to surface densities of approximately 25×10^{-6} g cm^{-2} and $50 \times 10^{-6}\,g\,cm^{-2}$, respectively. TQCM 3 remained uncoated as in STS-3 and served as a control sensor. TQCM 4 was coated with a layer of osmium to a surface density of approximately $60 \times 10^{-6}\,g\,cm^{-2}$.

In one of the many Orbiter attitudes for this mission, the payload bay faced in the direction of the velocity vector for a period of 42 hours so that atmospheric constituents impinged perpendicularly onto the CMP surface that contained TQCM's 2, 3, and 4. TQCM 1 was at 90 degrees to this velocity vector. This vehicle attitude (called +ZVV in STS parlance) existed for a number of periods during the STS-8 mission.

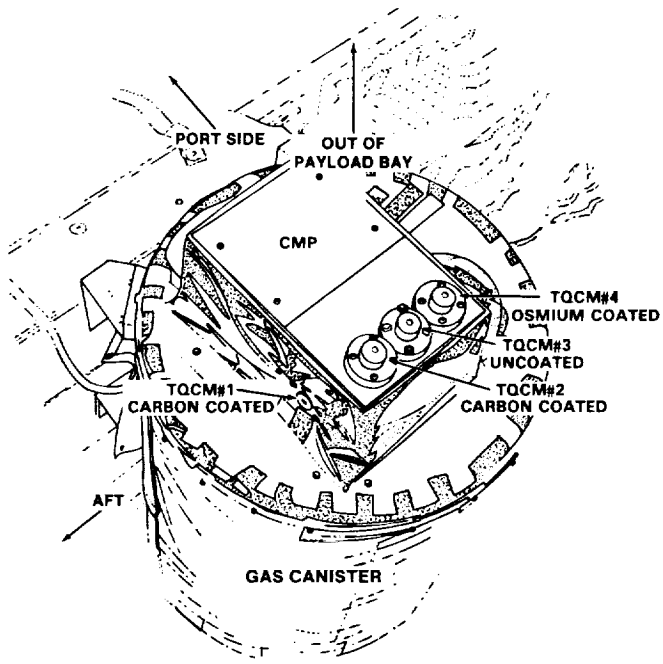

Fig. 1 CMP configuration, STS-8

* Presented at the 23rd Aerospace Sciences Meeting, January 14-17, 1985.

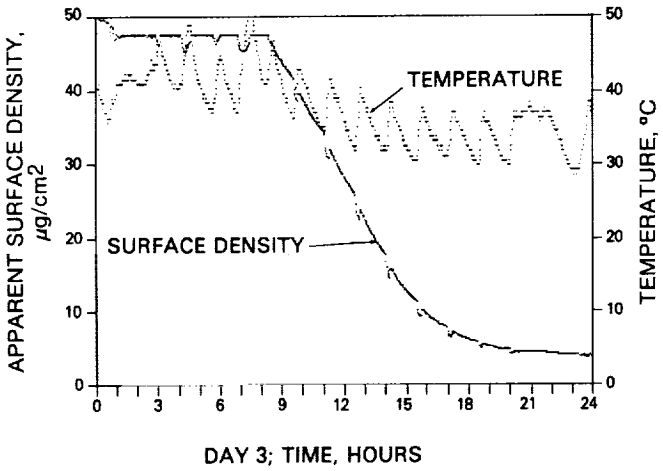

Fig. 2 TQCM 2, carbon coated

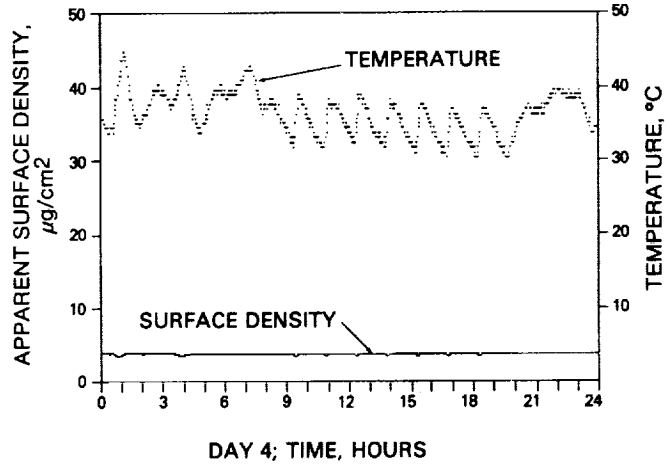

Fig. 3 TQCM 2, carbon coated

Another major change to the instrument was that it was converted from responding in real time to commands issued from the ground to a pre-programmed mode. This mode, which established only one temperature set point, was instead initiated during this flight by a command from an onboard astronaut.

The third major change to the measurement package involved a reconfiguration to make the CMP compatible with the Get Away Special (GAS) experiment canister. The portion of the instrument which housed the detector was mounted on the top surface of the GAS canister. Electronics, including the batteries and the tape recorder, were contained within the canister. The GAS canister provided a very flexible configuration that was almost independent of Orbiter operation.

The TQCM sensitivity was, as in the STS-3 CMP, 1.56×10^{-9} g cm^{-2} Hz^{-1}. The frequency data from TQCM's 1, 2, and 4 were halved for recording; TQCM 3 data were recorded at the instrument output frequency. Frequencies were recorded to the nearest Hertz. Data were collected every 102 seconds.

All of the TQCM's were intended to operate at approximately 15° C after they were turned on. Because of the limited time available to prepare for this mission, it was decided to proceed with the existing degraded thermal control system for TQCM 3. In addition to the problems experienced with TQCM 3, a thermal runaway condition (reaching a temperature in excess of 80° C) occurred with TQCM 2 at turn-on, which resulted in the loss of thermal control capability for TQCM 2. As a result, TQCM 1 temperatures were maintained between 14°

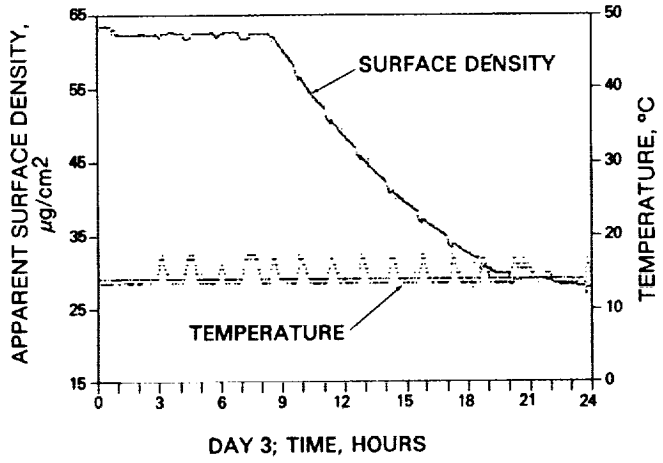

Fig. 4 TQCM 4, osmium coated

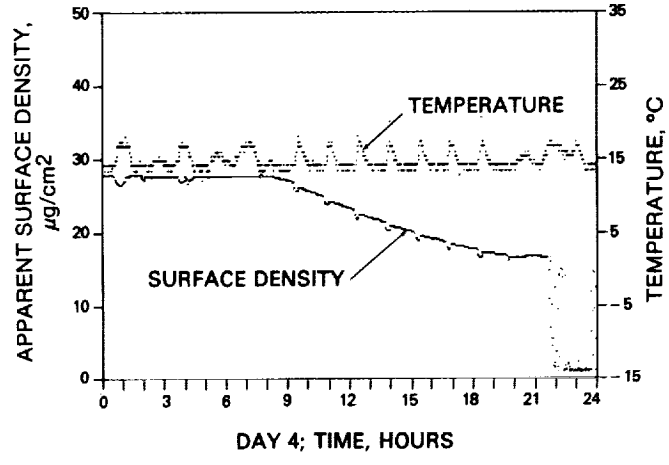

Fig. 5 TQCM 4, osmium coated

and 18° C, TQCM 2 (after recovering from the runaway condition) between 32° and 51° C, TQCM 3 between 7° and 24° C, and TQCM 4 between 13° and 17° C.

3.3 Results

Although data were obtained for approximately 97 hours during flight, in the interest of brevity, only the data for TQCM's 2 and 4 are reproduced here for days 3 and 4. The Orbiter attitudes during these 2 days resulted in almost the total loss of the carbon and osmium coatings.

The first +ZVV attitude was entered on day 3 at 08:15:19 (mission elapsed time) and exited on day 3 at 19:35:00. It was entered the second time on day 4 at 07:52:00 and exited on day 4 at 19:40:00. Figures 2 and 3 show the data from TQCM 2; Figures 4 and 5 show the data from TQCM 4.

Both Figures 2 and 4 show that the TQCM's reacted immediately to the incident oxygen flux within the atmosphere. In very general terms, they then both show a decreasing rate of material removal that has not been definitely explained, but this phenomenon might be attributed to decreasing amounts of coating being available for removal (as though areas were being removed leaving islands of the coatings behind that were more strongly bonded to the surface). By the end of the first EOIM exposure on day 3, essentially all of the carbon and most of the osmium coatings had been removed. During the second EOIM exposure (Figs. 3 and 5), essentially all of the remaining osmium was removed.

Using a model of the atomic oxygen density,[4] an average density at the Orbiter altitude of 222 km (120 n. mi.) of 2.65×10^9 atoms cm^{-3} was obtained. Using an orbital velocity of 7.78×10^5 cm s^{-1}, a flux of 2.06×10^{15} atoms cm^{-2} s^{-1} can be derived. Fitting a straight line to the early data (0900 to 1030, about one orbit) in the first +ZVV attitude, a mass loss of 7.23×10^{13} atoms s^{-1} is found. This produces a reaction rate of 28.5 atoms of oxygen per atom of carbon.

A similar calculation for TQCM 4 yields a loss of 3.90×10^{12} atoms s^{-1} for osmium. This produces a result of 528 atoms of oxygen per atom of osmium as an average for each orbit.

The plots of TQCM data show regular dips in the surface density data. These irregularities are due to thermal effects caused by the sun striking the TQCM surface which, in turn, increased the surface temperature. The dip begins at Orbiter sunrise and ends when the TQCM is shadowed by the Orbiter. While the data gathered during the period are difficult to analyze because of the varying solar flux due to angle, it appears that the average loss of surface material during the sunlit period is significantly higher than during the other periods.

A closer analysis of the atmospheric model[4] may yield a correlation of the differences in mass loss with orbital position.

3.4 Summary

The STS-8 flight of the CMP has provided data on the reaction of carbon and osmium with atmospheric atomic oxygen. This kind of instrument can be used for many similar measurements, such as reaction rate monitors in areas too complicated to model analytically.

References

1. "STS-2, -3, -4 Induced Environment Contamination Monitor (IECM) Summary Report," NASA Technical Memorandum, NASA TM-82524, Miller, E. R. ed., Feb. 1983.

2. Leger, L. J., "Oxygen Atom Reactions with Shuttle Materials at Orbital Altitude: Data and Current Status," Proceedings AIAA 21st Aerospace Sciences Meeting, Reno, AIAA Paper £83-0073, Jan. 10-13, 1983.

3. Triolo, J., Maag, C., and Kruger, R., "Results from a Small Box Real-Time Molecular Contamination Monitor on STS-3," Journal of Spacecraft and Rockets, Vol. 21, No. 4, July-Aug. 1984, pp. 400-404.

4. Hedin, A. E., "Tables of Thermospheric Temperature, Density, and Composition Derived for Satellite and Ground Base Measurements," Laboratory of Planetary and Atmospheres, Goddard Space Flight Center, Greenbelt, Maryland, Vol. 1, Jan. 1979.

4.0 ORBITAL ATOMIC OXYGEN EFFECTS ON THERMAL CONTROL AND OPTICAL MATERIALS: STS-8 RESULTS*

A. F. Whitaker, S. A. Little, R. J. Harwell, D. B. Griner, R. F. DeHaye

NASA George C. Marshall Space Flight Center
MSFC, Alabama 35812

A. T. Fromhold, Jr.

Auburn University
Auburn, Alabama 36849

Abstract

Various paints, metals, and organic and inorganic optical materials with applications to space telescope, tethered satellite, and advanced solar array technology were flown on STS-8 to determine quantitative effects resulting from exposure to the orbital atomic oxygen environment. Specular and diffuse requirements for the various material surfaces are described. Changes in optical characteristics, erosion rates resulting from exposure, and the effectiveness of protective overcoats in preventing erosion and maintaining specular qualities are discussed Mass loss rate for Chemglaze Z302, a polyurethane paint, was greater than any other material examined. This paint showed evidence of surface texturing, and therefore optical characteristics, with a dependency on direction of incident atomic oxygen. As expected, other paints which contain relatively inert fillers had lower mass rates than the Z302. Effects on silver are discussed along with an activation energy developed for the conversion of cold-rolled silver. Data on 23 materials are presented.

4.1 Introduction

The STS-8 Atomic Oxygen Effects Experiment, a follow-on experiment to that flown on STS-5, was configured to expose a large number of disk-type material specimens for reactivity assessment and to investigate temperature dependence, influence of ultraviolet irradiation, and material transfer aspects of atomic oxygen effects. The experiment provided an atomic oxygen fluence of 3.5×10^{20} atoms/cm^2 incident perpendicular to the experiment material surfaces over a period of 41.17 hr at 120 n. mi. The Marshall Space Flight Center (MSFC) portion of the experiment was developed to support the space telescope (ST) and tethered satellite (TS) projects and advanced solar array technology at MSFC. One hundred twenty-four specimens, mainly disk-type, representing 35 materials and/or processes comprised the MSFC experiment Of these materials, 10 paint specimens and 8 silver solar cell interconnects were maintained at temperatures of 210 $\pm$ 15° F and 142 $\pm$ 15° F during exposure, while the remainder of the materials were mounted in uncontrolled temperature regions estimated to be about 50° F. Most of the materials were for the ST and are shown in their specific application in Figure 1. Twenty-three of the exposed materials fall into the category of thermal control and optical materials and are discussed in this paper.

The evaluations and analyses to which these material specimens were subjected were similar to those described in (1). In addition, selected materials were subjects of special investigations including proton induced x-ray emission (PIXE), Rutherford backscattering (RBS), ellipsometry evaluations, transmission infrared spectroscopy, and electron spectroscopy for chemical analyses (ESCA). When appropriate and feasible, these evaluations were performed to yield data on oxide formation and surface electrical conductivity, identification of surface species and binding energies, and depth distribution of species.

*AIAA Paper 85-0415 Presented at the 23rd Aerospace Sciences Meeting, January 14-17, 1985.

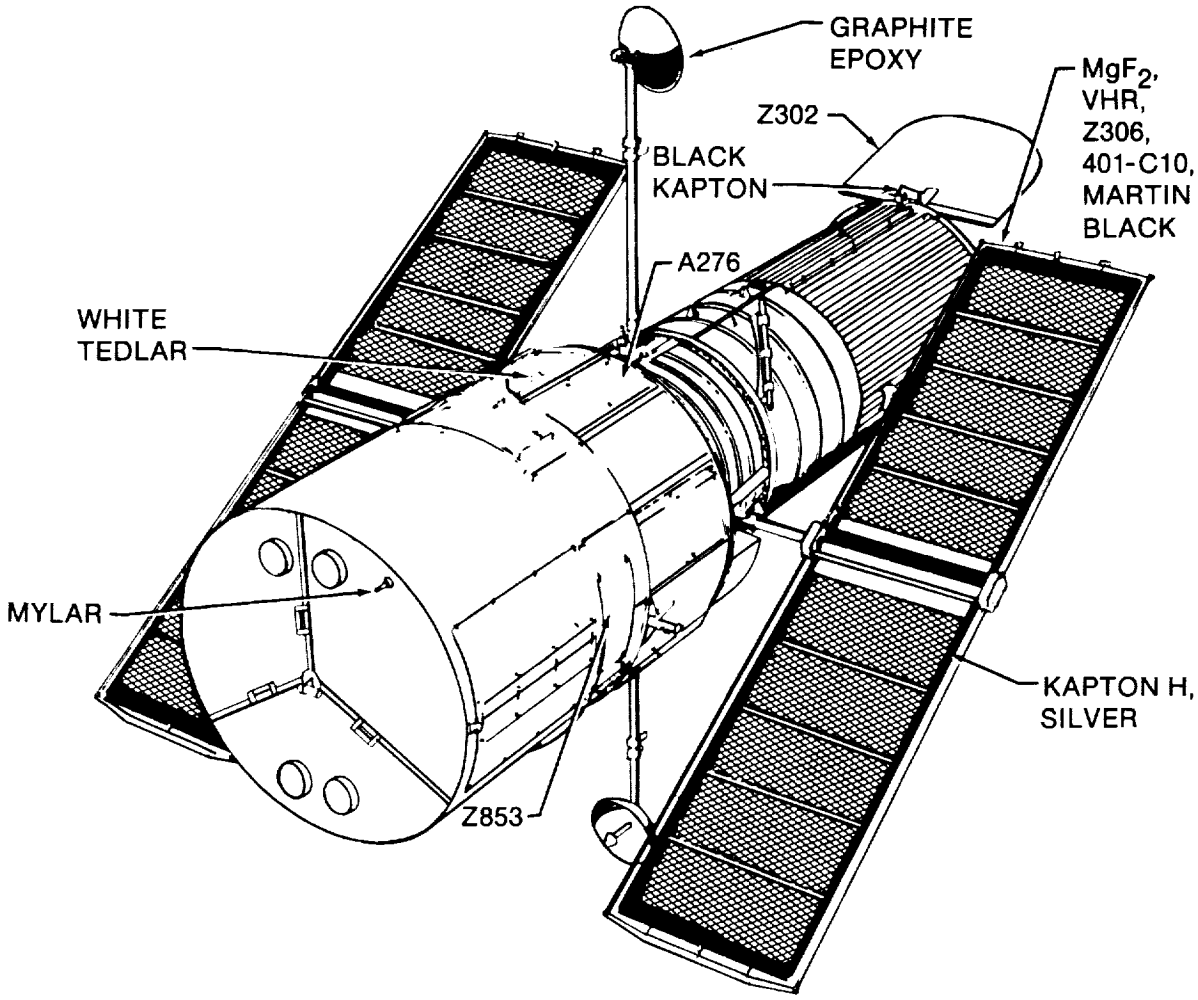

Fig. 1 The space telescope with nonmetallic surfaces identified.

4.2 Data Presentation and Analyses

4.2.1 Paints and Overcoats

Ten paints, including two with overcoats, applicable to the space telescope and to the tethered satellite, were evaluated. The diffuse paints, Chemglaze Z306 polyurethane and 3M 401-C10 epoxy, serve as ST light shield and baffle coatings for stray light suppression. The Chemglaze Z302, the glossy black polyurethane paint with a diffuse reflectivity requirement of 0.25 percent for the ST aperture door application, minimizes scattered light entering the telescope. The Chemglaze Z853 yellow polyurethane paint is applied to ST handrails and doors as crew aids, and the Chemglaze A276 glossy white polyurethane paint on the ST support systems module equipment section is part of the thermal control system. GSFC (Goddard Space Flight Center) green, an oxide paint, is the candidate coating for the tethered satellite body. The silicone overcoats applied to A276 and Z302 were intended to minimize atomic oxygen effects on these specular polyurethane paints. Two experimental paints, a glossy white and a glossy black, candidate substitutes for A276 and Z302, respectively, were also flown.

Optical properties including solar absorptivity (α_s), total diffuse scatter (TDS), total solar reflectivity (R_T), diffuse reflectivity (R_d), and specular reflectivity (R_s) and mass loss data for these paints, along with comments concerning exposure effects, are contained in Tables I, II, and III. Since no degradation dependency on temperature was noted, all optical data on a specified paint were averaged together. Optical properties other than TDS were measured on a Gier-Dunkle integrating sphere utilizing a Beckman DK2A spectrophotometer.

Table 1 STS-8 property data on diffuse paints

Specimen ID/evaluations	Z306 flat black		401-C10 flat black		Z-853 yellow	GSFC green
	α_s	TDS*	α_s	TDS*	α_s	α_s
Flight specimens, average optical property values for all temps.	.987 ±.001	.0132	.979	.0283	.406 ±.001	.538 ±.004
Control value for optical properties	.959 –	.0559	.974 ±.001	.0357	.440 –	.540 –
Mass loss/cm², total fluence $\left(\frac{mg}{atom}\right)$	$.10 \times 10^{-20}$		$.086 \times 10^{-20}$		0.09×10^{-20}	No change
Comments on exposure effects	+2.8% in α_s, more diffuse, porous surface		+0.5% in α_s, more diffuse		Porous surface	No observed effects

*Measurement made at normal incidence, 0.6328 μm.

Table II STS-8 property data on specular paints

Specimen ID/evaluations	Z302 glossy black					Z302 glossy black with OI 650 overcoat					Z302 glossy black with RTV 670 overcoat				
	α_s	R_t	R_d	R_s	TDS	α_s	R_t	R_d	R_s	TDS	α_s	R_t	R_d	R_s	TDS
Flight specimens, average optical property value for all temperatures	.993 ±.002	.7 ±.2	.4 ±.1	.3 ±.1	.0131	.962	3.8	1.6	2.2	.0028	.963	3.7	1.5	2.2	.0065
Control value for optical properties	.950 ±.001	5.0 ±.1	.5 ±.1	4.5 ±.3	.0063	.963	3.7	1.8	1.9	.0035	.967	3.3	1.2	2.1	.0037
Mass loss/cm², total fluence $\left(\frac{mg}{atom}\right)$	$.58 \times 10^{-20}$ ($RE = 3.9 \times 10^{-24}$ cm³/atom)					No change					No change				
Comments on exposure effects	= 4.5% in α_s, specular component converted to a total change, surface area considerably expanded into spike configuration.					α_s of control higher than uncoated Z302. No change in TDS.					α_s of control higher than uncoated Z302. TDS exceeds ST stray light requirement.				

Measurements were made from 200 to 2500 nm at energy increments representing 5 percent of the solar spectrum at zero air mass, and these incremental reflectances were averaged to derive the total solar reflectance. Diffuse reflectance measurements were made by directing the first reflection from the sample out of the integrating sphere (via the beam entrance port) and thereby eliminating the specular portion of the reflectance. Specular reflectance was derived from the difference in total and diffuse reflectances. Emissivity of the coatings was measured with a Gier-Dunkle DB-100 instrument with the samples at room temperature. Mass loss data was generated by weighing specimens prior to and following exposure.

As a result of exposure, the black paints showed an increase in α_s, and all the paints with specular components became diffuse, which is consistent with the STS-5 experiment results. The Z853 yellow paint decreased in α_s, and no change

Table III STS-8 property data on specular paints

Specimen ID/evaluations	A276 glossy white				A276 glossy white with ~1/2 to 1 mil OI 650 overcoat			
	α_s	R_t	R_d	R_s	α_s	R_t	R_d	R_s
Flight specimens, average optical property values for all temperatures	.245 ± .010	75.5 ± 1.0	74.8 ± 1.0	.7 ± .5	.257 ± .010	74.2 ± 1.0	72.3 ± .6	2.0 ± .5
Control value for optical properties	.247 ± .013	75.3 ± 1.2	70.7 ± 1.2	4.6 ± .1	.255	74.5	72.6	1.9
$\frac{\text{Mass loss/cm}^2}{\text{total fluence}}\left(\frac{\text{mg}}{\text{atom}}\right)$	$.10 \times 10^{-20}$				$.01 \times 10^{-20}$ (only one sample showed loss)			
Comments on exposure effects	Variations in thickness from specimen to specimen mask α_s changes, −85% in R_s.				α_s of control about +3% above uncoated A276.			

within measurement uncertainty was noted in α_s for the A276 white paint. As was expected, measurements showed no change in the GSFC green. The experimental paints flown performed no better than the A276 and the Z302. No change in emissivity was noted for any of the paints as a result of exposure. The silicone overcoats, which generally resist atomic oxygen attack, were applied to the paints to retain the specular character of their surfaces. The OI-650, a "glass resin" silicone, was successful, whereas the RTV 670 became slightly diffuse, suggesting that the RTV 670 was more reactive even though its mass loss was also negligible. Mass losses for those paints containing relatively inert fillers were essentially the same at 0.1×10^{-20} mg/incident atom. No reaction efficiency (RE) in terms of cubic centimeters per incident atom could be calculated for these paints because of the preferential surface attack. The Z302 surface, which recedes uniformly upon exposure, had a mass loss six times greater than the other paints and has the highest reaction efficiency ($RE = 3.9 \times 10^{-24}$ cm3/atom) of any material exposed.

Of particular interest is the Z302 paint's surface morphology, which is apparently created by the directional effects of incident atomic oxygen. Figure 2 shows scanning electron microscope (SEM) photographs of this paint obtained for the unexposed sample, the STS-5 exposed sample, and the STS-8 exposed sample. The atomic oxygen incident vector swept across the material surfaces during the STS-5 exposure and was perpendicular to the surfaces during the STS-8 mission. The coned structures evident on the STS-8 sample were also found on graphite samples flown. The optical scatter from these surfaces along with the OI-650 coated specimen are shown in the bidirectional reflection distribution function (BRDF) data in Figure 3. The unexposed Z302 shows an increase in the scatter function at the smaller angles, indicating a specular reflection component. After exposure, the Z302 shows no specular component but a rough Lambertian scatter surface. The large angle scatter, which is important to the ST aperture door application, increased by a factor of three to four on the STS-8 sample. Samples measured from the STS-5 flight reveal an increase in the backscatter but not as much during the STS-8 mission. The bow in the BRDF curve for the STS-5 samples indicates a surface roughness with spatial frequencies of the order of a few micrometers which concentrates the scatter at smaller angles. The SEM photographs support this analysis by showing reaction products on the surface in patterns a few micrometers in size. The OI-650 coating prevented any degradation of the large angle scatter, which indicates that the protective coating worked well for this application.

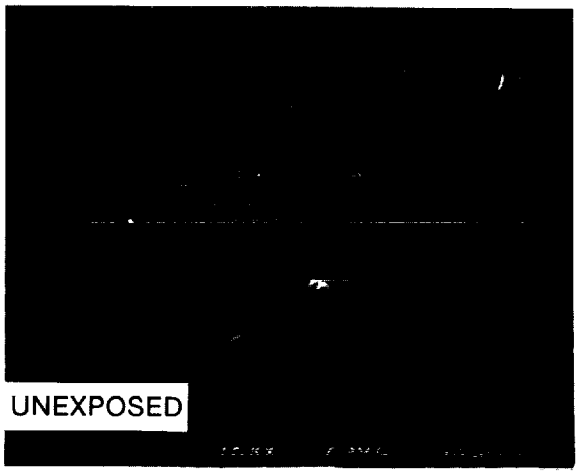

(a) Z302 control sample.

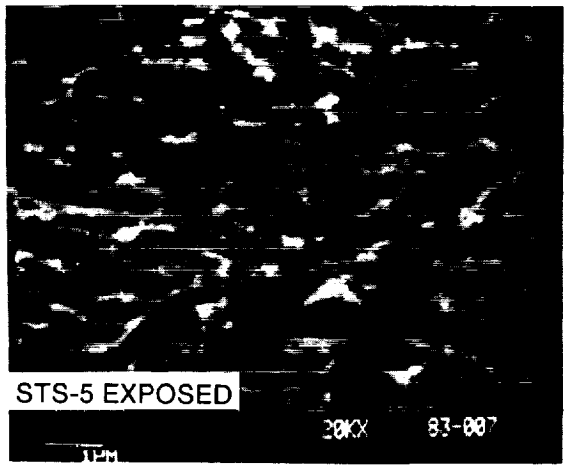

(b) Z302 sample exposed on STS-5 flight.

(c) Z302 sample exposed on STS-8 flight.

Fig. 2 SEM photographs of Z302 samples.

Surface analyses utilizing ESCA were made on selected paint samples. One consistent trend noted on the flight samples as compared to the control samples was a decrease in carbon content (based on the ratio of carbon to silicon) which is attributed to atomic oxygen reactivity. The A276 and Z302 showed a slight increase in oxygen content, and the 401-C10 showed a significant decrease (based on the ratio of oxygen to silicon). The broadening of silicon peaks in the Z302 indicates oxidation, although no change occurred in the N(1S) and O(1S) peaks. The higher binding energy form of silicon, probably SiO_2, was dominant in the flight 401-C10 samples and is indicative of complete oxidation of the silicon.

In summary, atomic-oxygen-vulnerable paints show small changes in α_s, improvements in diffusivity, and loss of specularity upon exposure. Even though overcoats for specular paints are available to prevent measurable erosion, they may not necesarily maintain their specularity. Finally, with the exception of the A276 paint, all of the paints examined by ESCA revealed increases in surface oxidation. This supports the original assumption that oxidation appears to be the dominant mechanism for material loss.

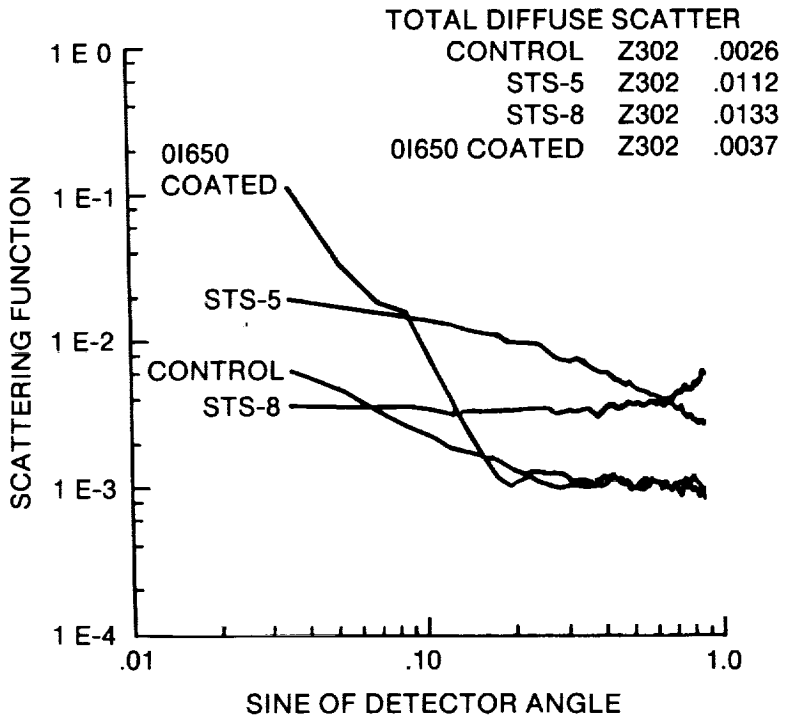

Fig. 3 BRDF data on Z302 paint.

4.2.2 Optical Materials

Nine specimens of mirror-type materials were flown which were representative of the ST primary mirror, the ST fine guidance system (FGS) optics, and the solar concentrator, which included elements of advanced solar array technology. These specimens consisted of 275 A of MgF_2 over aluminum, SiO_x systems over aluminum and silver, and proprietary dielectric films over aluminum and silver. Solar reflectivity measurements similar to those made on the paints were used to evaluate the FGS optics and the concentrator materials, whereas reflectivity measurements for the ST primary mirror materials were made over the range from 121.6 to 220.0 nm. No changes in reflectivity due to atomic oxygen exposure were noted for these materials within measurement accuracy of ± 1 percent. Examination of the ST material specimens at 150× under special lighting conditions revealed that three of four flight specimens had one to two crater-type areas which are suspected to be the result of on-orbit particle impacts.* As described, no measurable reflectivity degradation occurred either as the result of atomic oxygen exposure or as the result of the cratered areas. The PIXE spectrum of the MgF_2 coated aluminum ST materials indicated no significant atomic constituent differences observed between flight and control specimens. Further, ellipsometry data showed refractive index and absorption coefficient values for the flight specimens to be identical to that of the controls indicating no effects of atomic oxygen on aluminum protected by MgF_2 in this manner. The overcoat materials applied to these aluminum and silver mirrors appear to provide adequate atomic oxygen protection under these short duration exposures and reasonably benign thermal conditions.

4.2.3 Silver

Silver is utilized as solar cell interconnect material on the ST solar array. High electrical conductivity is required to maintain adequate spacecraft power. Previous exposure of these interconnects on the STS-5 experiment indicated that silver was highly reactive to atomic oxygen with a strong degradation dependency on temperature. To further quantify the atomic oxygen/silver interaction, a considerable number of silver specimens including interconnects, disk-type, and vapor-deposited films were flown. These silver specimens are identified in Table IV, and their

*Hertzig, H., GSFC, private communication.

Table IV STS-8 property data on silver

Silver types/configurations		Exposure conditions	
A.	Cold-rolled (solar cell interconnects)	A. (1)	Atomic oxygen (AO) normal, and at 45° angle to specimens, temperature controlled at 210 ± 15° F, 142 ± 15° F
		(2)	AO normal to specimens, temperature uncontrolled ~50° F
B.	Silver-plated and clad Invar, Pb/Sn solder-clad silver	B.	AO from reflected oxygen only, temperature uncontrolled
C.	Bare and chromate-conversion-coated silver	C.	AO normal to specimen, temperature uncontrolled
D.	Vapor-deposited films, 0.85 μm, 1.70 μm, 3.05 μm	D.	AO incident to films normal, at 45° angle and at 65° angle, temperature uncontrolled

exposure configurations are noted. The silver-plated and clad Invar specimens are candidate interconnect substitutes. Lead/tin solder and chromate conversion coating were evaluated for their effectiveness in protecting the silver. The vapor-deposited films were designed for two purposes: (1) to evaluate the atomic oxygen fluence/cosine law degradation dependency in silver, and (2) to assess as far as possible the concept of utilizing the resistance changes induced in a thin film due to atomic oxygen exposure as an environmental monitor.

All exposed, unprotected silver specimens were affected, including those which had no direct exposure but were subject only to reflected atomic oxygen atoms. However, the attack was less severe on those specimens with no direct exposure than on the directly exposed surfaces. The exposed surfaces were converted through oxidation processes to grey/black/brown loose scale or to thin interference films depending on the temperature of the specimen. The spalling of the scale was previously suggested[2] to be due to the conversion of silver to its oxide which has a larger lattice spacing and therefore requires a larger volume. As expected according to established oxidation theory, considerably more silver was converted to scale on the higher temperature surfaces. An exposed interconnect is shown in Figure 4, and SEM photographs comprise Figure 5. In the lower temperature interconnects where effects were less severe, the scale formation followed the machining ridges in the material. Further, cracking of the scale was more severe near the cutouts, and delamination or flaking of the scale seemed to occur at a certain plane in the material. These effects suggest possible stress involvement in addition to high reactivity in the silver conversion process. The vapor-deposited silver films ranging in thickness from 0.8 to 3.0 μm showed scale formation of definite area and thickness dependent on the initial film thickness. This suggests a stress relief role for the bulk or substrate material as Peters has hypothesized.* It appears that the critical thickness of scale sufficient to crack or spall is a function of both the initial surface stress condition and the bulk material stress.

An activation energy of 0.61 ± 0.9 eV over the temperature range from +50° to +210° F was generated for the conversion to scale of the cold-rolled silver interconnect material. Although the thickness of converted silver at the high temperature varied by about a factor of 2, the variation from the high temperature to the low was as great as a factor of 26, thereby providing well-resolved data. Measurements were made from specimens metallurgically mounted.

*Peters, P. N. MSFC, Interpretation of STS-8 Vapor-Deposited Silver Films, private communication.

These specimens are shown in Figure 6. This activation energy suggests a highly reactive process and requires further confirmation.

The lead/tin solder protected the low temperature silver, as would be expected since it was thick (~2.5 μm) and nonreactive, whereas the chromate conversion coating failed, probably because it was thin and porous. No strong dependency of the conversion process was noted on total incident atomic oxygen, and no conclusion could be reached concerning the role of the angle of incidence of atomic oxygen. Analyses for these effects were complicated by the strong thermal effects and the stress role of substrate material seen in the vapor-deposited films. The concept of using a thin film as an atomic oxygen monitor seems to be reasonable. Even though silver would not be the choice material, we were able, using the film's resistance data, to predict film thickness within 10 percent with the 3.0 μm vapor-deposited film. Better results probably were not obtainable since some diffusion of oxygen into the bulk occured in the the silver, and thus no well-defined scale/bulk electrical interface exists.

A number of evaluators attempted to determine with limited success the stoichiometry of the scale. Auger electron spectroscopy (AES) analysis revealed more oxygen but in low concentrations in the high temperature interconnect.[3] A separate AES analysis found no oxygen in the 142° F interconnect.*

*Dalins, Ilmars, MSFC, private communication.

When compared with control samples, ESCA evaluation showed a minute but consistent decrease in binding energy of the Ag 3d doublet, which is indicative of increased oxidation of metallic silver ($Ag \rightarrow Ag_2O \rightarrow AgO$). Chemical shifts of oxygen species to lower O(1S) binding energies occurred, but new forms of oxygen did not seem to be created. Both the presence of traces of carbon of an unknown origin on the flight samples and matrix effects prevented a reliable determination of surface oxygen to silver content. The RBS measurements revealed that underneath the scale, oxygen had penetrated the bulk to depths of about 1200 A in very dilute concentrations. In summary, these analyses to date show: (1) the scale to be somewhat nonstoichiometric but with increased oxidation of silver and (2) diffusion of oxygen occurring beneath the scale.

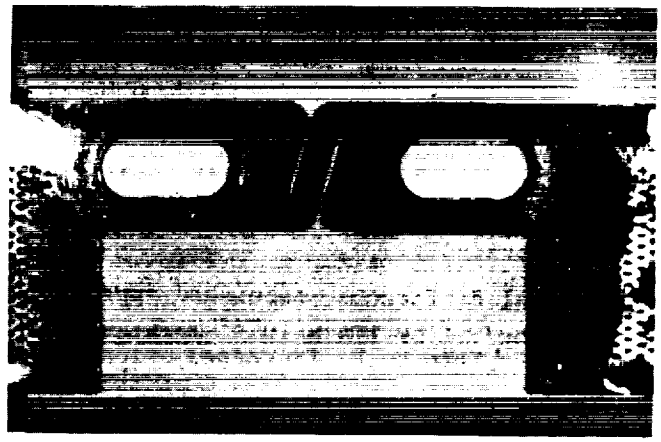

Fig. 4 STS-8 exposed silver interconnnect.

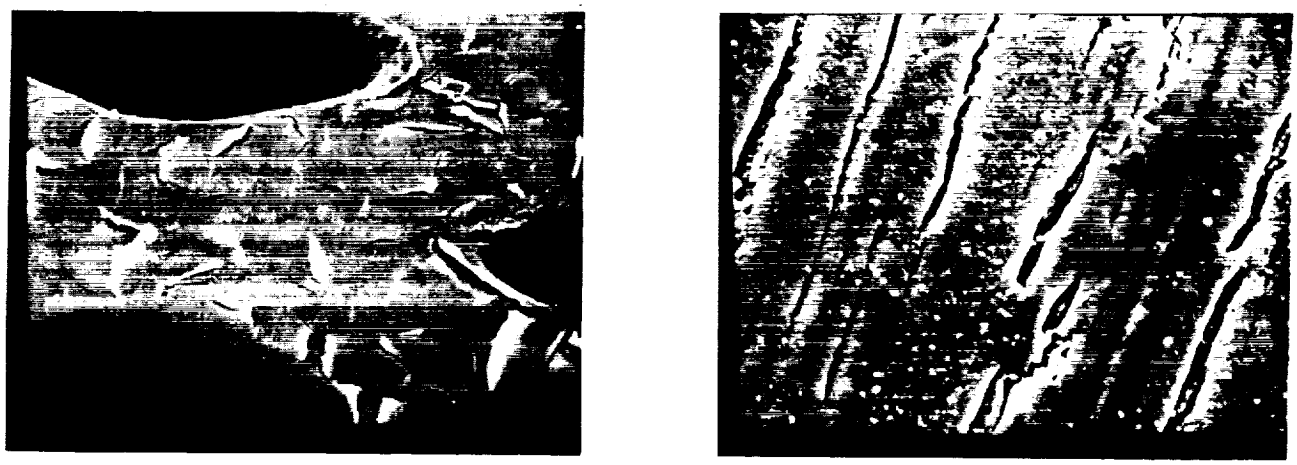

Fig. 5 SEM photographs of exposed silver interconnect.

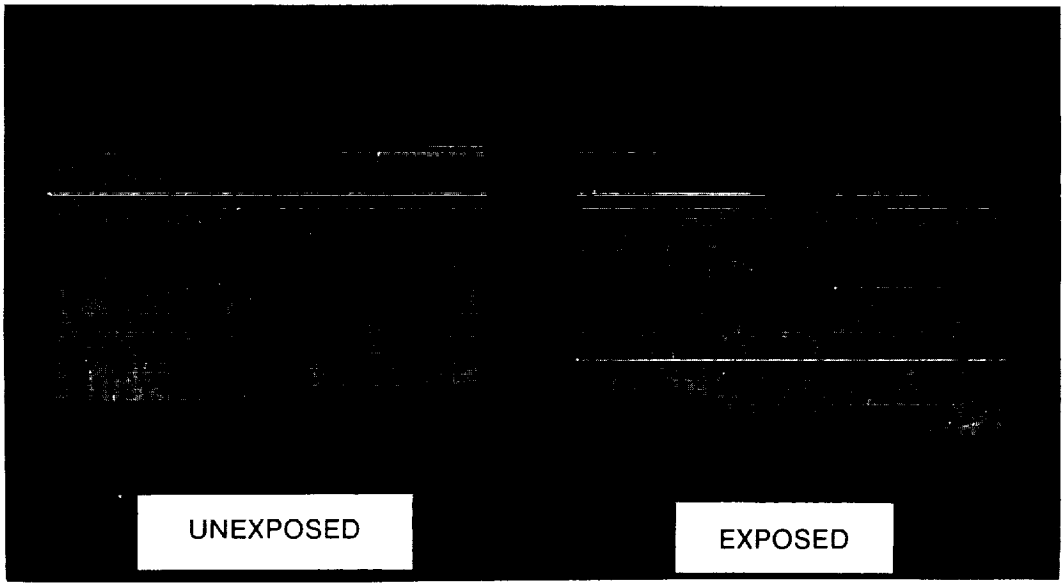

Fig. 6 Cross section of unexposed and exposed cold rolled silver.

4.2.4 Other Metals

Nine additional metals were exposed on STS-8: copper, lead, magnesium, molybdenum, nickel, platinum, tungsten, HOS-875 (FeCrAl alloy) in the bare and preoxidized condition, and Tophet-30 (NiCr alloy) in the bare and preoxidized condition. These metals are of interest for a variety of reasons. Copper and molybdenum are alternate solar cell interconnect materials, and, further, all of these metals have well-known high temperature oxidation characteristics. Under high temperature oxidation conditions, the HOS-875 and the Tophet-30 form their own protective oxide films of Al_2O_3 and Cr_2O_3, respectively. With the exception of some of the silver specimens, these metals were exposed on surfaces that were in the low temperature region, estimated to be about 50° F. The data generated to date regarding the results of the metals' exposure are shown in Table V. Following silver, the most reactive metal examined was copper with a measurable mass increase. When initial examinations of the metals revealed little reactivity, more sensitive evaluation techniques were attempted, and in many instances the sample preparation was not adequate for good resolutions under these evaluations. These metals generally showed low reactivity, possibly as a result of: (1) low exposure temperature, (2) low oxygen flux, and (3) limited exposure time.

4.3 Summary

Six nonmetallic material application areas on the space telescope are, or have been, of major concern in regard to atomic oxygen effects. These include the magnesium flouride coated mirrors, the Chemglaze Z302 painted aperture door, the Chemglaze Z306 painted light shields and baffles, the Kapton H solar array blanket substrate, the silver solar cell interconnects, and the Chemglaze Z853 coated crew aids. For short term exposures (~7 days), all data generated to date on magnesium flouride indicate no atomic oxygen effects either from chemical reactivity or diffusion. Oxygen would not be expected to replace flourine atoms. Diffusion of oxygen at ST altitude (~593 km at insertion orbit) cannot be answered because of mission duration, but oxygen density necessary to support diffusion is very low. Thus, the best information available indicates that atomic oxygen effects on the ST mirrors are not expected to be a problem. The erosion of Kapton H has been well documented with reaction efficiencies generated to predict thickness loss based on mission duration, spacecraft altitude and orientation, and solar activity. Erosion of Kapton H on the ST solar array blanket has been predicted, and the blanket has been redesigned to accommodate the expected erosion. Evaluations are currently underway to determine an overcoat for the silver interconnects

Table V STS-8 metals data summary

Metal	Exposure results
Silver	Well-defined visual changes, severe oxidation on all specimens, dilute penetration of oxygen in bulk, increases in refractive index, and decreases in electrical conductivity.
Copper	Visual difference, tarnished appearance, mass increase: $0.5\ mg/cm^2$ or 1.4×10^{-23} mg/atom, dilute penetration of oxygen into bulk, increased oxidation to CuO.
Lead	No visual change, no mass change.
Magnesium	No visual change, no mass change.
Molybdenum	No visual change, no mass change, dilute penetration of oxygen into bulk, increased oxidation to MoO_3.
Nickel	No visual change, no mass change.
Platinum	No visual change, no mass change.
Tungsten	No visual change, no mass change, decrease in refractive index, no trend in absorption coefficient.
HOS-875* - Bare - Preoxidized	No visual change, no mass change, no other changes discernible by SEM/x-ray diffraction.
Tophet 30* - Bare - Preoxidized	No visual change, no mass change, no other changes discernible by SEM/x-ray diffraction.

*(7)

that will extend on-orbit life but not add stress to the interconnect. Atomic oxygen on the Z306 painted baffles and light shields is expected to improve their diffusivity characteristics in the region of direct impact, thereby improving their light suppression characteristics. Further, to alleviate the concern for the transfer of loose surface particles from the exposed Z853 to experiment hardware during astronaut servicing, a silicone coating has been applied to the Chemglaze Z853 painted ST crew aids. Finally, overcoats to be applied to the Chemglaze Z302 on the ST aperture door are being evaluated not only for their low reactivity to atomic oxygen and good adhesion to Z302, but also for their ability to maintain the specular qualities of the paint.

Acknowledgments

The authors wish to thank the following people who were of considerable help during the design, fabrication, and evaluation of this experiment: Dr. Lubert Leger, Jim Visentine, and Ike Spiker of JSC, Dr. Ted Gull of GSFC, Dr. Wayne Stuckey of Aerospace Corporation, Dr. John Gregory of UAH, and Wayne Slemp of LaRC for accommodation and coordination; Dr. Palmer Peters of MSFC for interpretation of silver film data; Dr. Ilmars Dalins, James Coston, Wendell DeWeese, and Dave Nicolas of MSFC for metallurgical analyses; Bill Kennedy and Bobby Cothren for optical property and mass loss determinations; Jack Smith for engineering drawings; Ed White for design and fabrication; Max Sharpe for sample preparation; Dr. Carl Lowell and Carl Stearns of LeRC, Drs. Kasra Daneshvar, Dave Worley and Bruce Tatarchuk of Auburn University and Mohan Misra of MMC for individual evaluations. The typing of Ms. Jewell Cargile is especially appreciated.

References

1. Whitaker, A. F., "LEO Atomic Oxygen Effects on Spacecraft Materials," presented at AIAA Conference on Shuttle Environments and Operations, Oct. 1983.

2. Peters, P. N., Gregory, J. C., and Whitaker, A. F., "Quick Look Report on Silver Interconnect Samples 1-75-7A and 1-150-7A Flown on STS-5." unpublished.

3. Misra, Mohan, "Interaction of Atomic Oxygen and Silver Interconnects for STS-8 Flight Experiment" prepared under NAS8-30300.

5.0 EFFECTS OF STS-8 ATOMIC OXYGEN EXPOSURE ON COMPOSITES, POLYMERIC FILMS, AND COATINGS*

by

W. S. Slemp, B. Santos-Mason, G. F. Sykes, Jr., and W. G. Witte, Jr.

NASA Langley Research Center
Mail Stop 183
Hampton, VA 23665

Abstract

A series of candidate spacecraft materials including graphite reinforced composites, polymeric films, and thermal control coatings was evaluated in a Space Shuttle flight experiment to determine their durability in the low Earth orbit, atomic oxygen environment. Following the exposure flight, the response to atomic oxygen was determined by computing reaction efficiencies, and characterizing surface and optical property changes. The results indicate that thin, polymeric-matrix (graphite/epoxy) composites and polymeric films exhibit considerable surface erosion when exposed to the atomic oxygen environment. However, composites protected by experimental thin-film metallic coatings were not eroded. The optical properties of thermal control coatings exhibited only minor changes following space exposure. A novel polysiloxane-polyimide block copolymer was identified with a reaction efficiency about an order of magnitude less than that of the currently used polyimide thermal blanket material.

5.1 Introduction

After early Space Shuttle flights STS-1 through STS-3, substantial surface erosion of the polyimide film used as a component of thermal control blankets was detected. Property changes in thermal control coatings were also observed[1]. Dedicated experiments on Shuttle flights STS-4 and STS-5 confirmed the phenomena and provided some quantitative mass loss data on a variety of films and coatings[2]. The erosion and coating degradation have been attributed to reaction with atomic oxygen, the predominant species[3] in the low-Earth orbit (LEO) Shuttle environment. Due to the strong oxidizing potential of atomic oxygen and the impact energy (approximately 5 eV) provided by the orbital velocity of the Shuttle, it has been proposed that oxidation is the primary effect on organic materials[2]. This paper reports results from a recent Shuttle mission (STS-8) used to obtain quantitative interaction data on some widely used spacecraft materials and to evaluate several experimental polymers and coatings which might be more stable than many current materials used in the LEO environment. The materials evaluated included state-of-the-art graphite/epoxy composites, experimental metal-matrix composites, sputter deposited metal and sputter deposited metal-oxide thermal control coatings, and a series of polymeric films.

5.2 Experiment Description

The materials were mounted in the payload bay of the Shuttle and exposed to the LEO environment at an altitude of 225 km for 41 75 hours. During the exposure period, the Shuttle payload bay was open and faced the direction of flight. Most materials were mounted in the bay so that the surface to be analyzed was perpendicular to the flight velocity vector and thus received a maximum direct atomic oxygen exposure flux. This exposure provided a fluence of 3.5×10^{20} oxygen atoms/cm^2 perpendicular to the surface of the samples.

The specimen temperature during exposure was uncontrolled for all materials except for two small groups of polymer films. These latter films were mounted on two separate exposure plates, one held at 120° C and the other held at 65° C. The temperature of the remaining samples was not

*AIAA Paper 85-0415 Presented at the 23rd Aerospace Sciences Meeting, January 14-17, 1985.

determined during the exposure. However, estimates[4] based upon the optical properties (absorptance and emittance) of the relatively massive anodized aluminum sample holder, indicate that the temperature may have reached a maximum of about 60° C. This estimate assumes that: (1) the specimen holder was directly exposed to the Sun with no back surface heat loss and (2) the thin disc samples achieved the sample holder temperature during the exposure. For this paper, these exposure conditions are referred to as "LEO ambient conditions."

5.3 Materials

5.3.1 Composites

Both polymer- and metal-matrix composites were selected for study because of their potential for future use as high stiffness, low thermal expansion structural materials on spacecraft. For the polymer-matrix composites, two 177° C cured epoxy systems were evaluated as described in Table I. Both composite systems used Union Carbide Corporation T-300* graphite fibers. The composite panels for each graphite/epoxy system were made from prepreg tape purchased from the sources indicated in Table I. The tape was laminated into either 2-ply [± 45°] panels or 4-ply [± 45°]s panels and processed according to the manufacturer's recommended 177°C cure cycle. The composite of both epoxy systems has been extensively characterized[5].

Following processing, the polymer matrix composite panels were machined into either disc samples or strip coupons, as noted in Table I. The strip samples were used for tensile tests and the discs for mass loss and scanning electron microscopy (SEM) studies. The nine tensile specimens were mounted to the Shuttle exposure tray using an aluminum plate, as shown in Figure 1. The specimens were mounted on the plate with screws through fiberglass end tabs bonded to each specimen. The top five specimens were directly exposed to atomic oxygen impingement, but the bottom four received only indirect exposure. Both specimen surfaces (top and bottom) were accessible to atomic oxygen impingement because of the gap created by the tab thickness. Some shadowing from direct atomic oxygen impingement occurred on the top mounted specimens because of their position underneath tubes from another experiment, as shown in Figure 2.

The disc specimens were mounted in the aluminum trays shown in Figure 3. The composites were held in place by spring loading the back surface against an aluminum cover plate. The cover plate allowed for a 2.1 cm diameter specimen exposure area. Each disc specimen was exposed at LEO ambient conditions.

Two types of metal-matrix composites, graphite-magnesium (Gr/Mg) and graphite-aluminum (Gr/Al), described in Table I, were exposed in the flight experiment. The specimens were cut into discs from single-ply panels and exposed at LEO ambient conditions. The Gr/Mg contained precursor wire of P100 graphite fiber infiltrated with AZ91C Mg and two surface foils of AZ61A Mg. The Gr/Al sample was also a 1-ply thick material containing P100 graphite fibers infiltrated with 6061 Al and two surface foils of 6061 Al.

5.3.2 Coatings

Ten different coatings were evaluated in this flight experiment, and these are summarized in Table II. White and black paint coatings with both organic and inorganic binders, several metal and metal-oxide coatings, and a metallized transparent polymeric film coating were evaluated. The latter coating was included because of its use in second surface mirror applications. The table provides a detailed description of each coating and, where applicable, the manufacturer or source of each coating. The chromic acid anodized and sputter deposited coatings were experimental materials produced using standard anodizing and vapor deposition techniques. Table III summarizes the preflight optical properties of all coatings, and this data will be discussed in the results section of this paper.

5.3.3 Polymer Films

The polyimide film, Kapton (DuPont Corp.), is used in the Shuttle payload bay and on satellites as a component of thermal control blankets because of its high temperature and UV stability and its toughness. However, because of significant erosion in the LEO atomic oxygen environment[2], a modification or suitable substitute may be required for future long

*Identification of commerical products in this paper is provided to adequately describe the materials and does not constitute official endorsement, expressed or implied, of such products or manufactuers by NASA.

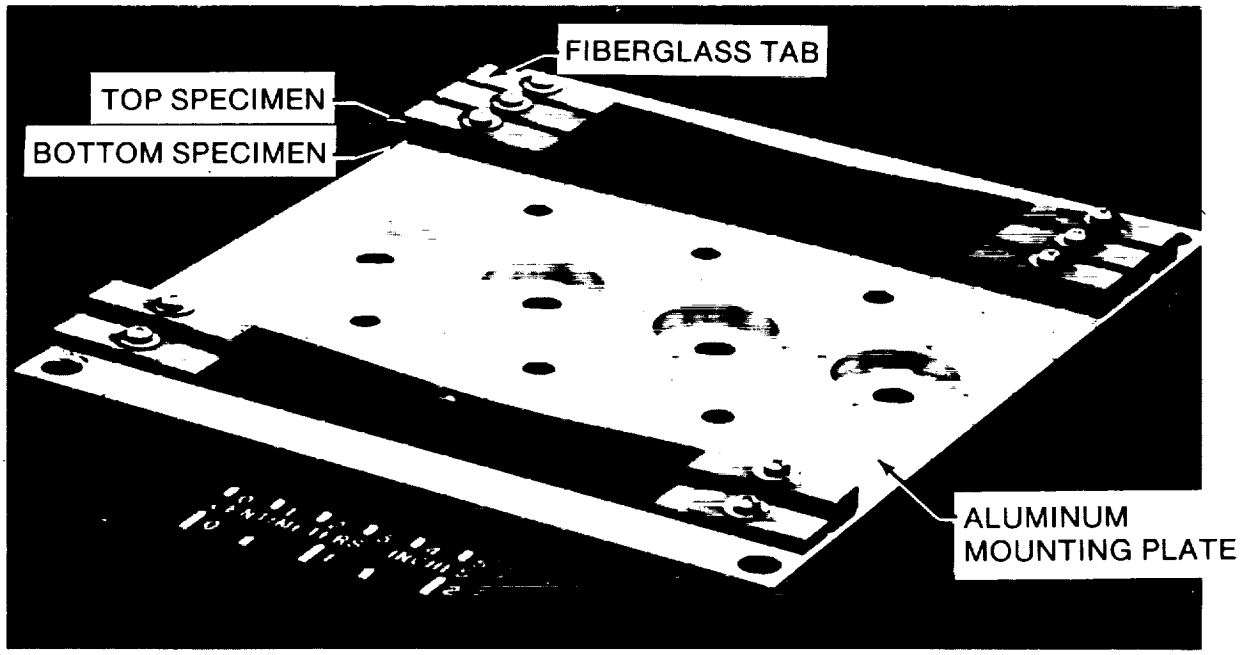

Figure 1.- Composite tensile specimens mounted on flight experiment base plate.

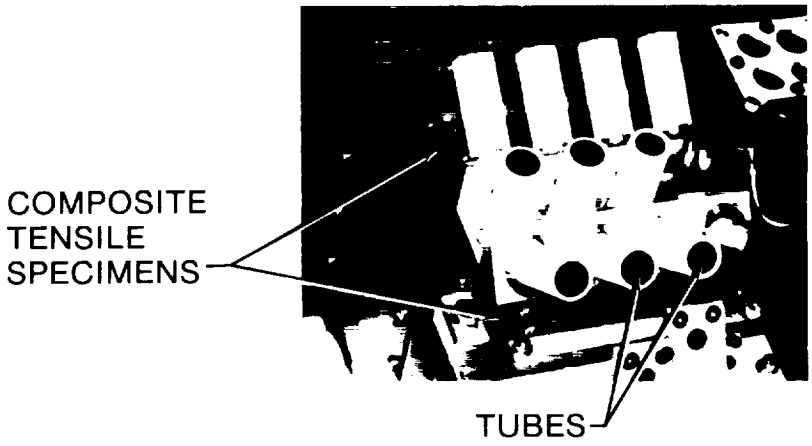

Figure 2.- Position of composite test specimens under environment sensor tubes.

term missions. Accordingly, a series of polymeric films with varying chemical structure were evaluated on the STS-8 Shuttle flight to provide guidelines that could be used for development of atomic oxygen stable polymer films.

The chemical structures of the 14 different polymer films evaluated in the flight experiment are given in Figure 4. As indicated, the films included PMDA based polyimides, BTDA based polyimides, BTDA based polyimide/polysiloxane copolymers, a polybenzimidazole, a pyrrone, and a polyester. The large group of polyimide films was exposed because the chemical and physical properties of these materials are similar to Kapton, and thus the series could provide clues to the effect of polyimide chemical structure on atomic oxygen stability. The polysiloxane/polyimide copolymers[6] were included because early Shuttle flight exposure data[2] indicated that polysiloxanes were not affected by atomic oxygen. The remainder of the polymer films were evaluated to provide information on a broad spectrum of chemical structures.

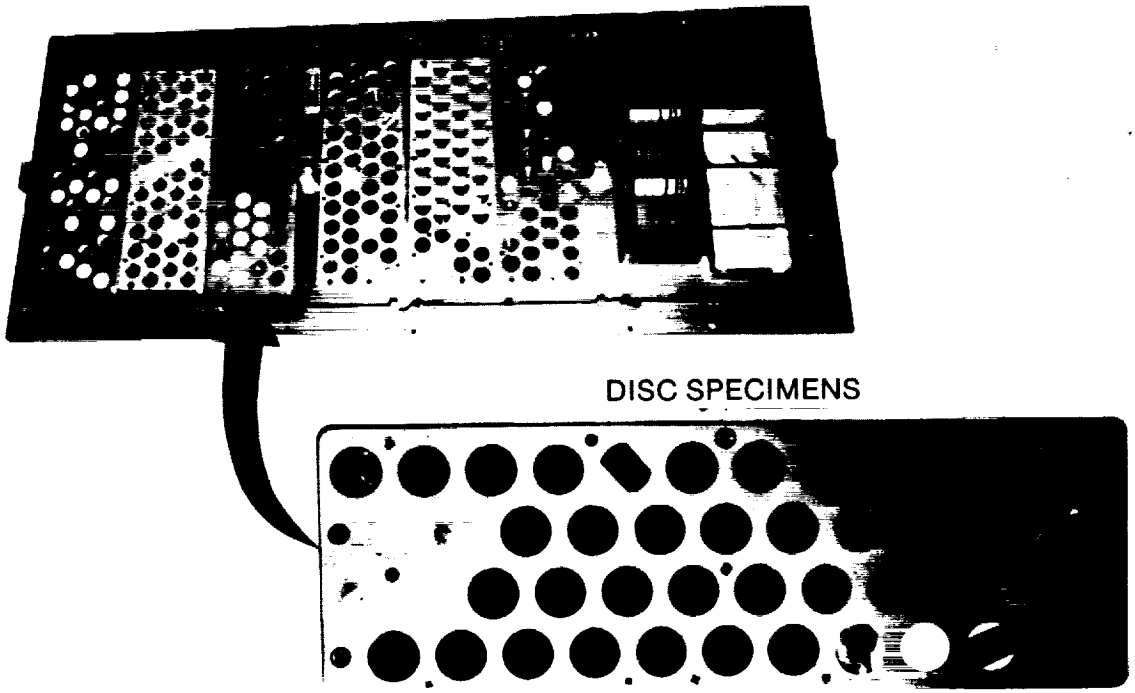

Figure 3.- Disc specimen mounting tray.

TABLE I.- SUMMARY OF POLYMER-MATRIX AND METAL-MATRIX COMPOSITES.

Material designation	Material	Source	Thickness	Fiber orientation	Exposure configuration
POLYMER MATRIX COMPOSITES					
T300/934	Graphite/epoxy	Fiberite Corp.	0.055 cm (4 ply)	[±45°]s	Strip-16.5 cm x 0.95 cm
T300/934	Graphite/epoxy	Fiberite Corp.	0.030 cm (2 ply)	[±45°]	Disc-2.5 cm dia.
T300/934	Graphite/epoxy	Fiberite Corp.	0.018 cm (2 ply)	[±45°]	Disc-2.5 cm dia.
T300/5208	Graphite/epoxy	Narmco Mat'ls.	0.030 cm (2 ply)	[±45°]	Disc-2.5 cm dia.
METAL MATRIX COMPOSITES					
P100/AZ91C	Graphite/magnesium	DWA Inc.	0.063 cm (1 ply)	[0°]	Disc-2.5 cm dia.
P100/AZ91C	Graphite/magnesium	DWA Inc.	0.063 cm (1 ply)	[0°]	Disc-1.0 cm dia.
P100/6061	Graphite/aluminum	DWA Inc.	0.063 cm (1 ply)	[0°]	Disc-1.0 cm dia.

TABLE II.- SUMMARY OF COATINGS INCLUDED IN STS-8 EXPOSURE EXPERIMENT

WHITE PAINT COATINGS

Coating designation	Source	Binder	Pigment	Substrate	Coating thickness
A276	Houghson Chem. Co.	Polyurethane	Titanium dioxide	Aluminum	0.02 cm
S13GLO	IIT Res. Inst.	Polydimethylsiloxane	Zinc oxide	Aluminum	0.02 cm
YB71	IIT Res. Inst.	Potassium silicate	Zinc orthotitinate	Aluminum	0.02 cm

BLACK PAINT COATING

Coating designation	Source	Binder	Pigment	Substrate	Coating thickness
Z306	Houghson Chem. Co.	Polyurethane	Carbon	Aluminum	0.02 cm

SECOND SURFACE MIRROR COATING

Coating designation	Source	Binder	Reflective coating
Silvered FEP Teflon	Sheldahl Inc.	0.013 FEP Teflon	2.000A silver & 200A Inconel

CHROMIC ACID ANODIZED COATINGS

Designation	Substrate	Coating	Surface
A-AL (LE)	6061-T4 AL	Thin layer AL_2O_3	Low emittance
A- AL (HE)	6061-T4 AL	Thick layer AL_2O_3	High emittance

SPUTTER DEPOSITED COATINGS

Designation	Coating	Substrate
Opaque nickel	1600A of 0.999 pure nickel	0.025 cm thick T300/5208 composite
Ni/SiO_2	600A SiO_2 over 1600A nickel	0.025 cm thick T300/5208 composite
AL/AL_2O_3	800A AL_2O_3 over 1800A of 0.9995 pure aluminum	0.025 cm thick T300/5208 composite

TABLE III.- OPTICAL PROPERTY CHANGES OF COATINGS EXPOSED TO THE LEO ENVIRONMENT

Coating	Preflight		Postflight	
	Absorptance	Emittance	Absorptance	Emittance
A276	0.255	0.89	0.278	0.90
S13GLO	0.193	0.90	0.188	0.90
YB-71	0.177	0.90	0.181	0.90
Z306	0.961	0.91	0.983	0.91
Ag/FEP	0.098	0.85	0.104	0.85
A-AL(HE)	0.410	0.68	0.405	0.68
A-AL(LE)	0.312	0.24	0.306	0.24
Ni	0.516	0.45	0.521	0.45
Ni/SiO_2	0.496	0.27	0.492	0.27
AL/AL_2O_3	0.291	0.78	0.285	0.78

The polymer films were mounted on two separate trays in the Shuttle payload bay. The disc specimen tray, shown in Figure 3, provided exposure without temperature control and, as noted previously, the temperature during exposure is unknown. These disc samples had an exposed surface diameter of 2.1 cm.

The film strip tray provided atomic oxygen exposure at controlled temperatures. Figure 5 shows the two temperature controlled base plates and mounted polymeric films. Each base plate was maintained at a different temperature. As noted earlier, one plate was held at 120° C and the other at 65° C. These polymeric film samples were each 5 cm square, and the individual strips were attached end-to-end with an acrylic tape. The long strips (several 5 cm square specimens taped end-to-end) were held against the heated base plates by a spring tensioning device attached to the ends of the film strips. All polymeric films were .002 to .005 cm in thickness.

5.4. Experimental Techniques

5.4.1 Tensile Properties

Polymer matrix composite tensile specimens were tested to failure in an Instron Universal Testing Machine at a strain rate of 0.013 cm/cm per minute. Each specimen was instrumented with two MTS Model 632.11B-20 extensiometers attached back-to-back on the middle 2.5 cm portion of the specimen to measure longitudinal tensile strain. Measurements from these two extensiometers were averaged. An Instron strain sensor No. 2640-003 was attached above the longitudinal sensors to measure transverse strains.

5.4.2 Infrared Analysis

FTIR spectra of polymeric films and polymeric-matrix composites were determined on a Nicolet 3600A FTIR system consisting of an 1180E data system, MX-1 optical bench, and a deuterated triglycine sulfate (DTG-5) detector. Composite spectra were obtained using a Harrick diffuse reflectance attachment, and film spectra were obtained using attenuated total reflectance (ATR) techniques. A more complete description of the procedures used for diffuse FTIR measurements is contained in reference 7.

5.4.3 Reaction Efficiency

The reaction efficiency in the atomic oxygen environment was calculated for the polymer films and composites and used to compare the relative response of each material. The efficiency was determined by dividing the specimen mass loss volume by the product of the exposed surface are and atomic oxygen fluence. The units of measurement are cm^3/oxygen atom.

5.4.4 Optical Properties

The solar absorptance was measured using a Beckman DK-1A spectrophotometer with a Gier-Dunkle Instruments integrating sphere. Reflectance was measured from 250 nm to 2500 nm, covering 95 percent of the solar spectrum. These data were

PMDA BASED POLYIMIDES

PMDA - pp' - ODA

PMDA - pp' DABP

PMDA - pp' - MDA

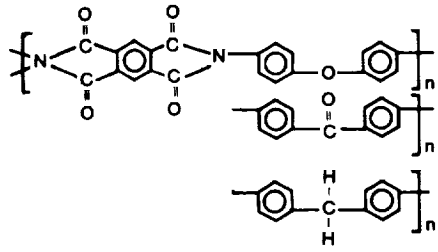

BTDA BASED POLYIMIDES

BTDA - mm' - $DDSO_2$

BTDA - pp' - ODA

BTDA - BENZIDENE

BTDA - DAF

BTDA - mm' - MDA

BTDA - pp' - DABP

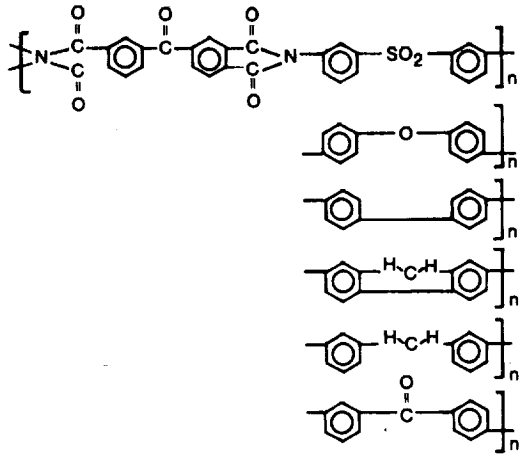

BTDA BASED
SILOXANE - IMIDE COPOLYMERS (PSX-PI)

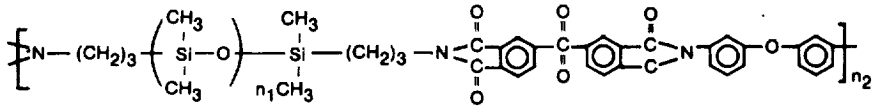

BJPSXPI-9 (25% wt. % SILOXANE)
BJPSXPI-11 (7% wt % SILOXANE)

PYRONE

PMDA-DAB

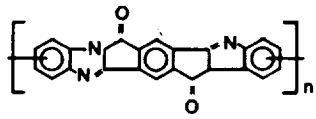

POLYBENZIMIDAZOLE

I-DAB (PBI)

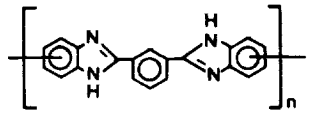

POLYESTER

PEN-2, 6

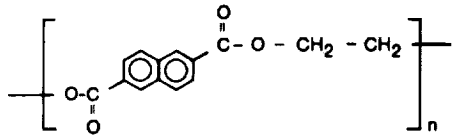

Figure 4.- Summary of polymeric films exposed on the STS-8 exposure flight.

recorded at 15 nm intervals throughout this spectral region. A computer program was used to calculate the solar absorptance from these data. A Gier Dunkle Instruments Model DB-100 emissometer was used for direct reading of total normal emittance for all coatings.

5.4.5 Surface Characteristics

A Cambridge Model 150 Scanning Electron Microscope (SEM) was used to examine the surfaces of control and flight exposed specimens. Prior to SEM examination, the surfaces of all dielectric specimens were coated with a vapor deposited gold-palladium film.

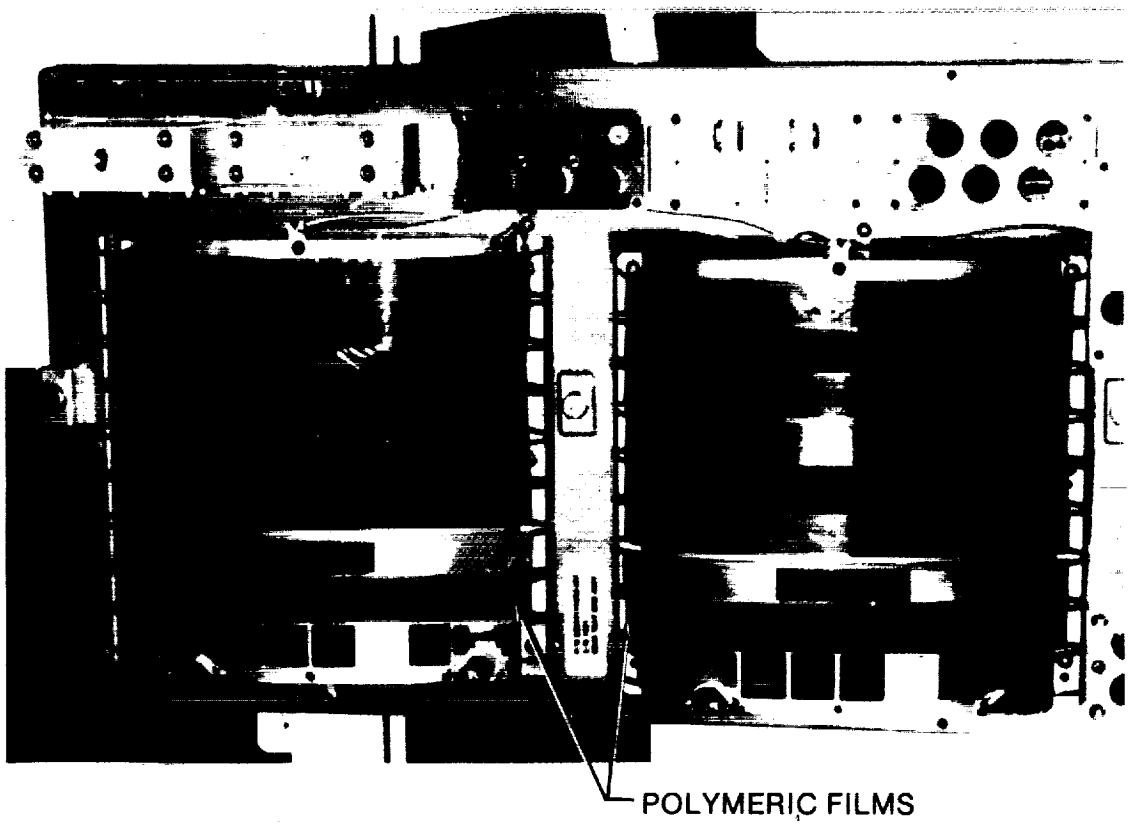

Figure 5.- Mounting of the polymeric film strips on the temperature controlled base plates.

5.5 Results

5.5.1 Composites

5.5.1.1 Polymer-matrix Composites. The surfaces of the polymeric-matrix composites were eroded as a result of exposure to the LEO environment. The erosion could easily be seen on specimens exposed to direct impingement of atomic oxygen as a much darker colored area compared to unexposed specimen surfaces. Specimen surfaces exposed indirectly to atomic oxygen were also darker than unexposed surfaces but to a lesser degree than those that received direct exposure. Figure 6 shows an example of the color contrast resulting from direct and indirect exposure to atomic oxygen. Shown are the fractured tensile test specimens that were partly shadowed during the flight exposure. As described previously, these specimens were located beneath another experiment and only portions of each strip received the direct impingement of atomic oxygen. These areas are identified as the darker bands across each specimen.

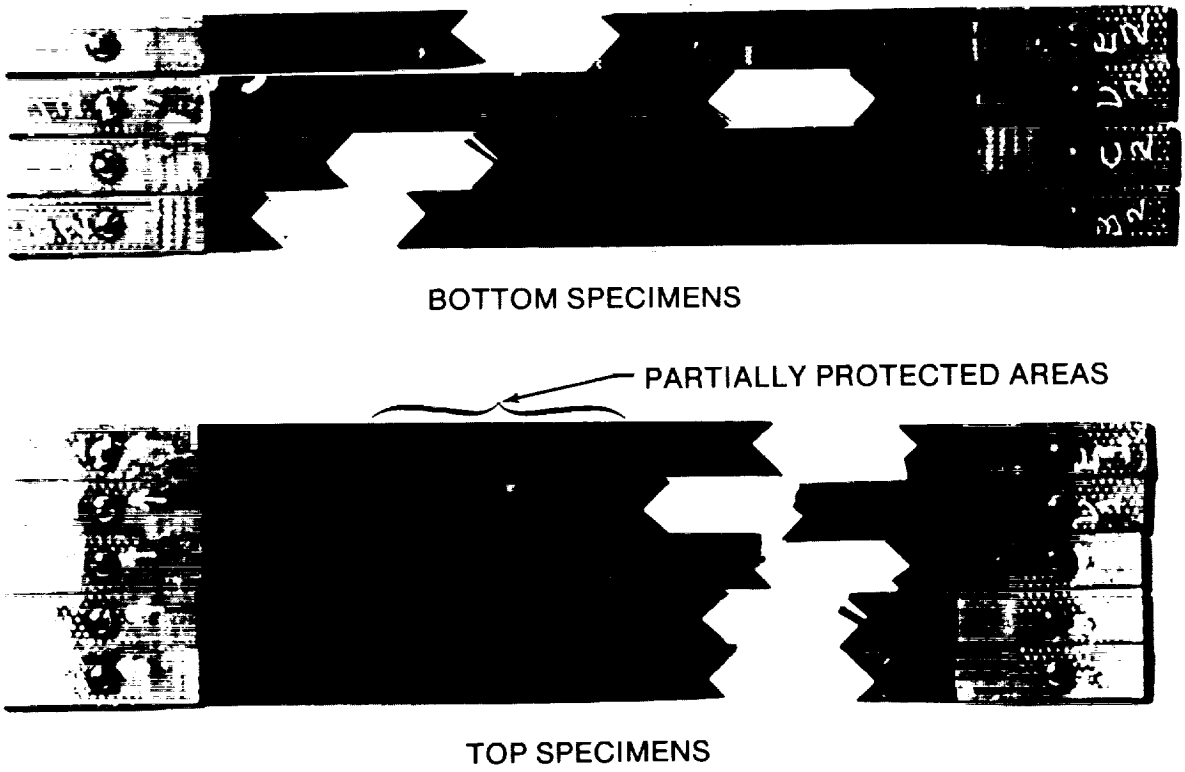

Figure 6.- Fractured composite tensile test specimens.

Figure 7 shows SEM photographs of the control surface and the eroded surface (in the direct impingement area) from the 934/T300 graphite epoxy specimen. The surface characteristics are very similar to surfaces reported earlier[8] for atomic oxygen eroded polymer films and shows the "rug-like' appearance. The thickness loss of this composite specimen was about 0.0009 cm. Both polymer-matrix composites exhibited this type of surface erosion following exposure. Using the mission fluence of 3.5 $\times$ 10^{20} oxygen atoms/cm^2 and the mass loss normalized for the exposed area of the specimens, the reaction efficiency as described previously was calculated. The average reaction efficiency for the T300/5208 composite was 2.9 $\times$ 10^{-24} cm^3/atom and the average for the T300/934 composites was 2.6 $\times$ 10^{-24} cm^3/atom. Both the 0.030 cm and the 0.017 cm thick T300/934 composites had the same reaction efficiencies.

Diffuse Reflectance Fourier transform infrared spectroscopy (FTIR) was used to evaluate the chemical change in these composites. Figure 8 presents the spectra of the exposed front and back sides of the T300/5208 composite and, for comparison, the spectrum of the control specimen. These spectra show that the changes occurring in this composite system on exposure to the atomic oxygen environment are related to oxidation of the epoxy matrix. Oxidation is indicated by the presence of the carbonyl absorption band near 1700 cm^{-1} in the spectra of the exposed specimens. Several other absorption bands are identified in the figure and these are characteristics of 177° C cured epoxy systems[9]. The appearance of the carbonyl bands in the spectra is similar to the results obtained from long-term air aging studies of epoxy composites[7]. The oxidation and accompanying mass loss of these materials during the flight exposure suggest that a suitable atomic oxygen resistant coating would be required for long-term LEO application of these materials.

Figure 9 presents results from tensile tests of the nine exposed strip specimens. This figure shows the average of the stress-strain curves for the flight exposed specimens and the control specimens. The standard deviations for the curves are indicated in two places on each curve. The stress strain curves exhibit the non-linear behavior found in tensile tests of $\pm$ 45° layup composite specimens. As shown, there was a 5 percent lower ultimate stress in the STS-8

exposed specimens, with no effect on the strain-to-failure or apparent modulus of the material. These data would suggest that atomic oxygen exposure affected only the outer ply fibers and/or matrix.

All of the composite specimens that received direct exposure of atomic oxygen and exhibited the banded surface appearance fractured in this banded area near the end of the specimen. The fractured surfaces of the specimens are shown in Figure 6. Because the surfaces of the specimens were eroded most severely in the banded area, fracture in this area was expected.

5.1.1.2 Metal-Matrix Composites. The Gr/Al sample had no weight change, but the Gr/Mg sample had a weight increase of 0.40 percent. When viewed in the SEM, the material protected by the retaining ring on each sample was a different shade than the exposed portion of the specimen. The discoloration was only visible in the SEM and could not be seen in a visual observation. No differences in surface chemistry or morphologies between the protected and unprotected areas were detected using SEM, EDAX, or "windowless" EDAX. The protected edge area of the Gr/Mg had a lower secondary electron yield than the center, atomic oxygen exposed, portion of the sample, suggesting that a thin oxide layer was formed in the exposed area. The presence of a thin oxide could also account for the slight weight increase noted for the graphite-magnesium composite.

5.5.2 Coatings

Table III provides a summary of the preflight and postflight optical properties of the coatings exposed in the STS-8 experiment. Overall, only minor effects on optical properties were observed, with the polyurethane based A276 white paint and Z306 black paint coatings showing the greatest change. For both of these coatings, the solar absorptance increased by 0.02, but the emittance was unchanged following LEO exposure.

Visually, the polyurethane binder coatings also exhibited the most notable changes following atomic oxygen exposure. The A276 surface changed from glossy to diffuse, and the Z306 became more diffuse in appearance. Figure 10 shows typical SEM photographs of the A276 white paint coating before and after exposure. The photographs are also typical of the exposed and unexposed Z306 coating. The SEM photos show that the polyurethane coatings had a more porous surface after exposure, thus improving the diffuse reflectance characteristics of both paints. The atomic oxygen appears to react with the polyurethane binder, leaving pigment particules on the surface. The particles were not disturbed during

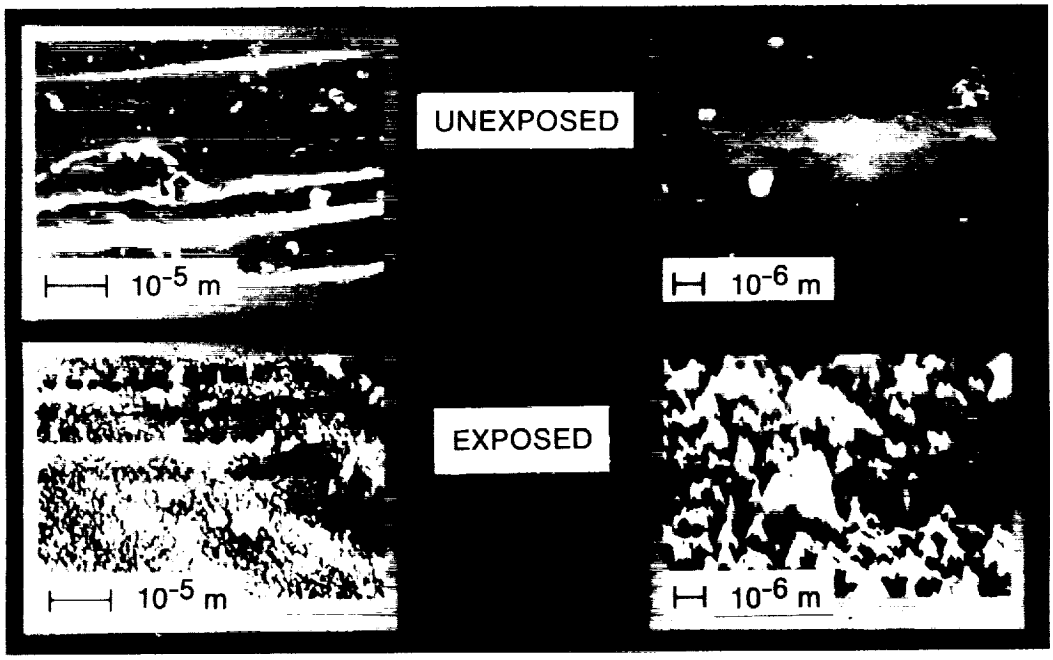

Figure 7.- SEM photographs of T-300/934 composite specimens before and after exposure.

normal handling of the specimens but were easily removed by gently wiping with a natural bristle brush.

The polydimethysiloxane based S13GLO and the potassium silicate (inorganic) based YB-71 white paints were very stable to the atomic oxygen exposure. As already noted, no change in solar absorptance and total normal emittance could be detected for these coatings. However, their post flight appearance was slightly more diffuse than the control specimens.

The metallized transparent second surface mirror coating also exhibited no change in optical properties as a result of STS-8 exposure. This indicates that fully fluorinated polymers are probably more stable to atomic oxygen than most polymeric systems and that the silvered-FEP Teflon coating could be used in LEO applications.

Two anodized aluminum coatings were evaluated in the exposure experiment, and both materials appear to be quite stable in the atomic oxygen environment. No change could be detected in optical properties, and both high emittance and low emittance coatings showed no visual change in post flight examination.

The three sputter-deposited coatings applied on graphite-epoxy composite substrates were also generally unaffected by the atomic oxygen environment. The opaque nickel coating appeared slightly rougher after exposure than the preflight coating, possibly indicating the initiation of a nickel oxide surface. However, SEM and EDAX characterization did not detect the oxide presence. The atomic oxygen stability demonstrated by these sputter deposited coatings suggests that this technique could be used to protect polymer matrix composites from erosion in long-term LEO applications.

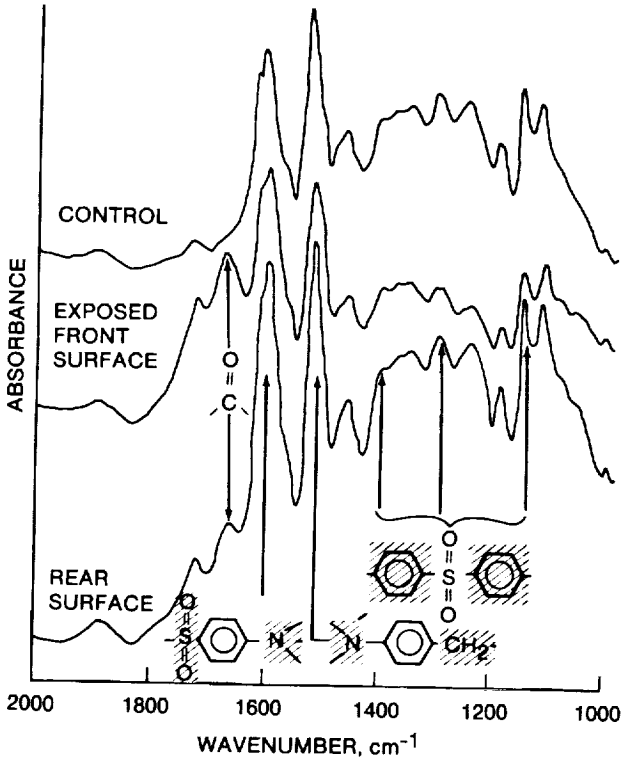

Figure 8.- DR-FTIR spectra of 2-ply T300/5208 composite exposed to space environment.

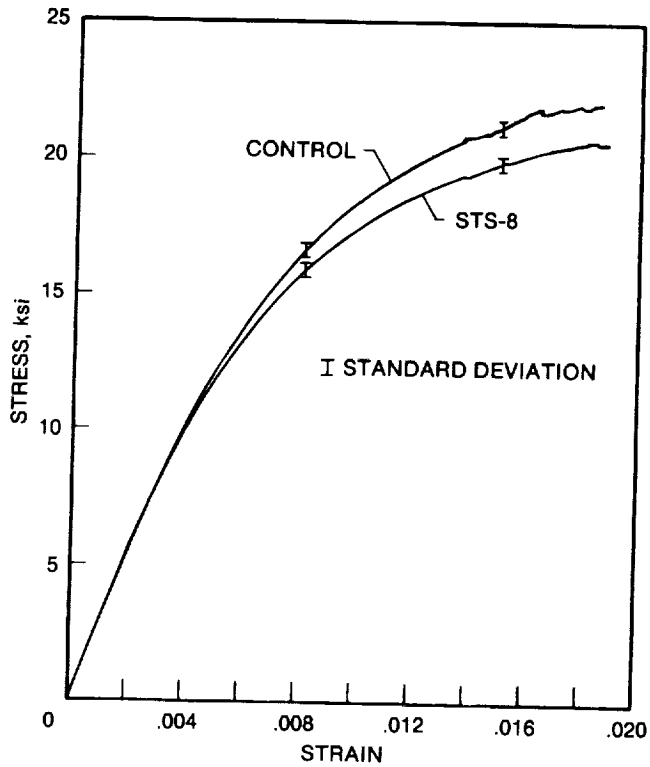

Figure 9.- Comparison of the averaged stress-strain data for the control and exposed T-300/934 graphite/epoxy composites.

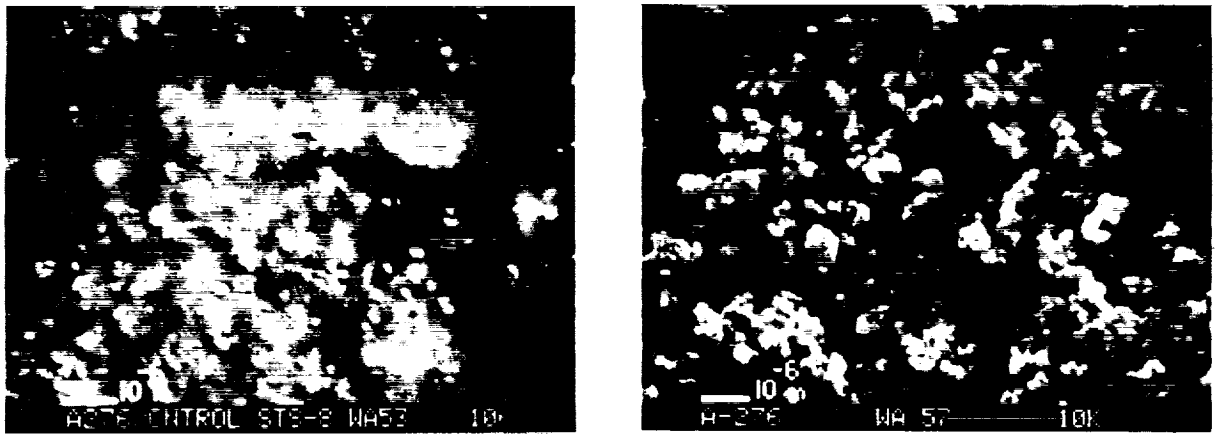

UNEXPOSED EXPOSED

Figure 10.- SEM photographs of the polyurethane base A-276 white paint before and after LEO exposure.

5.5.3 Polymer Films

All of the polymer films were affected to some degree by exposure to atomic oxygen. Visually, the exposed surface are on most films was changed from the normally smooth glossy finish to a dull, diffuse appearance. Only the two siloxane-imide block copolymers were visually unchanged after exposure.

SEM examinations of each polymer film generally showed a smooth, uniform surface before LEO exposure. However, following exposure, the surfaces of most polymers were extremely uneven and exhibited a "rug-like" appearance. Figure 11 shows the typical change in surface characteristics observed for most films. Shown are the before and after exposure SEM photographs of the PMDA-pp'-ODA polyimide film. The chemical structure of this material is identical to that of Kapton. The protrusions making up the "rug" surface point toward the velocity vector of the Shuttle flight and thus indicate the direction of atomic oxygen impingement. The atomic oxygen apparently oxidized and eroded away the material between the protrusions. The protrusion height is approximately 2-3 x 10^{-6} m. The SEM photo-graphs shown in Figure 11 are typical of all film materials evaluated, except for the two siloxane-imide copolymers.

Figure 12 shows the SEM photographs for one of the siloxane-imide (PSX-PI) copolymers. The SEM's of the unexposed (control) and atomic oxygen exposed materials are provided. The SEM's are typical of both copolymers and show that, following atomic oxygen exposure, the surface remains generally smooth. Some oxidation and erosion did occur, however, as shown by the relatively small cavities spread randomly across the surface. It has been shown[6] that when films of these copolymers are cast, the siloxane segments migrate to the surface to reach the lowest free energy state. This produces a siloxane-rich surface that apparently protects the polyimide substrate from atomic oxygen erosion. The two siloxane-imide copolymers evaluated in this study, BJPSXPI-9 and BJPSXPI-11, contained about 25 percent and 7 percent by weight of siloxane, respectively.

Table IV presents a summary of the atomic oxygen reaction efficiency observed for each polymer film. As indicated, all polymers showed some erosion and thus had a measurable reaction efficiency in the LEO environment. In each exposure temperature group (120° C, 65° C and LEO ambient temperature) there is a range of reaction efficiencies, indicating that polymer chemical structure has an effect upon atomic oxygen response. This is particularly evident in the large group of materials exposed at LEO ambient conditions (temperature not determined and uncontrolled) where the reaction efficiency varied by about an order-of-magnitude with film chemical structure. Overall, the polysiloxane-polyimide copolymers had the lowest reaction efficiency of all materials, and the PMDA-pp'-ODA (Kapton type polymer) had the highest reaction efficiency.

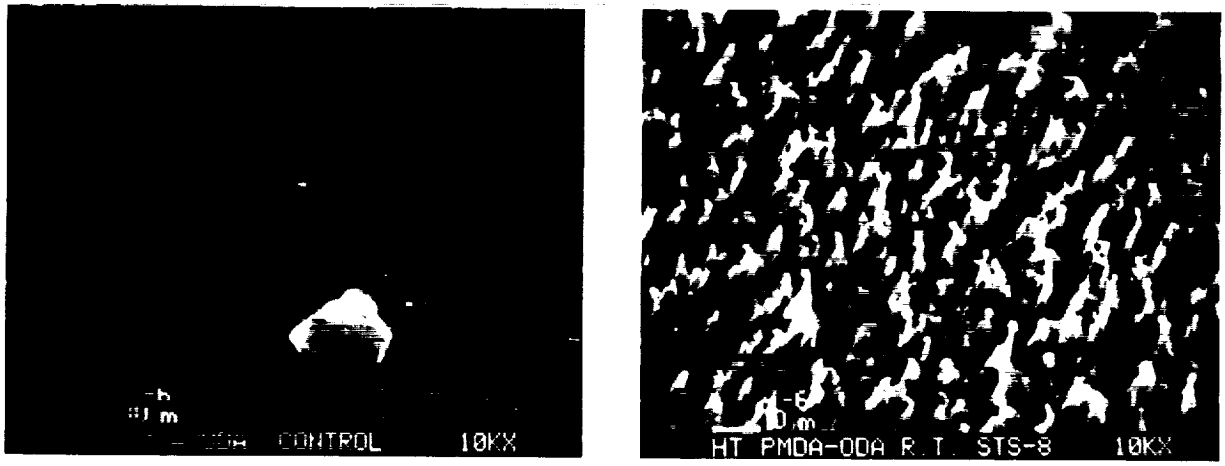

UNEXPOSED EXPOSED

Figure 11.- SEM photographs of the PMDA-pp'-ODA polyimide film before and after atomic oxygen exposure.

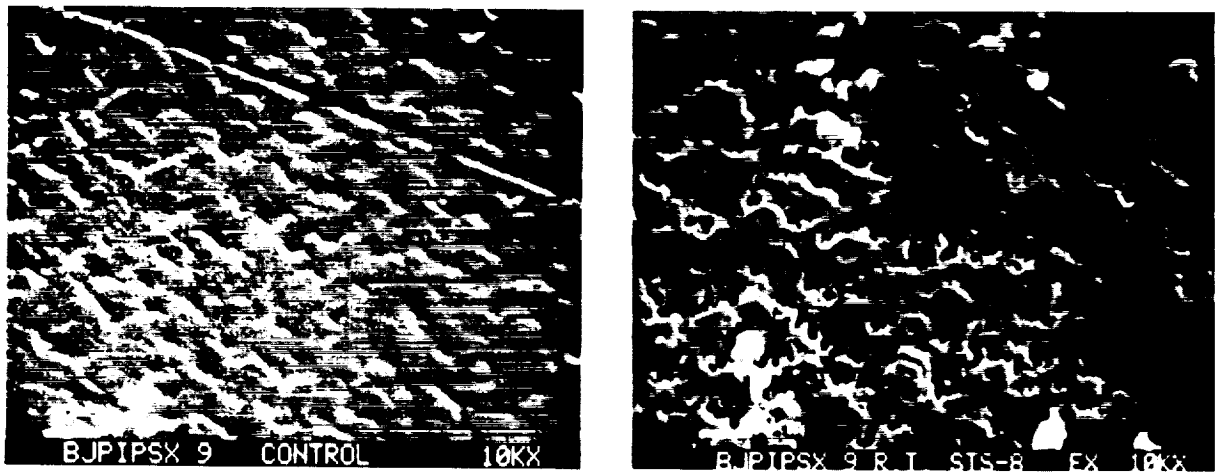

UNEXPOSED EXPOSED

Figure 12.- SEM photographs of the siloxane-imide copolymer film before and after atomic oxygen exposure.

The effect of exposure temperature on atomic oxygen response could not be determined because different groups of materials were exposed at each condition. With the exception of the two siloxane-imide copolymers, the reaction efficiency of all polyimides fell in the range 2.5 x 10^{-24} to 4.66 x 10^{-24} cm3/atom, indicating that temperature did not have a significant effect on atomic oxygen response.

Attenuated total reflectance infrared spectra were obtained on all films, but no significant chemical changes could be identified. This observation may indicate that the atomic oxygen interaction mechanism erodes the polymer surface by converting the material to gaseous products that are easily swept away.

5.6 Concluding Remarks

A series of candidate spacecraft materials including polymer- and metal-matrix composites, thermal control coatings and polymeric films were exposed to the atomic oxygen rich, low Earth orbit environment on Shuttle flight STS-8. Characterization of the materials following the flight shows that graphite-epoxy composites are eroded by atomic oxygen and will require protection for long-term use in the LEO space environment. Several metallic coatings were identified that could be used for protection of the polymer-matrix composites. The optical properties of a series of coatings including organic binder, metal, and metal oxide and a second surface mirror coating exhibited only minor changes

following exposure to the atomic oxygen. All of the polymeric films included in the exposure flight exhibited some erosion by atomic oxygen, and film chemical structure influenced the reaction efficiency. A novel polyimide-siloxane copolymer was identified that had about an order-of-magnitude lower reaction efficiency than the currently used polyimide thermal blanket material.

5.7 Acknowledgments

The authors wish to acknowledge the following individuals for their contributions to this flight experiment: Dr. S. S. Tompkins and G. A. Dries (Kentron International) for preparation and analysis of metal-matrix composite specimens. Dr. V. L. Bell for providing polymeric-films. Mr. R. M. Stewart for assistance in experiment assembly and optical property measurements on coatings. Dr. T. R. Gull, Goddard Space Flight Center, for accommodating the tensile composite specimens in the GSFC flight experiment.

TABLE IV.- POLYIMIDE FILM REACTION EFFICIENCIES TO THE STS-8 ATOMIC OXYGEN ENVIRONMENT

Polyimide type	Reaction efficiency, x 10^{-24} cm^3/atom	Exposure temperature, °C
PMDA-pp'-ODA	4.66	120
BTDA-pp'-ODA	3.97	120
PMDA-pp'DABP	3.82	120
PMDA-pp'-MDA	3.17	65
BTDA-BENZIDENE	3.08	65
BTDA-mm'-$DDSO_2$	2.29	65
BTDA-mm'-MDA	3.12	LEO ambient conditions*
BTDA-pp'-DABP	2.91	LEO ambient conditions*
PEN-2.6	2.90	LEO ambient conditions*
BTDA-DAF	2.82	LEO ambient conditions*
PMDA-DAB	2.50	LEO ambient conditions*
I-DAB	1.80	LEO ambient conditions*
BJPIPSX-11	0.56	LEO ambient conditions*
BJPIPSX-9	0.28	LEO ambient conditions*

*Exposure temperature was uncontrolled

5.8 References

1. Leger, L.: Oxygen Atom Reaction with Shuttle Materials at Orbital Altitudes. NASA Technical Memorandum 58246, May 1982.

2. Leger, L. J.: Oxygen Atom Reaction with Shuttle Materials at Orbital Altitudes-Data and Experiment Status. AIAA-83-0073, AIAA 21st Aerospace Sciences Meeting, Jan. 1983.

3. Hedin, A. E.; Reber, C. A.; Newton, G. P.; Spencer, N. W.; Brinton, H. C.; Mazer, H. G.; and Pottes, W. W.: A Global Thermospheric Model Based on Mass Spectrometer and Incoherent Scatter Data MSILS 2 Composition. J. Geophysical Research, Vol. 10, 1977.

4. Van Vliet, R. M: Passive Temperature Control in the Space Environment, MacMillan Company, New York, 1965.

5. May, C. A.: Exploratory Development of Chemical Quality Assurance and Composition of Epoxy Formulations. Air Force Materials Laboratory Report, AFML-TR-76-112, 1976.

6. Johnson, B. C.: High Performance Polyimide Copolymers: Synthesis and Characteristics, Ph.D. Dissertation VPI & SU, Blacksburg, VA, June 1984.

7. Young, P. R.; Stein, B. A.; and Chang, A. C.: Resin Characterization in Cured Graphite Fiber Reinforced Composites Using Diffuse Reflectance-FTIR, SAMPE Vol. 28, pp. 824-837, 1983.

8. Leger, L. J.; Visentine, J. T.; and Kuminecz, J. F.: Low Earth Orbit Atomic Oxygen Effects on Surfaces. AIAA-84-0548, AIAA 2nd Aerospace Sciences Meeting, Jan. 1984.

9. Levy, R. L.: Mechanism of Epoxy Moisture Effects, Air Force Materials Laboratory Report, AFML-TR-77-41, April, 1977.

6.0 EFFECTS ON THERMAL CONTROL PAINTS AT SHUTTLE ALTITUDES*

John J. Park

NASA Goddard Space Flight Center
Greenbelt, Maryland 20770

Abstract

Personnel of the Goddard Space Flight Center provided many thermal control paint samples for testing on the STS-8 flight. Ultraviolet stabilizers and antioxidants were added to commercial white paints to determine whether the additives would improve the stability of the paints. Data from the flight demonstrated that these inhibitors were not effective. Electrically conductive paints were made by adding conductive carbon particles to a silicone mixture and to a polyurethane matrix; the electrical resistance of the silicone increased about two times that of unflown samples, and the resistance of the urethane increased almost three times that of non-flight samples. Samples which showed the best stability and the least mass loss in low Earth orbit were a silicone used to protect Kapton, a white silicone paint having TiO_2 added as pigment, a black electrically conductive silicone paint, a white silicate paint, solder, and tantalum metal.

6.1 Introduction

The STS-8 flight offered the possibility of obtaining much more information on the reactivity of polymers than did the STS-5 flight. The addition of passive sample trays which were provided by Langley Research Center for the STS-8 mission meant that a large number of polymer varieties or modifications to the white Chemglaze A-276 and V-200 paints, along with specially prepared electrically conductive paints, and special silicone mixtures could be tested.

The sample tray was composed of a thin, 12- by 8-in. assembly having forty-six 25-mm-diameter holes. Each hole had a cavity beneath it to contain thin discs which could be either painted or metallic. The top cover of this assembly had holes slightly smaller than the discs so that the enclosed discs could not fall out. A circular spring forced the disc forward to maintain a steady force and prevent motion. The front surface faced out of the bay and was exposed to the atmosphere.

6.2 Sample Selection

Individual paint samples were sprayed onto 1-in-diameter aluminum discs. To retain the discs, the diameter of the exposed opening in the holding frame was 15/16 in. The discs were pushed outward by a flat spring. This technique also provided an unexposed area, which appeared afterward as a shiny "rim" for comparison with the area exposed to space. The rim provides an obvious optical comparison at any magnification.

The suspected reactants found in space which might cause the polymer degradation were the oxygen atom and sunlight. Consequently, antioxidants and ultraviolet (UV) stabilizers were selected as additives to protect polyurethane paint. Small quantities of the UV stabilizers Tinuvin 292 and Tinuvin 900 and the antioxidant Irganox 1010 were obtained from Ciba-Geigy Corporation. A combination of these various additives was added to small amounts of white paints.

The Chemglaze II white A276 (Hughson Chemical Company) has been used on the Space Shuttle because of its good abrasion resistance. The Chemglaze II white V200 is among Hughson's V-series which is claimed to have good abrasion resistance, wear properties, and flexibility. The V200 requires a catalyst, but the A276 is a single-component paint which air dries by reacting with the air moisture. To these paints the Irganox and Tinuvin inhibitors were added, both singly and in combination, up to 5 percent by weight of the individual additive.

* Presented at the 23rd Aerospace Sciences Meeting, January 14-17, 1985.

The RTV-615 silicone (a General Electric product) was used as the base material for certain applications. This silicone resin must be devolatilized before it is used in space to reduce its high outgassing; the devolatilization step involves a vacuum treatment at 140 to 150° C for 24 hours in a vacuum of about 10^{-6} torr. After the vacuum treatment, the silicone is mixed with the usual 10-percent curing agent and cured at room temperature. The result is a low outgassing silicone. By adding the white TiO_2 powder, a white paint was produced; by adding conductive carbon particles, a black conductive carbon paint was produced.

A black conductive urethane paint was also prepared, and an inorganic silicate paint was selected for flight. Tantalum metal and unmelted lead-tin solder were the metallic samples chosen.

6.3 Results

6.3.1 Modified A276 Paint

The standard A276 paint, with no intentional additives, was used for comparison; as mentioned previously, this paint has been used extensively on Space Shuttle surfaces. Its degradation in space had been noted after the first few Space Shuttle flights, specifically after the STS-3 flight.

Three additional modified samples of A276 were flown. Each contained 5 percent of Irganox 1010 antioxidant, but in two of them, a UV stabilizer was added (a different stabilizer in each, and 2.5 percent of each stabilizer). No problems were encountered in preparing these modified samples.

Each sample was measured for optical properties prior to flight. After the flight, these properties were remeasured to enable a direct evaluation of the changes.

The values for the A276 are presented in Table 1. The values for initial and final absorptance and emittance are reported. All of the changes were relatively small and almost uniform. The final emittance for all samples was 0.91, but the standard A276 increased 0.03 while the other samples with additives changed upward by 0.02. The variation in absorptance was more variable, though the value was either positive or negative by 0.01. However, the A276 containing only Irganox as an additive did not show a change in absorptance. Nevertheless, the fact that the emittance for all samples ended at 0.91 and tne changes in absorptance were 0, +0.01, or −0.01 indicates that the paints with additives did not produce a significant improvement over the standard A276 paint. Perhaps a longer flight might show more significant changes.

6.3.2 Modified V200 White Paint

As mentioned previously, the V200 paint is a more flexible paint which requires a catalyst for curing. The standard V200 paint was flown for comparison to those samples containing additives. The same three additives were used as in the A276 samples. The amount of UV stabilizer was either 2.5 or 5.0 percent, and the amounts of antioxidants were also either 2.5 or 5.0 percent. Thus, there was more variation than for the A276 samples.

Following the flight, it was noted that samples 2H, 2N, and 2U were a pink color. This was most evident when the white rim of the specimen was used for comparison. The pinkest specimen was 2N. All three contained the Tinuvin 292 UV stabilizer. Even though the 1R sample in the A276 series also contained the Tinuvin 292, it did not show the pink color after flight. The chief difference between the A276 and the V200 paints is the need to catalyze the V200, which may be the reason for the change in color. See Table 2.

The values for the absorptance and emittance of the modified V200 samples showed much more change than did those values for the A276 paint. The standard V200 paint showed increased absorptance of 0.02 and increased emittance of 0.02. However, those samples with additives showed much larger changes in absorptance. The 2N sample, which contained 2.5 percent of all three additives, changed from 0.24 to 0.34 in absorptance; this 2N sample was also the pinkest in color. The 2U sample, which contained 2.5 percent of Irganox 1010 and 5.0 percent Tinuvin 292, changed from 0.25 to 0.31 in absorptance. The samples which appeared pink remain pink at present, more than 4 years after flight.

The stablest V200 paint was the 2M sample. This sample contained 5.0 percent of both Irganox 1010 and Tinuvin 900. It showed an increase of only 0.03 in emittance and no change in absorptance. This compares well with the standard V200, which had an

Table 1

Sample	Irganox	Tinuvin		Initial		Final	
	1010	292	900	A	E	A	E
1Z	0	0	0	.26	.88	.25	.91
1B	5	0	0	.25	.89	.25	.91
1R	5	2.5	0	.26	.89	.27	.91
1W	5	0	2.5	.26	.89	.25	.91

Table 2

	Percent Additive						
Sample	Irganox	Tinuvin		Initial		Final	
	1010	292	900	A	E	A	E
2Z	0	0	0	.22	.89	.24	.91
2H	5	5	0	.27	.89	.30	.91
2M	5	0	5	.28	.88	.28	.91
2N	2.5	2.5	2.5	.24	.89	.34	.91
2U	2.5	5	0	.25	.88	.31	.90

increase of 0.02 in absorptance. Apparently, the addition of the Tinuvin 900 makes the V200 more stable. However, the short time test for these paints during the STS-8 flight does not provide enough data for confidence in a longer time test.

6.3.3 Silicone Samples.

There are numerous uses of silicone materials on spacecraft. Because of their clarity, silicone materials are used in applications such as solar cell cover adhesives. Because of their thermal stability, they are used in applications which may encounter large temperature changes such as solar cell adhesives. Unfortunately, the high cost of silicones limits their use to very selective applications. However, prior flight data had shown that polymeric materials, notably epoxy and urethane materials, were not resistant to the atomic oxygen atmosphere at low Earth orbits. The fact that data for silicone had not been reported was a deciding factor in selecting silicones and making modifications to them.

6.3.3.1 Kapton Protected by Silicone. The prior information on the degradation of Kapton during Space Shuttle flights suggested a test of silicone as a means of protecting Kapton. Thus, a film of Kapton was affixed to the aluminum disc, and then a film of Dow Corning's 6-1104 single-component clear silicone was brushed over the Kapton. This silicone cures within a week at room temperature by reacting with the atmospheric water.

On the disc the sample could be weighed, which would then permit a measurement of weight loss. The optical properties were also compared to those of nonflight samples, because three identical samples were prepared, but only one was flown. The data were determined after flight, but no preflight measurement was made on the sample which was

flown. Thus, there is a comparison only between two nonflight samples and one flight sample.

The flight results show that silicone can protect Kapton very well. The data are presented in Table 3. The weight loss for the total sample was only 0.19 percent. In fact, the total weight loss may be smaller. There may have been some slight transfer of material to the sample holder because of the contact pressure of the screws and the spring-loaded method of retaining the samples. It was noted that the silicone discs stuck lightly to the holder. The values for the optical measurements show only a decrease of 0.01 in absorptance and an increase of 0.01 in emittance for the Kapton.

Table 3 Kapton Protected by C6-1104 Silicone

Weight loss	0.19 percent	
Optical data	A	E
Control (nonflight)	= 0.46	=0.90
Control (nonflight)	= .46	=.90
Flight	= .45	=.89

6.3.3.2 White Silicone Paint. The silicone paint was prepared by adding TiO_2 pigment to the devolatilized RTV-615 resin. This mixture was briefly ground in a pestle to produce a smooth paint. The curing agent was added to the mixture, and the paint was brushed onto the primed aluminum disc.

The data are presented in Table 4. These data again show the stability of the silicone resin to the oxygen flux. The weight loss is 0.22 percent, a comparable value to the prior data for the silicone/Kapton combination. The paint is also optically stable, showing no change in absorptance and only a 0.01 decrease in emittance. These optical data are much more stable than for the A276 and the V200 white paints mentioned previously.

Table 4 RTV-615 Silicone with TiO_2 Pigment

Weight loss	0.22 percent	
Optical data	A	E
Control (nonflight)	= 0.19	=0.87
Control (nonflight)	= .19	=0.87
Flight	= .19	=0.86

6.3.4 Black Conductive Paint.

Black paints, along with white paints, are used for thermal control. In addition, an electrically conductive polymer is sometimes needed to permit uniform voltage levels or to prevent space-charge buildup. In order to test for the above possible future needs, two black paints were prepared. By adding conductive carbon particles in sufficient quantity to a resin, the electrical conductivity of a polymer film can be adjusted within narrow resistance ranges. The resins chosen were a polyurethane and a silicone.

The first paint, identified as black conductive silicone (BCS), was prepared by mixing 5 g of XC-704 into 10 g of RTV-615 resin. This was brushed onto Kapton which had been affixed to the aluminum disc and then permitted to cure. The other paint, black conductive urethane (BCU), was prepared by adding 4 g of the same XC-704 conductive carbon particles to 10 g of the Chemglaze Z-004, a clear urethane often used as a conformal coating. This is a single-component urethane which cures upon exposure to the atmosphere. This paint was brushed onto the Kapton on the aluminum disc.

Weight loss as well as changes in electrical conductivity for each paint sample were determined for each paint sample. To measure the resistance of these surface films, two electrodes located in a wooden block in the shape of a 1/2- by 1/2-in. square were placed on the black films, and the electrical resistance between the electrodes was measured using a digital resistance meter. It was necessary to weight the electrodes to limit the erratic changes in the readings. To provide a sufficiently constant reading, two 1-lb weights were placed on top of the wooden block holding the electrodes.

6.3.4.1 Black Conductive Silicone. The two conductive paints provided surprising results. First, the weight loss of the BCS was essentially zero. The weight of the flown disc was within 1 μg of the weight before flight. This was so surprising that repeated weighings were made, even though the silicones discussed above had very low weight loss percentages. In no instance was the change in weight with time great enough to calculate at 0.01 percent; normally, the weight change was no more than 0.002 percent. This further verifies the stability of silicones at low Earth orbit.

Resistance measurements were compared to those for the two discs which remained in the laboratory. The electrical resistance of the BCS paint which was flown was 3200 ohms per square, an increase of about 2 times for the average of the two samples which were not flown. The data are presented in Table 5.

Table 5 Data for Black Conductive Silicone

Weight loss	Less than 0.01 percent	
Resistance		
Control (nonflight)	2650 ohms per square	
Control (nonflight)	1090 ohms per square	
Flight	3200 ohms per square	
Optical measurements	A	E
Control (nonflight)	= 0.96	=0.89
Control (nonflight)	= .96	= .88
Flight	= .96	= .88

Optical measurements of BCS also showed that it is extremely stable. In comparison to nonflight control discs, the absorptance and emittance are essentially unchanged at 0.96 and 0.88, respectively, for the flight sample.

6.3.4.2 Black Conductive Urethane. This black paint showed a large percentage weight loss and a large change in optical properties.

The BCU disc was weighed before and after flight, and it showed a 6.7 percent weight loss. This is a much larger loss than for any of the above samples. However, prior flight data had indicated that urethanes are not stable in low Earth orbit, and these results are not surprising.

The electrical resistance values showed a large change also. In comparison to nonflight samples, the electrical resistance of 73,200 ohms per square for the flight sample was almost three times that for the nonflight samples. The data are presented in Table 6.

Table 6 Data for Black Conductive Urethane

Weight loss	6.7 percent	
Resistance		
Control (nonflight)	28,100 ohms per square	
Control (nonflight)	21,400 ohms per square	
Flight	73,200 ohms per square	
Optical Measurements	A	E
Control (nonflight)	= 0.95	= 0.88
Control (nonflight)	= .95	= .89
Flight	= .99	= .94

The optical measurements demonstrated a drastic change, as the data show. The appearance of the flight sample was much blacker than the control specimens. This more diffuse surface has been noted for numerous surfaces after exposure at low Earth orbits. However, the reflectance curve shows this sample to be an almost perfect absorber in the 0.3- to 2.4-μm region of the solar spectrum. The values of 0.99 for absorptance (an increase of 0.04 from the control) and a value of 0.94 for emittance (an increase of 0.05 and 0.06 from the controls) show these changes.

This particular sample was later photographed. The appearance of the surface at high magnification in the scanning electron microscope (SEM) showed the reasons for the optical changes. As can be seen in Figure 1, the numerous sharp peaks in the surface are the reason for the optical and visual changes.

6.3.5 Other Materials

6.3.5.1 MS74 Paint. This paint, developed by C. Shai, Goddard Space Flight Center, is a very stable white silicate paint. It has been applied to many spacecraft surfaces because of the stability it has exhibited in testing. This paint was sprayed onto the aluminum disc, and optical measurements were made before flight.

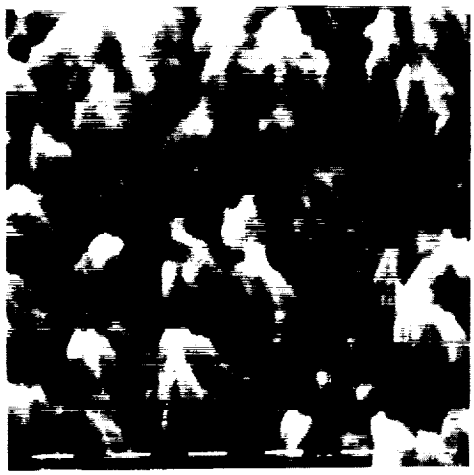

Fig. 1. Black conductive urethane (BCU) after exposure, having an absorptivity of 0.99 and an emissivity of 0.94 at 5000× with 1-μm markings.

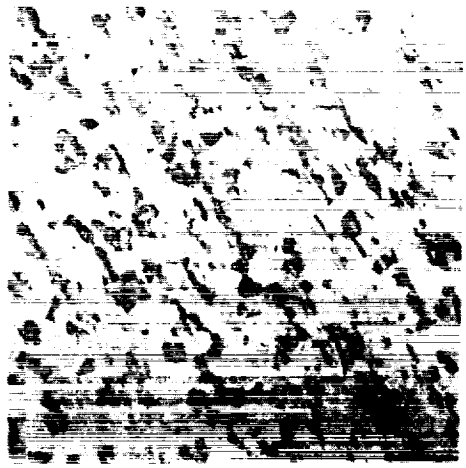

Fig. 2. Exposed surface of lead-tin solder at 640×.

The MS74 values were 0.14 for absorptance and 0.92 for emittance. The postflight values were 0.18 for absorptance and 0.92 for emittance. No visible change was noticed at the rim of the disc.

6.3.5.2 Solder. A piece of lead-tin solder was taped to a Kapton surface on the aluminum disc. The ends of the solder were also captured and held by the cover plate. Only SEM pictures were made. (See Fig. 2.) The SEM picture shows a slight etching of the surface, but no visible attack can be noted, not even with a microscope using 100× magnification.

6.3.5.3 Tantalum. A disc of tantalum was obtained which was approximately 1 in. in diameter. It was affixed to the aluminum disc and also held in place by the outer frame.

After flight, optical examination could not detect any reaction. In fact, the back side of the tantalum was as free of effects as the exposed side. There was also no evidence of change in the surface using the SEM.

6.4 Conclusions

This sample set of polymeric materials, two metals, and one inorganic paint showed a wide range of reactivities to the atmosphere at low Earth orbit.

Modifications to the Chemglaze II A276 and V200 paints that were obtained by adding an antioxidant or a UV stabilizer, alone or together, did not significantly make the paints more stable optically. In fact, the additives usually resulted in a greater change in absorptance and emittance than for the standard A276 and V200 paints.

Various samples of silicone mixtures demonstrated that the silicone molecule is very stable in low Earth orbit. A single-component silicone protected a Kapton film, a white silicone paint with TiO_2 pigment exhibited small weight loss and small optical property changes, and a black conductive silicone paint exhibited essentially no weight loss and little change in optical properties. The largest differences were for a black conductive urethane which had a 6.7 percent weight loss, became an almost perfect absorber in the 0.3- to 2.4-μm optical range, and exhibited a surface having numerous sharp peaks at high magnification.

A white silicate paint was also very stable in the space atmosphere. A rod of solder was very lightly etched by the atmosphere. A tantalum disc was not affected by the atmosphere and was probably the most resistant material to the oxygen flux.

Acknowledgements

The majority of the paint samples were provided through the assistance of Mr. J. Hirschfield, and the optical measurement data were produced by John Henninger. Carroll Clatterbuck prepared the additional paint samples, and Brad Parker provided the SEM pictures.

7.0 EVALUATION OF OXYGEN INTERACTIONSWITH MATERIALS (EOIM): STS-8 ATOMIC OXYGEN EFFECTS*

Kevin A. Smith

TRW Electronics and Defense Sector
Redondo Beach, California 92373

Abstract

Six test samples were flown on STS-8. Unprotected Kapton** and Kapton overcoated with 4000 nm of sputtered indium tin oxide were exposed to ram neutral atomic oxygen impingement (total fluence 3.5×10^{20} atoms cm^{-2}). Unprotected Kapton and Kapton overcoated with 11 000 nm of vacuum-deposited SiO_x were exposed to reflected oxygen impingement. The unprotected Kapton exposed to ram impingement exhibited significant increase in spectral absorptance. Sources of silicon oxides and aluminum oxides formed a protective layer on the Kapton surface providing partial protection from oxygen attack. Preferential unidirectional chain scission of unprotected regions of the polyimide occurred during the erosion process. The unprotected Kapton exposed to reflected impingement and both protected Kapton samples exhibited little degradation. Capture of small alumina particles (~2 to 5 μm) suspected to be from solid rocket exhaust occurred on the surfaces of the test specimens. Two contaminated samples with oxygen inert substrates were exposed to ram atomic oxygen flux. The flight results indicate that certain classes of outgassed contaminants may be removed from critical spacecraft surfaces which undergo this exposure.

7.1 Introduction

The advent of the Space Transportation System (STS) has resulted in the opportunity to routinely examine materials exposed to the space environment. Examination of many materials returned by the Space Shuttle has revealed significant effects attributed to the ambient orbital environment. Neutral atomic oxygen interaction[1] with materials at Space Shuttle altitudes appears to be the most plausible explanation for the effects observed. From data gathered on the initial STS flights, concern mounted in regard to the stability of Kapton in the low Earth orbital (LEO) environment.

Kapton, a polyimide with many applications in aerospace technology, undergoes mass loss, surface roughening, and thermophysical and mechanical property changes upon exposure to the LEO oxygen flux.[2] These changes result in significant implications concerning the utilization of Kapton for long-lived spacecraft in LEO (e.g., Space Station). Kapton has been utilized in many applications including thermal control and is currently under consideration as the baseline material in the flexible substrates for lightweight, high-power solar arrays because of its inherent strength, temperature stability, and high surface resistivity.

Specifically, TRW was interested in:

1. Physical changes of Kapton following exposure to the neutral atomic oxygen environment.

2. Means to protect the Kapton surface without appreciably altering either its optical or mechanical properties.

3. Differential removal of various classes of contaminant materials on the surface of an oxygen-inert substrate due to the neutral atomic oxygen flux.

7.2 STS-8 Exposure

Because of an upper stage anomaly on TDRS-A (STS-6), the TDRS-B was delayed from its scheduled launch on STS-8. Consequently, an expanded version of the STS-5 experiment replaced the TDRS-B

*AIAA Paper 85-7021 Presented at the Shuttle Environment and Operations II Conference, Nov. 13-15, 1985.

**Registered trademark Dupont Company.

mission. This experiment allowed TRW and 13 other organizations to obtain additional quantitative data concerning LEO atomic oxygen effects.

The STS-8 initial circular orbital altitude (β angle was 30°) was 296 km. This altitude was maintained for 56 orbits at a calculated mean neutral atomic oxygen density of 5.8×10^8 atoms cm^{-3}. Higher dansity was then obtained by lowering the Space Shuttle circular altitude to 222 km and orienting the payload bay into the velocity vector for 41.75 hr (~28 orbits) with a calculated mean atomic oxygen density of 2.7×10^9 atoms cm^{-3}. The total fluence is estimated to be 3.5×10^{20} atoms cm^{-2} following corrections for the actual solar activity during the STS-8 mission period.[3] Exposure at this altitude resulted in > 95 percent of all atomic oxygen fluence. The TRW-provided samples facing directly into the velocity vector experienced essentially all atomic oxygen impingement normal to the surface.

7.3 Sample Location and Experimental Configuration

All TRW samples were located on the Marshall Space Flight Center (MSFC) sample holder (Fig. 1). This holder was designated as tray no. 2 and was located in the forward port side of the payload bay on the DFI unit support structure. Approximately 300 material samples with much diversity in material content were flown on STS-8.

Both coated and uncoated Kapton samples were flown so that the changes in each could be ascertained and compared. The first location described on the MSFC tray provided direct exposure (ram) to the atomic oxygen flux. The sample configuration in this location consisted of a 25.4-µm-thick uncoated aluminized Kapton disc which was 2.5-cm in diameter (designated as unit A) with a 25.4-µm-thick aluminized Kapton annular ring with an inner diameter of 0.953 cm and an outer diameter of 2.5 cm. The polyimide exposed side of the annular ring was coated with 4000 nm of sputtered indium tin oxide (ITO) (Fig. 2). The ITO-protected annular ring was placed on top of the Kapton disc, and the entire unit was placed in the MSFC specimen holder tray (Fig. 1). The purpose of the experiment was to ascertain the changes in the unprotected Kapton versus the protected Kapton.

The second location of protected and unprotected Kapton samples (designated as unit B) was located on MSFC tray no. 2 (Fig. 1) and was flown facing downward onto the mounting but elevated about 1.91 cm above it. Consequently, this sample unit experienced only reflected, sputtered, or contaminant source material.

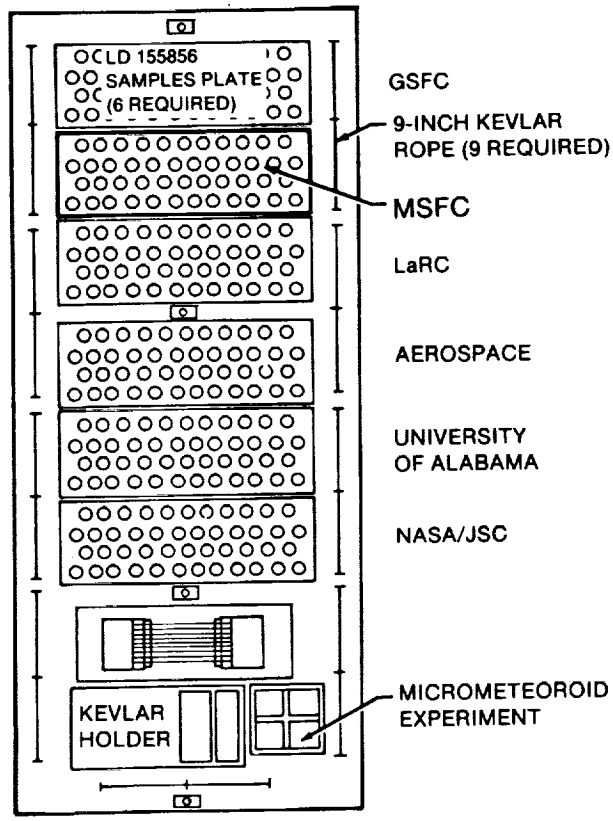

Fig. 1 Tray no. 2.

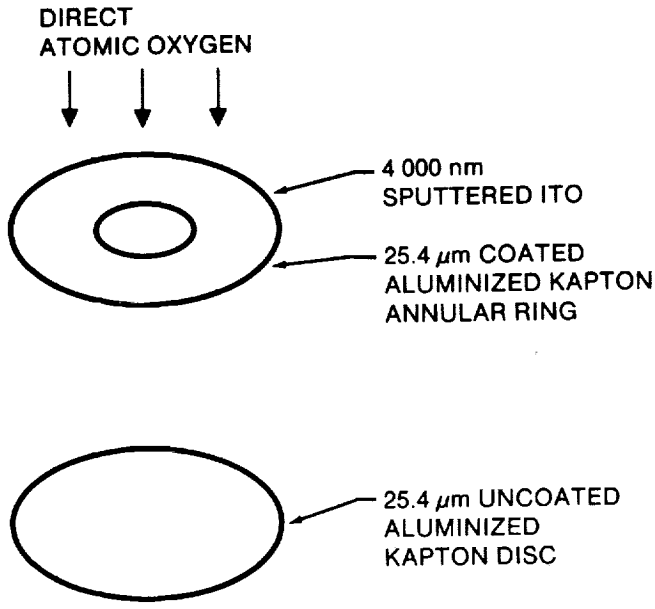

Fig. 2 Direct flux (unit A) exploded configuration.

The sample configuration in this location consisted of a 50.8-μm-thick uncoated aluminized Kapton disc which was 2.5 cm in diameter with a 50.8-μm-thick aluminized Kapton annular ring with an inner diameter of 0.953 cm and an outer diameter of 2.5 cm. The polyimide side of the annular ring was coated with 11 000 nm of vacuum-deposited silicon oxide (SiO_x) (Fig. 3). The silicon oxide-protected annular ring was placed on top of the Kapton disc, and the entire unit was placed in the MSFC specimen holder tray (Fig. 1).

Two oxygen inert samples were provided to determine the relative removal propensity of typical outgassed materials from two general classes of contaminant source materials. The two samples were circular electroless nickel wafers (99.997 percent pure) which were 2.5 cm in diameter and 0.318 cm thick. One side of each wafer was highly polished. Following a cleaning procedure, 1500 nm of chromium was vacuum deposited on the polished surface. Without breaking vacuum, 33 000 nm of gold was vacuum deposited over the chromium. The optical constants (n and ik) of the gold samples were then obtained with ellipsometry by measuring ψ and Δ ($\lambda = 0.6328\ \mu m$, $\phi = 70°$). The samples were then subjected to vacuum outgassing per American Society for Testing Materials procedure E-595-77 utilizing two contaminant sources. One sample received 8370 nm of outgassed material from Chemglaze Z-306 (polyurethane), and the other received 4390 nm of outgassed material from DC93-500 (silicone) as determined by ellipsometry. The contaminant films were anisotropic, and there was minor contamination attributed to diffusing pump oil based on the measured refractive index.

7.4 Results and Discussion

7.4.1 Film Thickness Loss

The results of the thickness change measurements (based on mass loss, utilizing bulk film density) before and after flight are shown in Table 1. Flight samples were compared with control samples

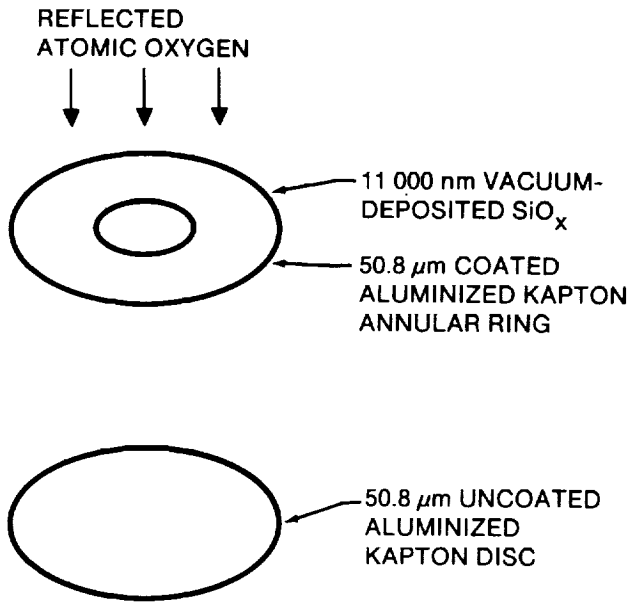

Fig. 3 Reflected flux (unit B) exploded configuration.

Table 1 Film thickness loss*

Unit A	Thickness (μm)	Thickness loss (μm)	Reaction efficiency 10^{-24} cm³/atom
ITO ring	25.4	0.05	0.01
Uncoated Kapton	25.4	0.5	0.1
Unit B			
SiO_x ring	50.8	0.05	0.01
Uncoated Kapton	50.8	0.2	0.06

*See text regarding error.

before and after flight. All sample weight changes were within 2σ of the microbalance accuracy. Consequently, the data may represent trends, but they are not indicative of the absolute numbers. The very small weight changes were expected because of the small exposed area of unprotected Kapton. The accuracy of the measurements was also a function of cutting variations, film thickness variations, differential interstitial water quantities (no moisture control was employed in the weighing technique) and water/gas adsorption changes. The observed weight changes could also be due to contaminant (molecular) and particular adhesion to the surface of the Kapton and the protected Kapton. Carbonaceous compounds (Fig. 4) and particle impacts (Fig. 5) have been found on the surfaces of the samples and may have contributed to the weight uncertainty. The majority of alumina particle impacts on unit B surfaces appear to be low velocity tangential impacts. It was speculated that most initial kinetic energy of the incident particles (on unit B surfaces) was lost because of previous impacts with adjacent surfaces before contacting the experimental surfaces. It was postulated that the observed particles originated from previous solid rocket motor activity (Fig. 6). Observation of the trends, however, indicates:

1. The ITO coating protected the Kapton from surface erosion during direct atomic oxygen exposure by a factor of 10 as compared to unprotected Kapton.

2. The SiO_x coating protected the Kapton in "reflected" attack by a factor of 4 as compared to unprotected Kapton exposed to "reflected" oxygen flux.

3. "Reflected" attack of uncoated Kapton occurred at a reduced rate as compared to direct attack by a factor of 2.5.

7.4.2 Solar Absorption and Emittance Changes

The measured changes in solar absorptance utilizing preflight and postflight values are shown in Table 2. All spectral measurements (0.28 to 2.5 μm) were made with a Beckman 5240 spectrophotometer. The apparent change in absorptance for the ITO ring (unit A) is within experimental error. The 11-percent change in the Al/Kapton exposed to direct oxygen attack is probably primarily due to the surface roughening effect produced. The 6.6-percent increase in spectral absorptance of the SiO_x ring (unit B) may be due to both contamination observed on the surface (Fig. 4) and numerous particle impacts (Fig. 5).

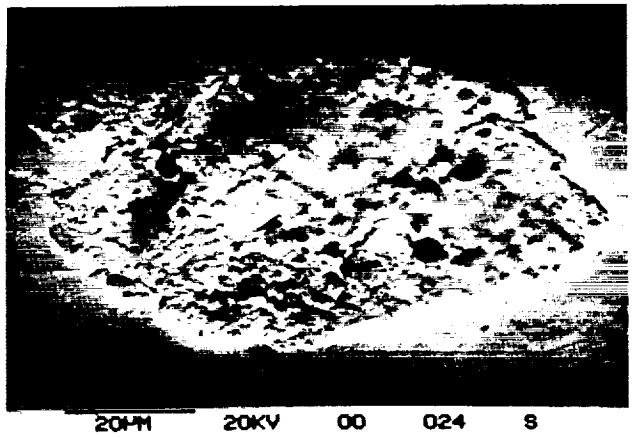

Fig. 4 Carbonaceous matter found on unit B SiO_x-protected surface, SEM: 1000×.

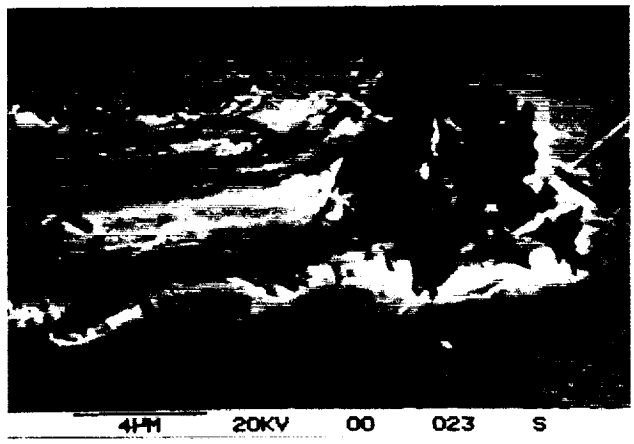

Fig. 5 Alumina particle with SiO_x debris at path termination, SEM: 5000×.

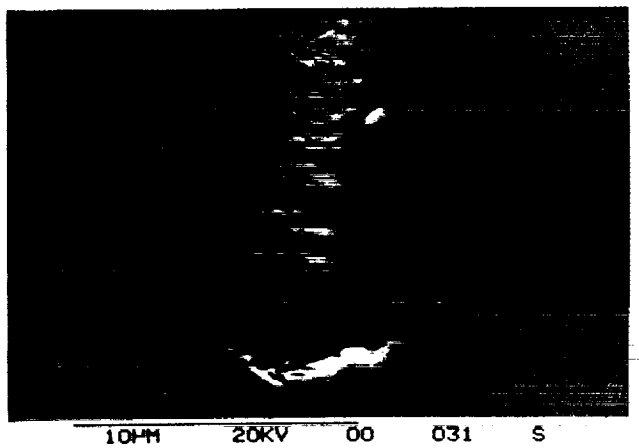

Fig. 6 Alumina particle track on unit A with ITO debris, SEM: 4000×.

Table 2 Spectral absorptance (0.28 to 2.5 μm) and normal emittance (2 to 26 μm)

	Absorptance		
Unit A	Unexposed	Exposed	% Δ
ITO ring	0.546	0.552	+ 1.1
Al Kapton	0.435	0.483	+ 11.0
Unit B			
SiO_x ring	0.588	0.627	+ 6.6
Al Kapton	0.467	0.405	– 13.3
	Emittance		
Unit A	Unexposed	Exposed	% Δ
ITO ring	0.712	0.716	+ 0.56
Al/Kapton	0.678	0.696	+ 2.65
Unit B			
SiO_x ring	0.784	0.782	– 0.26
Al Kapton	0.776	0.769	– 0.90

Because of the unit B configuration (Fig. 7), significant aluminum and alumina transfer probably occurred from the bottom of the SiO_x annular ring to the polyimide surface located beneath it.

The 13.3 percent decrease in spectral absorptance observed for the uncoated Kapton in unit B may be due to removal (mechanical, sputtering) of the aluminum and alumina layer from the SiO_x annular ring above it (Fig. 7). Diffuse layers of aluminum and alumina were detected with secondary ion mass spectroscopy (SIMS) on this unit B surface. It was possible that other (extrinsic to unit B) sources of aluminum were contributing to the deposition. The scanning electron microscope (SEM) showed that no morphological changes occurred in the exposed Kapton surface of the unit B sample (Fig. 8). The unprotected Kapton surfaces of unit B appeared as untouched as the control samples. The reason for this is unclear. Reflected atomic oxygen attack may have been inhibited by the protective aluminum and

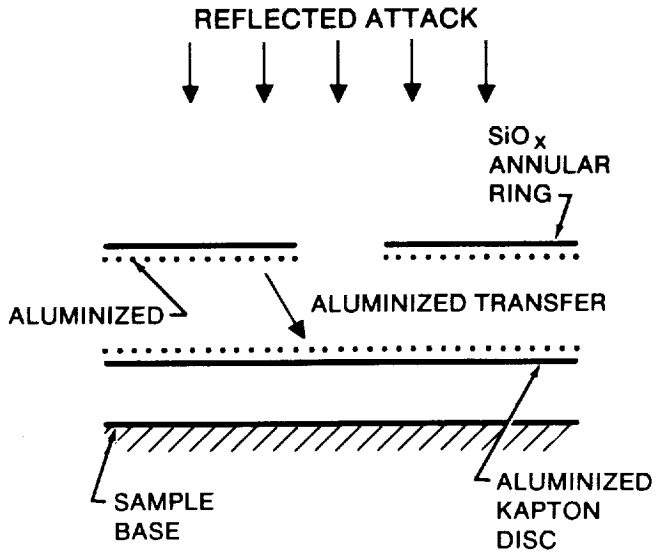

Fig. 7 Side view of sample configuration illustrating tendency for aluminum transfer.

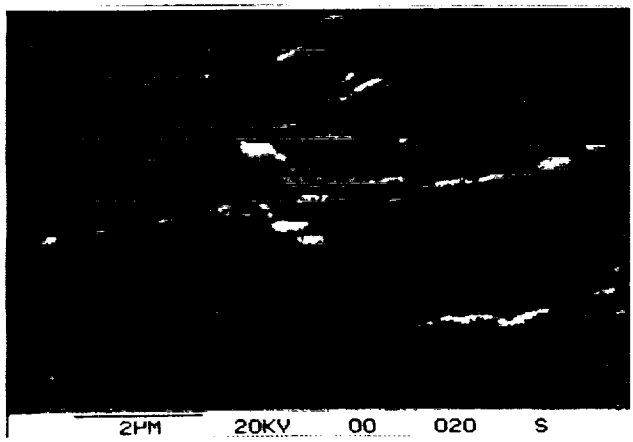

Fig. 8 No change in surface morphology for unit B unprotected Kapton, SEM: 10 000×.

alumina surface layers. It is also possible that some kinetic activation energy is required at the time of impact in order to initiate the oxidation mechanism. This requisite activation energy may not have been available for this sample configuration and location.

Table 2 illustrates the normal emittance measurements (2 to 26 μm). The measurements were obtained before and after flight with a Gier-Dunkle DB100 infrared reflectometer. The only significant change was the 2.65-percent increase in emittance of the Kapton sample exposed to the ram atomic oxygen flux. The resultant surface area increase is probably responsible for the small increase in emittance observed.

The specular (within approximately 5° of the reflected incident beam) versus diffuse components of the reflected incident radiation in the waveband 0.28 to 2.5 μm was investigated for the unit A unprotected Kapton exposed to the direct atomic oxygen flux. The results are reported in Table 3. The diffuse component of the reflected spectral radiation increased over 200 percent from the unexposed to the exposed condition. The loss in specularity was attributed to the increase in surface roughness.

7.4.3 Surface Resistivity Changes

All measurements were made under room conditions. All uncoated Kapton samples (both flight and control) exhibited surface resistivities greater than 200 GΩ square^{-1}. There was no measurable change in surface resistivity (>200 GΩ square^{-1}) for the unit B annular ring coated with SiO_x. The ITO surface resistivity (unit A) decreased by a factor of 5

Table 3 Specular vs. diffuse reflectance* of spectral incident radiation

	Components		
	Specular	Diffuse	Total
Unexposed	0.41	0.16	0.57
Exposed	0.17	0.35	0.52

*See text.

for the flight sample (a drop from 11.25 to 2.11 GΩ square^{-1}). Differential surface water adsorption, loss of indium oxide, or surface contamination may be responsible for the observed increase in conductivity. Ion microprobe analysis indicates there was an increase in soluable salts on the surface compared with the control sample.

7.4.4 Surface Morphology and Secondary Ion Mass Spectroscopy

The use of the scanning electron microscope illustrates the smooth Kapton surface (Fig. 8) even at 10 000× magnification. Although Figure 8 is a micrograph of unit B unprotected Kapton exposed to the reflected oxygen flux, its smooth appearance is nearly identical to the control samples. The smooth, undisturbed surface morphology was also observed on the SiO_x-coated annular ring. This unit B Kapton exposed to the reflected flux exhibited high surface concentrations of aluminum and alumina compared to the respective control sample as measured by wavelength dispersive x-ray (WDX) analysis and SIMS. The nominal aluminum thickness is estimated to be in the 1200- to 3880-nm range. The observed protection of the Kapton with thicknesses in this range have been reported elsewhere.[4] This indicates that transfer of aluminum and alumina probably occurred as a result of mechanical rubbing, oxidation processes, or sputtering of adjacent surfaces. The location of the overlying aluminum source for deposition on the Kapton surface below is illustrated in Figure 7. It is possible that low yield sputtering of aluminum occurred from other adjacent surfaces also. The kinetic energy of each incident

*Atomic Oxygen Working Group Meeting , Washington D.C., Jan. 23-24, 1984.

oxygen atom is about 5 eV. Aluminum was also found on the coated side of the unit B SiO_x annular ring albeit in lower surface concentrations than the Kapton below. The exposed area of the Kapton in unit B exhibited a higher secondary electron yield compared to the control sample. This indicates the presence of an oxide layer in the exposed region.

Numerous particle impacts were observed at both unit A and unit B locations (Figs. 5 and 6). Higher numbers of impacts were observed on the unit A samples as expected. The particle in Figure 5 was identified as aluminum oxide and was suspected to have an origin associated with previous solid rocket motor activity. Tangential alumina particle impacts also occurred on the ITO-coated annular ring of unit A but in much lower frequencies (Fig. 6) than on unit B. Eighteen impacts were observed on the unit A samples, and five impacts were observed on unit B samples.

The ITO-coated annular ring surface morphology was very smooth. There was no apparent oxygen attack, and in nearly all areas the surface appeared identical to the control surface. However, in very isolated regions, degradation of the polyimide surface occurred (Fig. 9). It was suspected that oxidation occurred as a result of oxygen attack in areas where the protective ITO coating was missing. The track of degradation could be simply due to oxidation of unprotected Kapton. However, because of the observation that tracks of degradation occurred, it was suspected that this pattern was due to preferential chain scission underneath adjacent protected surface layers with subsequent roof collapse of the cavities (Fig. 10). This pattern was repeated in two other regions of the specimen. Approximately 0.001 percent of the surface was affected in this way.

A maze of fine scratches was detected on the surface of the unit A unprotected Kapton. The small scratches end in a fairly well-defined region (Fig. 11) where the overlap of the annular ring protected the polyimide material from oxygen attack.

The unprotected surface exposed to ram in unit A exhibited a higher surface concentration of alumina and silicon than the respective control sample as determined by WDX and SIMS. The estimated thickness of this contaminant layer was 1850 to

*Atomic Oxygen Working Group Meeting, Washington D.C., Jan. 23-24, 1984

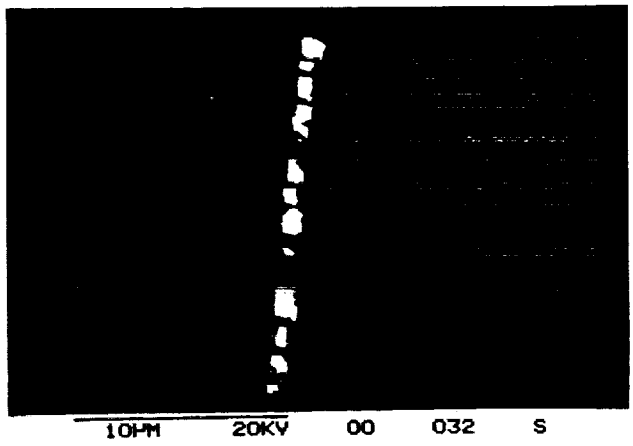

Fig. 9 Preferential oxygen attack where protective ITO coating was missing, SEM: 3000×.

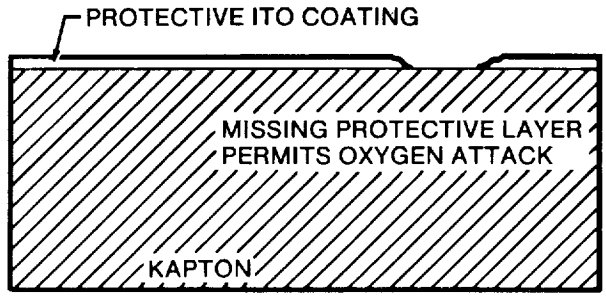

(a) Initial configuration.

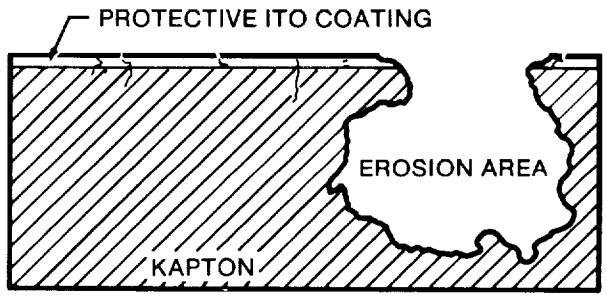

(b) Enlarged hole.

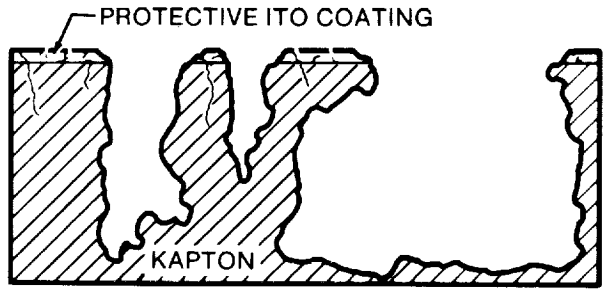

(c) Roof collapse as erosion continues.

Fig. 10 Kapton erosion progression.

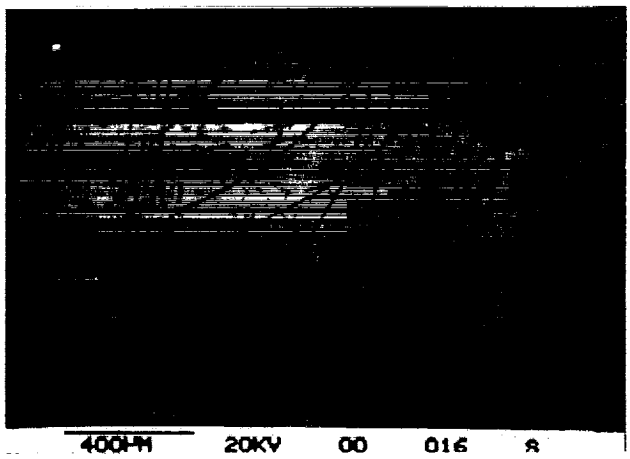

Fig. 11 Protected and unprotected Kapton surface, SEM: 50×.

4270 nm. The contaminant layer contained isolated high concentrations of Na and K which were attributed to human contamination products (e.g., saliva and skin flakes). The alumina concentrations are probably due to low-yield sputtering, mechanical rubbing, or oxidation products from either the aluminized layer above the Kapton (ITO annular ring, Fig. 7) or other local sources. The silicon oxide concentrations are probably the result of silicon-based RTV outgassing from local and Orbiter sources as reported earlier.* Atomic oxygen attack occurred preferentially where alumina or silicon oxide contamination was absent (Figs. 12 and 13). The observed pattern of erosion is similar to the ITO example albeit much more extensive. The greater extent of the erosion was attributed to the lower protective efficiency of the contaminant layer compared with the protective ITO coating. The preferred chain scission was evident in Figure 12 as shown by the unidirectional long track marks. Other patterns may have been induced by atomic oxygen eddies within the eroded area of the Kapton material itself. Many investigators have observed the "carpet-like" structure and "spider-web" strands shown in Figure 14.* It was thought that strand formation was attributed to the visual remnants of the last vestige of the contaminant layer seen just before total roof collapse (similar to Fig. 10).

The gold-coated nickel discs with the outgassed contaminant material from DC93-500 and Chemglaze Z-306 were measured for contaminant thickness following flight exposure using the same optical constants (real and imaginary refractive index of the substrate, n and ik). The change in contaminant thickness is reported in Table 4. Much of the polyurethane-based contaminant had been removed, while the silicone-based material actually increased in thickness ostensibly due to oxygen enrichment and contaminating extrinsic sources. The outgassed organic material from DC93-500 also began to approach the refractive index of SiO_2. Laboratory control specimens under room temperature and pressure lost approximately 15 percent of their contaminant thicknesses. Consequently, we can conclude that certain classes of outgassed contaminants may be removed from critical spacecraft surfaces during exposure to the LEO neutral atomic oxygen flux. Additional investigation is required.

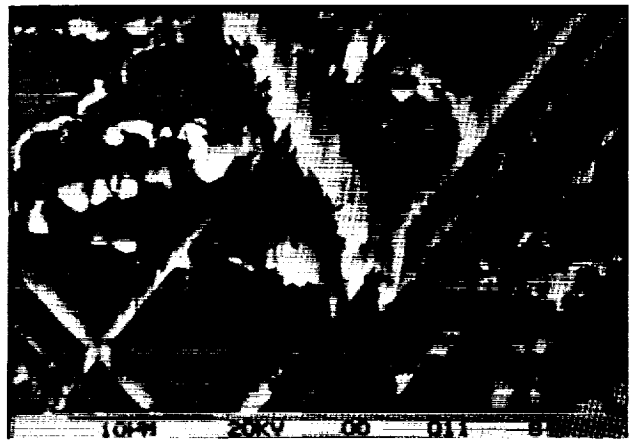

Fig. 12 Preferential atomic oxygen attack on uncoated unit A Kapton, SEM: 2000×.

Fig. 13 Preferential atomic oxygen attack on uncoated unit A Kapton, SEM: 5000×.

*Atomic Oxygen Working Group Meeting, Washington D.C., Jan. 23-24, 1984

Fig. 14 "Spider" strands as last vestige of contaminant on unit A uncoated Kapton, SEM: 10 000×.

Table 4 Contaminant thickness change following atomic oxygen exposure

	Average initial contaminant thickness (nm)	Average final contaminant thickness (nm)
Chemglaze Z-306	8370	340
DC93-500	4390	5370

7.5 Conclusions

- Protective coatings or oxidative inhibitors for Kapton must be developed for use in long-term LEO applications.
- Significant increases in spectral absorptance occurred when uncoated Kapton was exposed to direct oxygen flux.
- Emittance was not appreciably changed, perhaps because of the small amount of erosion incurred.
- Larger samples are required to obtain a definitive assessment of the surface and bulk resistivity changes.
- Optical property changes and contaminant thickness can be measured with ellipsometry when a fixed angle of incidence is obtained.
- Contamination (alumina and silicon oxides) acting as a protective layer reduced the overall erosion of the Kapton material.
- Capture of small alumina particles (~2 to 5 μm) suspected to be from solid rocket motor exhaust occurred on the surfaces of the test specimens.
- Indium tin oxide provides an excellent protective coating against atomic oxygen attack. Further study should be conducted to determine the charging characteristics and the mechanical and thermophysical change/stability induced by utilizing this coating.
- SiO_x was not adequately tested in this study to determine its protective quality against oxygen attack. Further study is required.
- Certain classes of outgassed contaminants may be removed from critical spacecraft surfaces because of the LEO neutral atomic oxygen flux. Additional investigation is required.

Acknowledgements

The author acknowledges the technical contributions of Mr. Roy Batista, Mr. William Hewitt, Dr. George Inouye, Mr. Keith Maruya, Dr. Louis Rosales, Mr. Charles Ruth, Mr. Pedro Valdovino, and the TRW Thermophysics Laboratory in the preparation and analyses of the samples utilized in this study.

The author thanks Ms. Antoinette Iverson for preparation of the manuscript.

References

1. Leger, L. J., "Oxygen Atom Reaction with Shuttle Materials at Orbital Altitudes," NASA TM-58246, May 1982.

2 Smith, K. A., "Degraded Physical Properties of Aluminized Kapton Flown on STS-3," TRW IOC R213.2.83.200, May 1983.

3 Visentine, J. T.; Leger, L. J.; Kuminecz, J. F.; Spiker, Ivan K.; "STS-8 Atomic Oxygen Effects Experiment," AIAA Paper 85-0415, Jan. 1985.

4. Banks, B. A.; Mirtich, M. J.; Rutledge, S. K.; Swec, D. M.; "Sputtered Coatings for Protection of Spacecraft Polymers," NASA TM-83706, April 1984.

8.0 PROTECTIVE COATINGS FOR ATOMIC OXYGEN SUSCEPTIBLE SPACECRAFT MATERIALS - STS-41G RESULTS*

A. F. Whitaker, J. A. Burka, J. E. Coston, I. Dalins, S. A. Little, R. F. DeHaye

NASA George C. Marshall Space Flight Center
MSFC, Alabama 35812

Abstract

Sixteen materials consisting of metallizations, silicones, and FEP Teflon were applied as protective coatings to selected spacecraft material surfaces and exposed on STS-41G to the low Earth orbit atomic oxygen environment. Evaluations of their protective effectiveness were made through assessing their mass loss/gain characteristics, maintenance of base material optical properties, and imperviousness to atomic oxygen attack. Generally, all coatings provided some degree of protection for the underlying material. In some cases, the overcoat appeared to be too thin to provide adequate protection.

8.1 Introduction

Metallizations, silicone coatings, and FEP Teflon applied to various atomic oxygen susceptible spacecraft materials were exposed to the space environment on Space Shuttle mission STS-41G. These coatings were subsequently evaluated for their effectiveness in protecting the underlying material. The protective overcoats had been chosen based on their known stability in an oxidizing environment, the prior experience with them as an overcoat, and the availability, ease, and convenience of application. The data generated from this investigation were utilized to address pressing atomic oxygen issues on spacecraft hardware in fabrication at the time. In several cases, materials were utilized in unique applications as overcoats.

The materials flown were mounted on the Space Shuttle remote manipulator system (RMS) and exposed to the ram direction (Fig. 1) to obtain a total atomic oxygen fluence (mass spectrometer and incoherent scatter model calculations for a ram surface at 120 nm) of 2.45×10^{10} atoms/cm^2. Materials were configured into 1-in-diameter disc-type specimens or into thin foils as shown in Figure 2a. Thermal labels mounted with the specimens on the substrate indicated generally that the substrate temperature reached 200° F. The duration at this temperature during the approximate 40 hr of exposure is unknown.

Evaluations of the effectiveness of the coatings in protecting the substrate material were based on sample weight loss or gain, optical property measurement, and impenetrability to atomic oxygen.

8.2 Data Presentation and Analyses

8.2.1 Paints and Overcoats

Two paints and three overcoats, candidates for space telescope external surfaces, were exposed on STS-41G. Test results on these exposed materials are shown in Table I. The Chemglaze Z302 paint, which was overcoated with either OI-651, RTV-602, or MN41-1104-0 silicone, was required to maintain its specularity. The requirement for the Chemglaze Z853 paint, which was overcoated with MN41-1104-0, was to remain intact and thus produce no loose particles that could be transferred to scientific instruments during crew servicing of the telescope. The effect of overcoating these paints was to increase their initial absorptivity by 1 to 2 percent. Evaluations of these flown materials showed mass loss to be negligible, as expected. Optical data indicate an increase in diffuse reflectance of the surfaces of the RTV-602 and the MN41-1104-0 but no changes to the OI-651. The MN41-1104-0 appears to be adequate for protecting the Z853 paint even though a slight darkening of the overcoat occurred as a result of ultraviolet (UV) exposure during this flight. On the other hand, the optical property changes of decreased

*AIAA Paper 85-7017 Presented at the Shuttle Environment and Operations II Conference, Nov. 13-15, 1985.

Fig. 1 Exposure of material samples on the Space Shuttle RMS

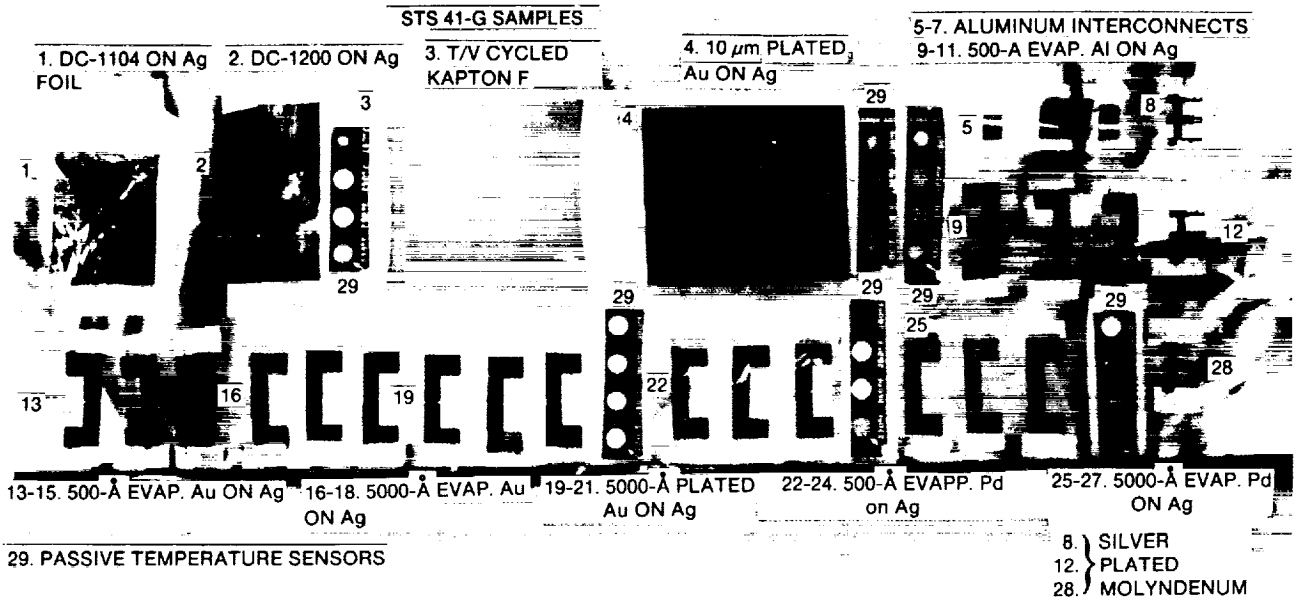

Fig. 2a Coated silver specimens after exposure

Table I STS-41G property data on overcoated paints

Evaluations	Z302 glossy black with OI 651 overcoat	Z302 glossy black with RTV-602 overcoat	Z302 glossy black with MN41-1104-0 overcoat	Z853 glossy yellow with MN41-1104-0 overcoat
Exposed flight specimens optical property, absorptivity (α)	.972	.969	.970	.469
Nominal control values of absorptivity (α)	.972	.973	.972	.458
Mass loss of flight specimen due to atomic oxygen exposure	None	Negligible	Negligible	Negligible
Comments on exposure effects	Maintains specular character of Z302	Loss of Z302 specular character	Loss of Z302 specular character	Loss of Z853 specular character, slight α increase partially due to UV darkening

NOTE: The effect of applying an overcoat to these paints is to increase the initial absorptivity by 1 to 2%.

absorptivity and increased diffuseness which occurred as a result of exposure made the RTV-602 and the MN41-1104-0 unacceptable as overcoats for the Z-302 specular paint.

8.2.2 Kapton H and Kapton F

Kapton F, which is Kapton H with an FEP Teflon overcoat, is a candidate for replacement of Kapton H as a solar array structural substrate. As determined for earlier flight specimens, the low reactivity of Teflon to atomic oxygen makes it a reasonable candidate for protecting atomic oxygen susceptible materials. But the fact that it has some reactivity implies that a thin layer does have some life limitations. A sheet of Kapton F (0.1 mil FEP Teflon on each side of 1.0 mil Kapton H) that had been thermal vacuum cycled from $-70°$ C to $+150°$ C for 35 cycles prior to flight was exposed on this experiment. The objective was to determine if atomic oxygen would penetrate any delaminations and/or cracks induced by the thermal vacuum cycling. Microscopic examination of the material after flight indicated that it was intact with no atomic oxygen penetration of the Teflon overcoat to the Kapton H substrate. Two primary issues remain that must be solved before Kapton F can be considered as a viable substitute for Kapton H. First, the degradation of Kapton F resulting from the combination of long-term UV irradiation and atomic oxygen exposure must be determined to be within acceptable design limits, and, second, a successful method of bonding other solar array elements to Kapton F must be developed.

In addition, a sheet of Kapton H (Fig. 2b), folded so that one half of its length was unexposed, was flown to gather additional data on Kapton H The exposed portion of the Kapton H sheet was found to have variations in its thickness in patterns conforming to the indentations of the RMS's beta cloth surface to which it was mounted. This seemed to indicate that oxygen was reflecting from the ridges into the "valleys" where the greatest thickness losses were incurred. Thickness losses, due to atomic oxygen exposure, were determined from weight measurements of disc-type specimens cut from this sheet and ranging from 0.11 to 0.25 mil. This evidence further indicates that the reflections are a factor in atomic oxygen degradation of materials.

8.2.3 Metallization Overcoats for Silver

Vapor deposition facilities for aluminum, gold, and palladium are readily available at solar cell manufacturers. Thus, if these coatings proved to protect silver solar cell interconnects against atomic oxygen attack, processing of them onto interconnects

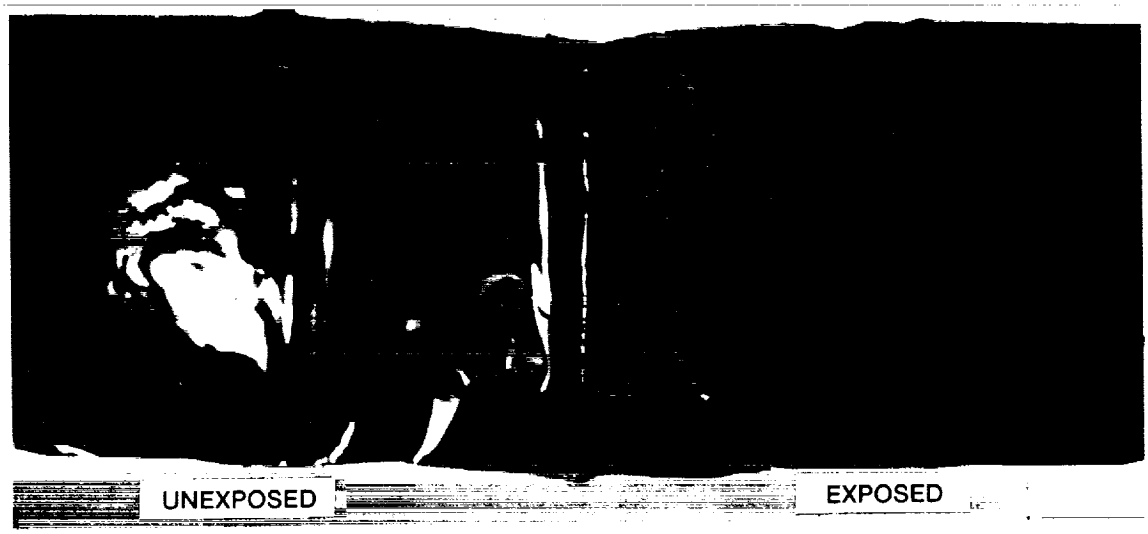

Fig. 2b 0.5 mil Kapton H showing both unexposed and exposed areas

could, with little impact on fabrication schedule, easily become a minor addition to the manufacturing process for cell assemblies. It was with this plan in mind that these coatings were pursued for use on silver. The interconnects flown are shown in Figure 2 and labeled as specimens 13 through 27. These interconnects are configured in a "Block C" shape with acid-etched grid patterns and slots to provide stress relief. One-half of each interconnect was coated. The interconnects were held in place on the flight foil sheet with Teflon tape on both the coated and the uncoated ends.

Figures 3a through 3d show scanning electron microscope (SEM) photographs of the 500-A aluminum-overcoated silver interconnect before and after flight exposure. The aluminum provided some protection even though it was not totally impervious to the atomic oxygen. Figure 3a shows a smooth aluminum overcoat which is typical of the as prepared surface. The coating interface on the interconnect surface is obvious in Figure 3b with the lighter region indicating aluminum. Scale and surface roughening occurred on the uncoated area of all interconnects similar to that reported previously on exposed, bare silver. Figures 3c and 3d show numerous spots and streaks on the coated area where the silver has oxidized. Wrinkling of the overcoat occurred in one area near a grid hole. This is an indication of poor adhesion which probably resulted from contamination during the coating process. While the aluminum coating was generally protective, 500 A appeared to be too thin to prevent oxidation of the silver.

Palladium was evaluated as a silver overcoat in thicknesses of 500 A and 5000 A . Figures 4a through 4d show a flight-exposed 5000-A palladium-overcoated interconnect. While the unexposed specimen surfaces were smooth and uniformly coated with the palladium, the flight-exposed specimen showed discoloration and spots in the palladium coating. Energy dispersive x-ray spectroscopy (EDXS) evaluation of these spots shown in Figures 4c and 4d indicated silver only. Oxygen had obviously penetrated the overcoat and oxidized the silver. The silver, which expands upon oxidizing, appeared to have cracked the overcoat and produced bowed, cracked formations of silver oxide. The 500-A palladium flight specimen showed significantly more degradation of the silver substrate than the 5000-A coated specimen. It is not known how these spots originate. Perhaps one factor might be surface asperities of silver where the overcoat is thin or inadequately coated. Auger electron spectroscopy (AES) examination of the palladium film revealed a drastic increase in the amount of oxygen in the exposed area by comparing the oxygen content of the exposed area, the area protected by the tape, and the back side of the exposed area. This indicates that ram direction impinged atomic oxygen penetrated the palladium and suggests that oxygen can diffuse through the film to the silver substrate. Interestingly, the AES data further showed the more

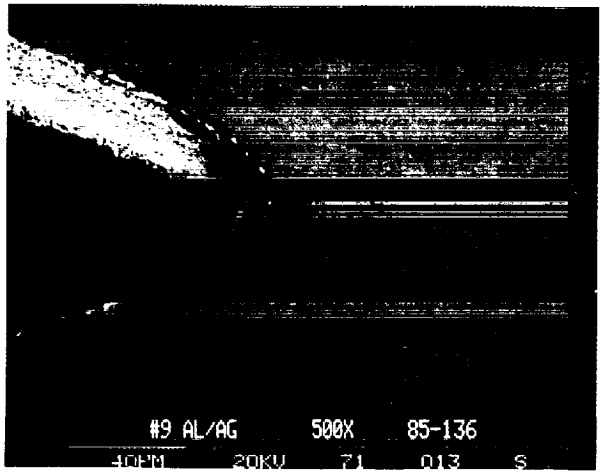

(a) Coated unexposed

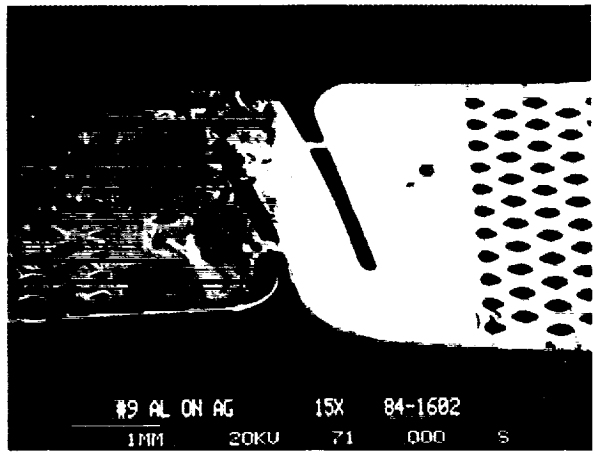

(b) Bare/Coating interface

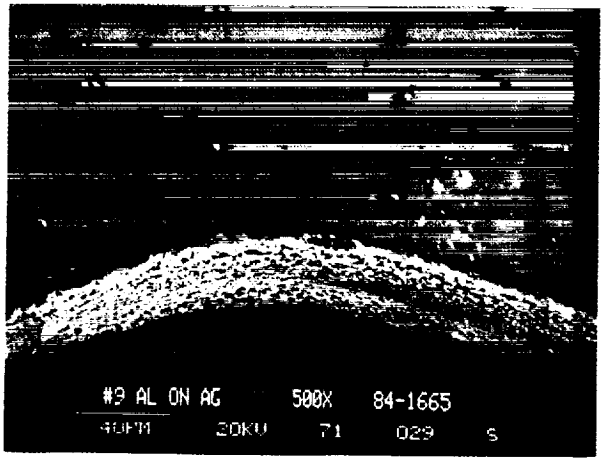

(c) Coating exposed

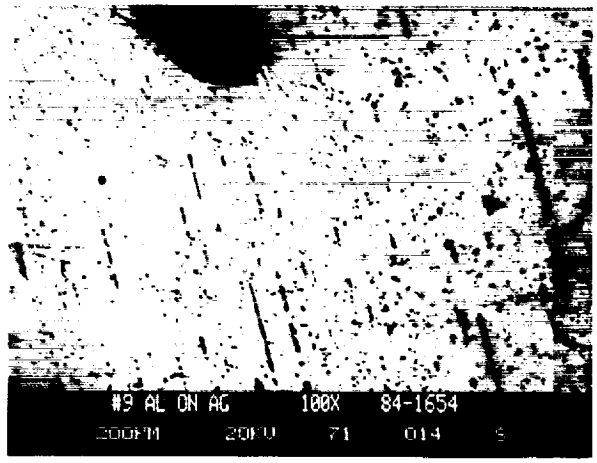

(d) Coating exposed

Fig. 3 SEM photographs of control and exposed aluminum-coated interconnects

massive 5000-A palladium film to contain more oxygen than the thinner 500-A film. It follows that greater protection is offered by the thicker film because of the greater oxygen diffusion path length, and the onset of the substrate oxidation is delayed.

Gold was flown which was deposited in 500-A, 2500-A, and 5000-A thicknesses on silver. Electroplated and vapor-deposited gold were exposed to determine if one process was more protective than the other. Vapor-deposited gold thicknesses of 500 A and 5000 A were applied to the interconnects. Electroplated gold thicknesses of 2500 A and 5000 A were deposited on silver foil (specimen no. 4 on Figure 2a) and the interconnects, respectively (Table II). Preflight SEM photographs of the vapor-deposited and electroplated surfaces are shown in Figure 5. The electroplated surface, which was grainy and had a larger effective surface area, would be expected, by virtue of its preparation method, to provide better than line of sight protection.

All flight specimens were visibly darker in the gold-coated areas which were exposed. Areas protected under the tape which held the specimens in place still had the original bright gold or silver luster. Even though all exposed gold-coated and bare surfaces were dark, no scaling was detected on the 500-A coated interconnect area or the 5000 A gold electroplated interconnect area. However, scaling was evident on the 2500-A gold-electroplated foil and the 5000-A gold vapor-deposited interconnect The

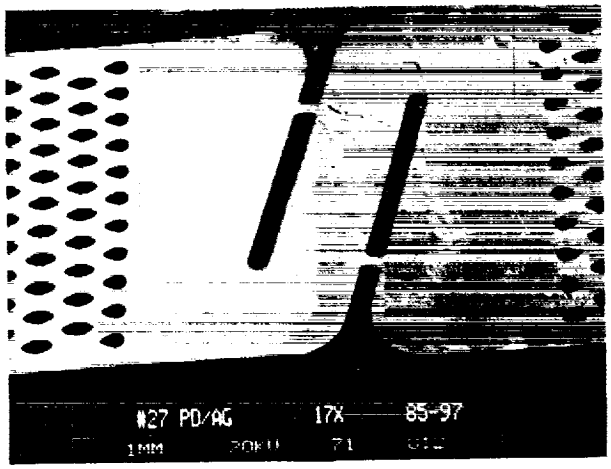

(a) Bare/Coating interface

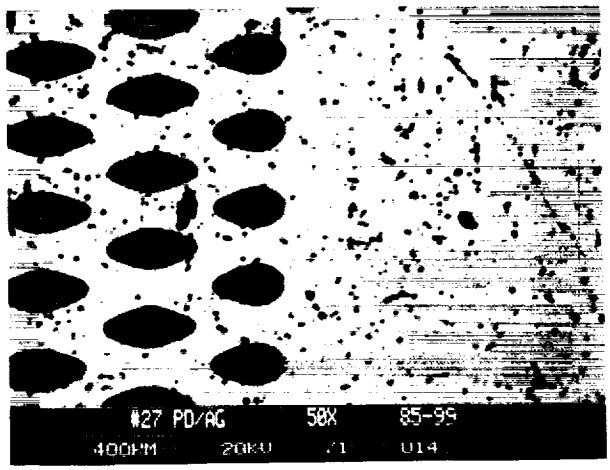

(b) Coating exposed

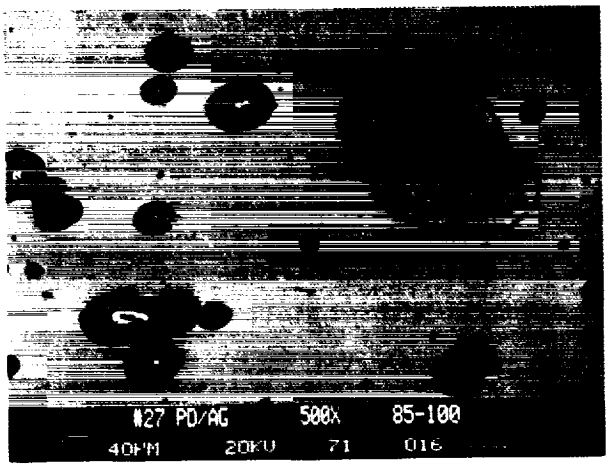

(c) Coating exposed

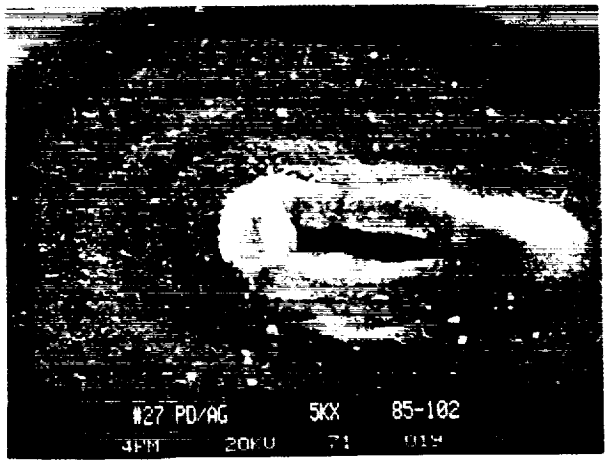

(d) Coating exposed

Fig. 4 SEM photographs of exposed palladium-coated silver interconnects

5000-A gold vapor-deposited interconnect showed evidence of a hydrocarbon-contaminated surface (Fig. 6a) which was traced to predeposition processing. This same pattern of spots was evident after exposure (Fig. 6b) and apparently corresponds to the site of scale initiation. It is suspected that the hydrocarbon contamination mixed with the gold coating and provided high diffusivity paths to the silver substrate for the atomic oxygen. No contamination was traced to the other samples. Cracking and scaling of the surface of the electroplated foil (Fig. 7) was similar to that seen previously on silver surfaces freshly attacked by atomic oxygen.

The visible darkening of the gold-plated surfaces was initially thought to result from intermetallic diffusion involving gold and silver. However, adjacent areas under the protective tape showed a sharp contrast in color with definite boundaries at the tape edge which tend to eliminate this explanation based on thermal diffusion alone. Further, thermal vacuum exposure at 200° F failed to produce the same effect in the coated samples. Some limited silver/gold diffusion was revealed by depth profiling the 5000 A of plated gold. Traces of silver were detected on the upper gold surface by AES evaluation. These traces are presumably either reaction products of atomic oxygen interaction or the decomposition of the silver oxide by the ambient atmosphere upon return. Primarily as a result of the contamination problem in the 5000-A vapor-deposited gold specimens, no absolute distinction could be made regarding vapor deposition versus electroplating protection. Generally, the 5000-A

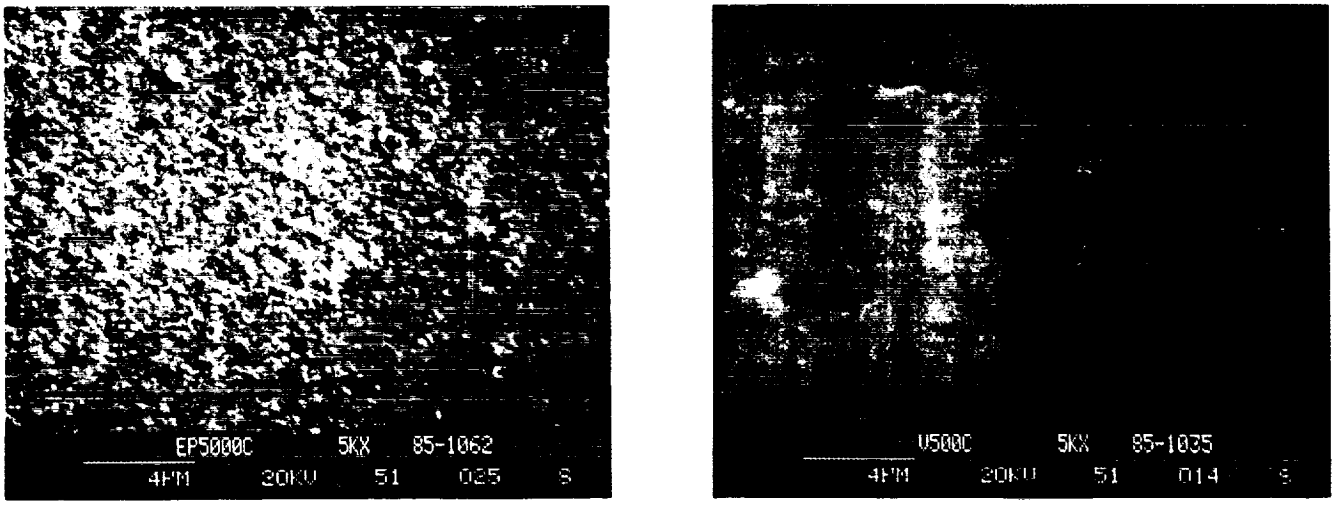

(a) Vapor-deposited Au

(b) Electroplated Au

Fig. 5 SEM photographs of preflight vapor-deposited and electroplated gold on silver

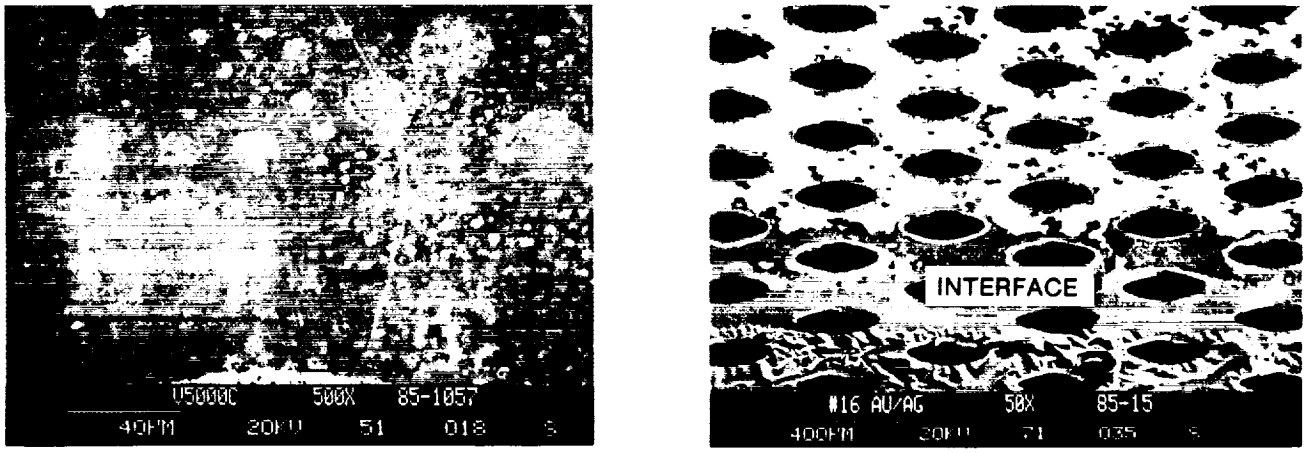

(a) Silver interconnect surface prior to gold deposition

(b) Exposed vapor-deposited gold interconnect

Fig. 6 SEM photograph of contaminated silver surface prior to coating and with exposed 5000-A vapor-deposited gold

electroplated gold seemed to provide the best short-term protection for the silver of any of the gold coatings.

8.3 Conclusions

Silicone coatings have previously been shown to provide substrate protection from atomic oxygen. Those silicones termed "glass resins" have indicated minimal surface reactivity as overcoats for specular paints, maintaining the very stringent requirements of limited diffuse reflectance. Because of its poor cohesion and easy transferability, the DC 1200 primer failed to protect the silver. The DC 1104 provided good protection for the silver. The film was thick, generally in the range of 0.2 mil, and nonporous. No oxygen diffused through this coating to the silver substrate during this short STS exposure. To successfully utilize this coating on silver, it must be determined that its application does not add undue stress to the interconnect system.

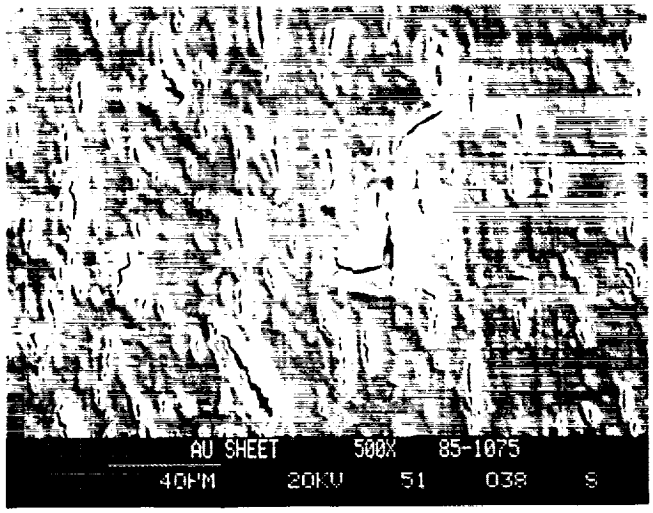

Fig. 7 Exposed 2500-A electroplated gold on silver foil

The applied thin metallizations of aluminum, palladium, and gold are inadequate for protecting silver under conditions of combined atomic oxygen and thermal vacuum. Once the atomic oxygen diffuses through these coatings to the silver, the oxidation of the silver is initiated. Some intermetallic diffusion may accompany this process to accelerate the result. The thicker films seem to retard the onset of oxidation as would be expected. However, based on the postflight evaluations, the film thicknesses to 5000 A of the overcoat samples, flown for approximately 40 hr into the spacecraft ram direction at 120 nm and evaluated here, would not be expected to provide long-term protection

Sources

1. L. J. Leger, et al, "STS Flight 5 LEO Effects Experiment - Background Description and Thin Film Results," presented at AIAA Shuttle Environment and Operations Meeting, October 1983. AIAA-83-2631-CP.

2. A. F. Whitaker, et al, "Orbital Atomic Oxygen Effects on Thermal Control and Optical Materials - STS-8 Results," presented at AIAA 23rd Aerospace Sciences Meeting, January 1985. AIAA-85-0416.

3. Peters, Palmer N., Gregory, John C., and Whitaker, Ann F.: Quick Look Report on Silver Interconnect Samples, 1-75-7A and 1-150-7A Flown on STS-5, unpublished.

Acknowledgments

The authors wish to thank the following people who were of considerable help during the design and analyses of this experiment: Dr. Lubert Leger, Jim Visentine, and Ike Spiker of JSC; Herman Gilmore, Dave Nicholas, and Ed White of MSFC. The typing of Ms. Jewell Cargile is greatly appreciated.

9.0 REACTION OF METALS IN LOWER EARTH ORBIT DURING SPACE SHUTTLE FLIGHT 41-G*

Albert T. Fromhold, Jr. and Kasra Daneshvar

Auburn University
Auburn, Alabama 36849

Ann F. Whitaker and Sally A. Little

NASA George C. Marshall Space Flight Center
MSFC, Alabama 35812

Abstract

The effects of the ambient space environment on metals which have applications to space telescope were studied by exposing specimens of Cu, Ag, Au, Ni, Cr, Al, Pt, and Pd on flight 41-G (STS-17). Data obtained by ellipsometry, Rutherford backscattering, and proton induced x-ray emission before and after flight are summarized. Although the effects of the space environment were most pronounced for silver, there were significant changes in the surface properties of the majority of the other metals. The surface optical constants proved to be the most sensitive measure of surface changes. These changes are attributed to the interaction of the metals with atomic oxygen.

9.1 Background

The basic problem was to ascertain the corrosive effects of the space environment, especially atomic oxygen, on metal specimens in the region of low Earth orbit. Eight different metals which have applications to space telescope, as well as corresponding control specimens, were measured by ellipsometry and Rutherford backscattering (RBS) before and after flight. Proton induced x-ray emission (PIXE) was used to analyze the elemental concentrations of the samples after flight. Bar graphs comparing the surface optical properties (refractive index and absorption coefficient) before and after flight for both the flight specimens and the control specimens illustrate the changes attributed to exposure to the space environment.

9.2 Rutherford Backscattering

The objectives of the RBS measurements were to determine the sample thickness before flight as an independent check on the thickness deduced from the evaporation monitor and to ascertain whether any significant surface layers were formed during flight or any significant decreases in thickness occurred during flight due to surface erosion. The thicknesses before and after flight are listed in Table 1. A comparison of the RBS data taken after flight with that taken before flight shows some differences, but these differences are generally not systematic enough or large enough to be considered statistically significant, with the possible exception of silver, in which a 40-percent increase in thickness occurred in the flight specimen.

Table 1 Rutherford backscattering data

Metal	Before flight: L (A)		After flight: L (A)		Ratio B/A	Ratio F/C
Ag	B	2325	F	3214	1.00	1.42
	A	2325	C	2268		
Ni	B	1931	F	1906	0.99	0.96
	A	1951	C	1986		
Pd	B	6401	F	6368	1.01	0.98
	A	6342	C	6513		
Cu	B	2033	F	2107	0.96	0.99
	A	2115	C	2130		
Au	B	4994	F	5173	0.95	0.97
	A	5254	C	5310		
Cr	B	895	F	814	1.03	1.06
	A	870	C	766		

*AIAA Paper 85-7018 Presented at the Shuttle Environment and Operations II Conference, Nov. 13-15, 1985.

9.3 Proton Induced X-Ray Emission

The objectives of the PIXE measurements were to provide an independent confirmation of the specimen elemental metal, to ascertain the major impurity metals, and to see what trace impurities were present on the sample surfaces after the flight. In particular, it was considered likely that the trace impurities on the surface might be different for the flight and the control specimens because of the chemical reactions with atomic oxygen which were possible for the flight specimens.

The PIXE results indicated that the evaporated metal films did contain significant impurity metal concentrations, and there were differences in the trace impurities on the sample surfaces depending upon whether the sample was a flight or a control sample. The amount of information obtained by this technique is voluminous and varied. Some of our data indicate that the higher the atomic weight, the fewer changes in the surface concentration of an impurity will occur.

9.4 Ellipsometry Data

Optical constant data consisting of refractive index n and absorption coefficient k were obtained for each of the 16 metal specimens (eight flight and eight control) both before and after the STS 41-G (STS-17) mission was completed. The data obtained in this study are presented in a series of bar graphs depicting the value of the optical refractive index n and the optical absorption coefficient k for the various metal specimens chosen for this study. The specimens were evaporated layers of silver, gold, palladium, platinum, nickel, copper, aluminum, and chromium on metal substrates. The nominal thickness of the layers ranged from 500 to 5000 Å, with more quantitative values for the thicknesses listed in Table 1. The intense mercury green line (5461 Å) was employed for the measurements.

First let us describe our so-called "standard" plot. A standard plot contains eight individual bars on a graph. Each standard plot is for one optical constant obtained from one metal either prior to flight or following the flight. Either the optical refractive index n or the optical absorption coefficient k is represented by each of the eight bars in a standard plot. All data on the plot are either preflight or postflight. In each standard plot, data are presented for two samples of the same elemental metal. Data prior to flight for the two samples are designated as A and B. The sample represented as B was subsequently flown and exposed on the STS-17 mission. The other sample, represented as A, is the control. Postflight data on these two samples are designated by F for the flight sample (B before flight) and C for the control sample (A before flight). Thus we have the correlation:

	Before flight		After flight
Sample:	A	=====>	C
Sample:	B	=====>	F

A given standard plot contains either A,B data or C,F data. Such standard plots are presented in pairs in the figures in this report for the purpose of drawing comparisons and obtaining other information. On a given figure containing two standard plots, four types would be possible based on the various combinations. However, we have found it useful to restrict the figures to the following three combinations.

	Before flight		After flight
n:	A,B	+	C,F
	+		
k:	A,B	+	C,F

Standard plot pairs illustrating n and k (n,k pairs) for a given metal before flight (A,B) indicate the overall quality of the samples, since at that point in time the data for the two specimens of a given metal should not differ in any essential way. For example, Figure 1 illustrates these results for the gold specimens utilized in this study.

Let us now describe in greater detail the actual data contained in a given standard plot. Figure 1, for example, gives the refractive index and absorption coefficient data for the two samples of gold before the flight. The letters A and B denote the sample in question. Two of the four bars for sample A give the results of two independent determinations (labeled a and b) for a given position on the sample surface. The other two bars for sample A give the results of two independent determinations (again labeled a and b) for a different position on the sample surface. The two positions on the sample surface are labeled 1 and 2, respectively. Good agreement between the a,b data for a given position gives confidence in the

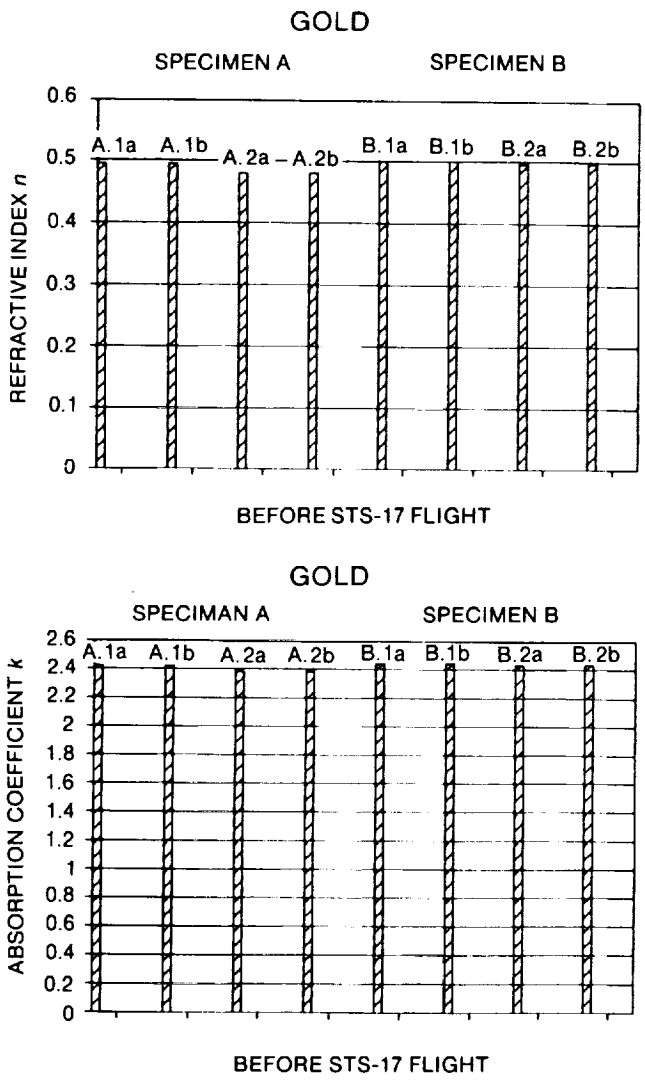

Fig. 1 Standard plots illustrating refractive index n (upper plot) and absorption coefficient k (lower plot) for Au specimens A (control specimen) and B (flight specimen) prior to flight. (Keys 1a and 1b designate independent measurements on one surface area of the sample, whereas 2a and 2b designate independent measurements on a different surface area of the sample.)

experimental precision of the measurement; good agreement between the data for positions 1 and 2 gives us confidence that the surface of the sample is homogeneous.

The need for precision requires no explanation. The need for surface homogeneity is less specific since it is based on several considerations. Two considerations are (1) the general confidence in good sample preparation and (2) the pragmatic consideration that there is no way to preserve an accurate memory of the area measured after the sample is removed from the ellipsometer. That is, the measurement does not mark the area physically, so once the sample is removed from the ellipsometer and subsequently returned for remeasurement, one must rely on the fact that the values obtained are characteristic of any part of the surface.

In summary, agreement between the data labeled A.1a and A.1b demonstrates measurement precision, as would the agreement between the data labeled A.2a and A.2b. Agreement between the A.1 and A.2 data demonstrates sample homogeneity. Exactly analogous statements can be made for the B data shown in the same standard plot (see Fig. 1), since that data is the corresponding data for the second of the two samples. Agreement between the A and B data gives us the required confidence that prior to the Space Shuttle flight the control and flight samples are essentially the same, and, if they are not exactly the same, at least we quantify the differences between the two samples. This represents a basic requirement for drawing meaningful conclusions by comparing the data on the two samples after flight.

It can be inferred from the standard plot for the refractive index of gold shown in the upper half of Figure 1, for example, that the data are precise (cf. A.1a and A.1b, A.2a and A.2b, B.1a and B.1b, and B.2a and B.2b), that the surface is homogeneous (cf. A.1 and A.2 data, and B.1 and B.2 data), and that the two samples are essentially identical in optical properties (cf. A data with B data). It is clear from the plot in the lower half of Figure 1 that these conclusions hold also for the absorption coefficient data.

Each of the other seven figures for the remaining metals in the study gives a similar picture of the optical quality of the sample it represents. Although the limitations of space preclude showing all of these figures, it was noted from these figures that the experimental precision is excellent for all 16 samples, and the surface homogeneity varies from excellent for Cr, Pd, and Al to very good for Au, Ag, Pt, Cu, and Ni. As might be expected, there is somewhat more variation in the sample to sample data for a given metal, though, as already noted, the data for the Au samples are in very good agreement. The sample to sample agreement is excellent for Cr, very good for Au, Ni, and Pd, and reasonably good for Cu and Al. For Pt, the agreement is quite good for the refractive index, but there was a sample to sample difference of about 15 percent for the absorption coefficient. For

Ag, the sample to sample agreement for the absorption coefficient was within about 5 percent, but there was a factor of 2 difference in the refractive index between the two samples.

Even though the sample to sample difference in n observed for silver is a bit surprising, such differences are not uncommon in the literature. (For example, values which have been cited for the refractive index of silver vary from 0.066 to 0.240 to 3 at wavelength 6328 Å.) More importantly, our observed difference turned out to be of the same order as the aging effect, which in turn was relatively small compared to the much larger changes which occurred upon exposure to the Space Shuttle environment in orbit.

Now let us present a different type of comparison based on the same standard plots, namely, a comparison of the data for a given optical constant before and after flight. Standard plot pairs illustrating either n or k for a given elemental metal before and after the flight serve two important purposes. Comparison of the A and C data demonstrates the aging effect on the optical constants during the several weeks' time period spanning the STS-17 mission. This aging effect must, of course, be factored into any changes noted in the flight sample during this period. Comparison of the B and F data in juxtaposition with the A and C data then allows one to deduce the specific effects of exposure during the Space Shuttle flight on the metal specimen in question. There are AB,CF plot pairs for each of the two optical constants of a given metal. With eight different elemental metals, this gives rise to 16 possible figures.

Figures 2 and 3 depict the effects of the Space Shuttle flight exposure on the Cr and Cu specimens. Each figure contains two standard plots for the same optical constant of the same elemental metal. The standard plot in the upper half of the figure shows the preflight data, and the standard plot in the lower half of the figure shows the postflight data.

Figure 2 shows that the refractive index of chromium is decreased by exposure to the space environment. Figure 3 shows that the absorption coefficient of copper is decreased by exposure to the space environment. Space precludes showing all 16 figures depicting n and k for the eight metals studied, but the results showed that by far the greatest changes which can be attributed to exposure to the space environment occurred for silver. The changes were very large for both the refractive index and the

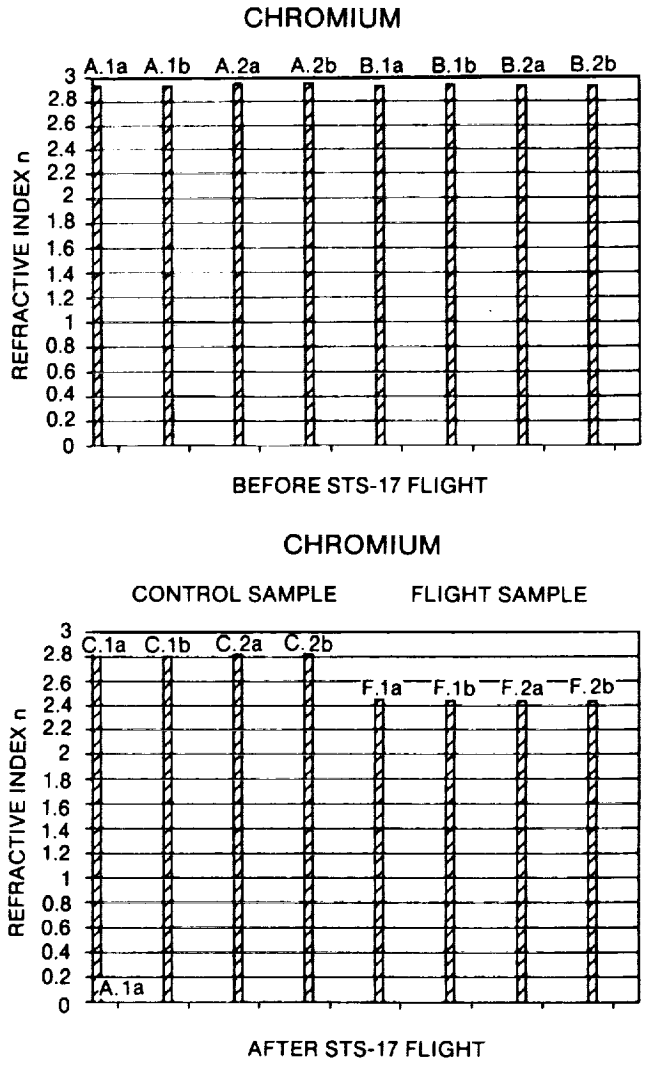

Fig. 2 Standard plots illustrating refractive index n for Cr specimens A (= = >C) and B (= = >F) before (upper plot) and after (lower plot) the flight. (Keys 1a and 1b denote independent measurements on one surface area of the sample, whereas 2a and 2b denote independent measurements on a different surface area of the sample.)

absorption coefficient. Changes in both optical constants due to space exposure were found also for palladium, copper, and chromium, although the effects are not as large as for silver, and likewise (but to a somewhat lesser extent) in gold and aluminum. There was also a change in the refractive index of platinum, but this was of the same order as the sample to sample variation in the absorption coefficient of platinum prior to flight. The majority of our samples, therefore, show some effects which can be attributed to flight exposure. These effects are now further examined.

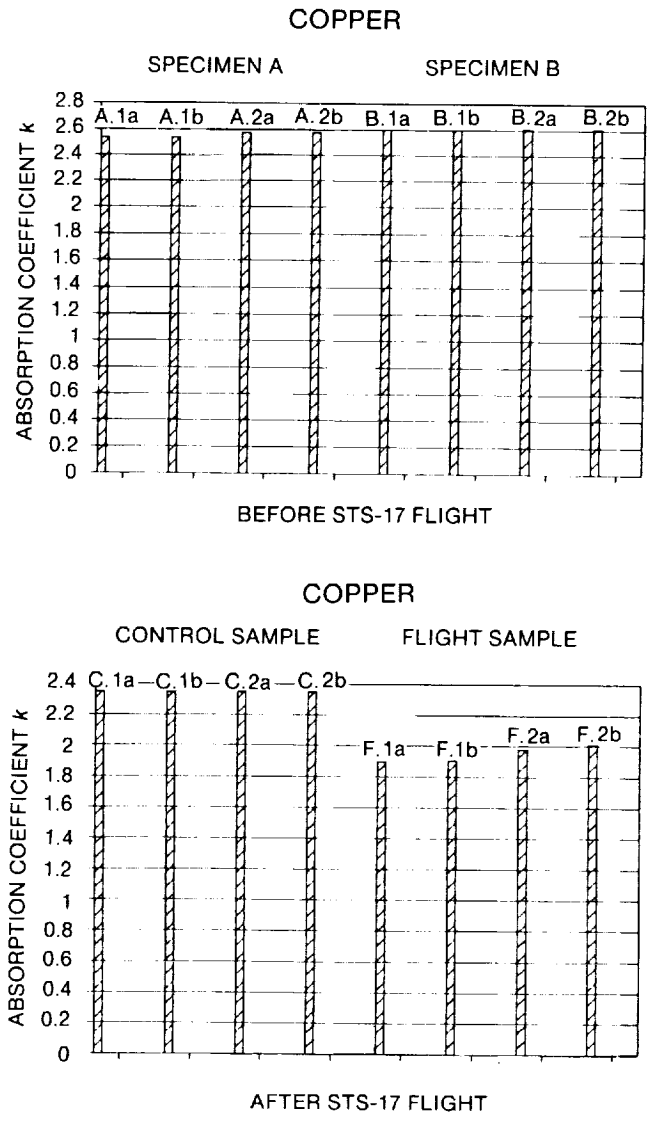

Fig. 3 Standard plots illustrating absorption coefficient k for Cu specimens A (= = >C) and B (= = >F) before (upper plot) and after (lower plot) the flight. (Keys 1a and 1b denote independent measurements on one surface area of the sample, whereas 2a and 2b denote independent measurements on a different surface area of the sample.)

Utilizing the fact that the precision of the measurements taken on a given area of each sample at a given time was extremely good, an averaging of these data was carried out, and plots were made in which the averaged data for the two spatial sites on a given sample are given as adjoining bars. Also included in this new series of plots are both A,B and C,F data for either n or k. Of course, this type of plot differs from the standard plots illustrated previously.

On a given figure we include both the n data plot (upper half) and the k data plot (lower half). These results for the elemental metals gold and silver are shown in Figures 4 and 5, respectively. A comparison of the A and C data in a given plot shows, for example, the aging effects in the control specimen over the weeks spanning the mission, whereas a corresponding comparison of the B and F data includes aging but shows especially the much larger

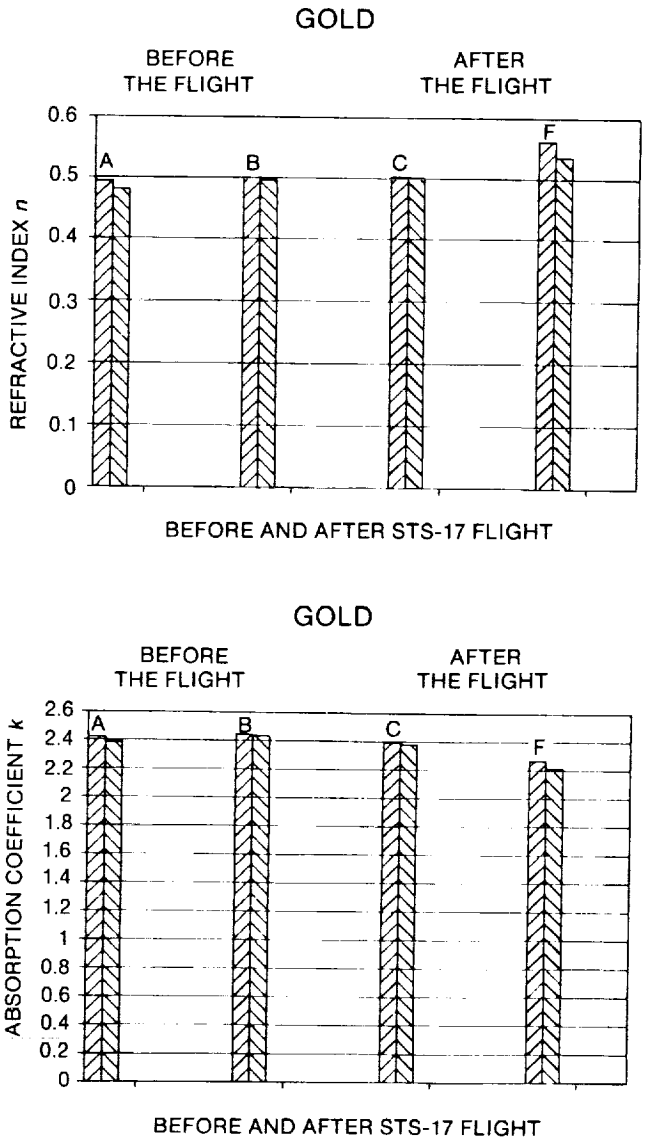

Fig. 4 Plots illustrating refractive index n (upper plot) and absorption coefficient k (lower plot) on two areas of Au specimens A and B before flight and on two areas of the same Au specimens after flight (A= = >C; B= = >F).

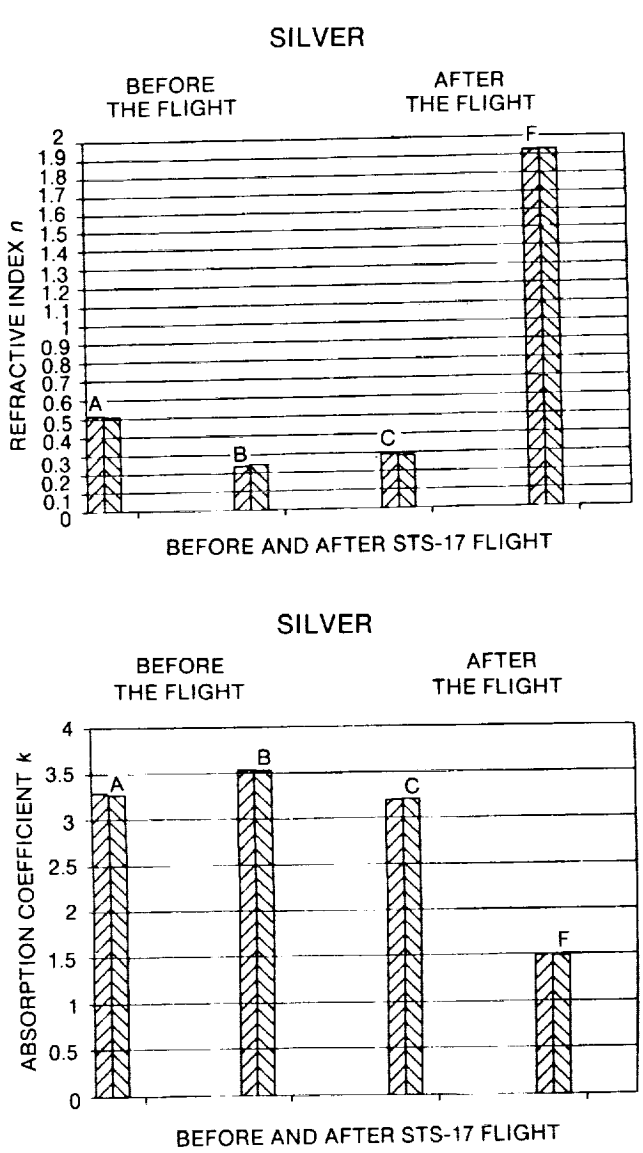

Fig. 5 Plots illustrating refractive index n (upper plot) and absorption coefficient k (lower plot) on two areas of Au specimens A and B before flight and on two areas of the same Ag specimens after flight (A = = >C; B = = >F).

effects produced by flight. It can be noted from the upper plot in Figure 5 that the aging effect on the refractive index of silver was a factor of 2, as noted by comparing the A and C data, whereas the change due to exposure (including aging) of the flight sample was a factor of 8, as can be noted by comparing the B and F data. On the other hand, it can be noted from Figure 4 that gold underwent a negligible aging effect. Nickel, copper, and aluminum exhibited some aging effects.

A comparison of the A and B data in such plots shows convincingly that the sample to sample variations are significantly smaller than the variations produced by exposure during flight, as indicated by a comparison of the C and F data. Figure 4, for example, shows that the sample to sample variations in n and k for Au were quite small compared to the relatively small changes in n and k attributed to flight exposure.

To emphasize the especially large space-exposure effects observed for silver relative to the other metals, it can be noted from Figures 4 and 5 that the 10 percent or so variation in n for gold due to flight exposure is rather small compared to the factor of 8 or so variation in n for silver during the same flight exposure.

The ellipsometer data clearly demonstrate that nonhomogeneity in the surface of a given sample was never a problem. In addition, the data demonstrate that the aging effects are really quite unimportant, with the possible exception of n for silver. On the contrary, the data demonstrate that experimentally significant changes did occur in the flight specimens during the mission.

9.5 Summary

Qualitative and quantitative data on space telescope materials which were exposed to atomic oxygen in low Earth orbit during the 41-G (STS-17) mission were obtained utilizing the experimental techniques of Rutherford backscattering, particle induced x-ray emission, and ellipsometry . A group of eight samples and their controls were measured before and after flight. Information herein includes characterizations of the surface of each speciman using ellipsometry techniques, reporting of the thicknesses of the evaporated metal specimens using RBS, and reporting of the trace impurity species present on and within the surface using PIXE. Pronounced changes in the optical constants of the surfaces of the flight specimens occurred relative to the surfaces of the control specimens.

Acknowledgement

This work was supported in part by NASA Contract H-78184B.

10.0 RESULTS OF APPARENT ATOMIC OXYGEN REACTIONS WITH SPACECRAFT MATERIALS* DURING SHUTTLE FLIGHT STS-41G

D. G. Zimcik
Communications Research Center
Ottawa, Ontario, Canada

C. R. Maag
NASA Jet Propulsion Laboratory
Pasadena, California 91109

Abstract

An experimental package flown on Space Shuttle mission STS-41G was designed to investigate the effect of atomic oxygen in low Earth orbit on polymeric-based spacecraft materials. The experiment included specimens of advanced composite materials, i.e., carbon-epoxy and Kevlar-epoxy both with and without protective coatings, in addition to a number of thermal protective paints and films. These materials specimens were attached directly to the lower arm boom of the Space Shuttle remote manipulator system and positioned normal to and in the direction of flight for a total of approximately 38 hours of equivalent normal exposure at 225-km altitude. In addition, a carbon-coated atomic oxygen fluence monitor together with a photographic record obtained by the Canadian payload specialist on board provided detailed information on the environment experienced by the exposed specimens.

A description of the effect of atomic oxygen interaction experienced by the exposed specimens is presented in this paper. Mass loss measurements together with high resolution scanning electron microscope photomicrographs are presented to quantify the effect and identify the resultant surface morphology. Postflight analysis indicated that the specimens experienced the effect of a very aggressive environment which resulted in significant changes to exposed surfaces.

10.1 Introduction

Experience on Space Shuttle (SS) flights has shown that atmospheric interactions with spacecraft in low Earth orbit (LEO) can have significant effects on the performance of materials, particularly those of a polymeric base, after only short exposure Polymeric materials are important elements of spacecraft design with applications for structural members in the form of advanced composite materials or thermal protection in the form of films and coatings. Future spacecraft will continue to use polymeric materials in thermal coatings or as advanced composite material structural members in order to achieve the size, stiffness, and pointing requirements of large third generation spacecraft.

Unfortunately, there is the potential for every satellite, whether in LEO or higher, to be affected by the LEO environment. The use of the Space Shuttle to launch satellites (which allows a benefit of check-out of the satellite before deployment and boost) and the capability to repair satellites on orbit increases the possible exposure. Even the short time spent in the SS orbit or a parking orbit prior to boost for an expendable launcher may have serious effects on exposed materials. Such a concern exists for the Galileo spacecraft being developed by the NASA Jet Propulsion Laboratory (JPL). Galileo is an interplanetary spacecraft that will orbit Jupiter. The present deployment altitude and parking orbit is 196 km at 30° inclination.

Erosion of materials could affect the spacecraft in three ways. The number one concern would be the loss of surface conductivity. This would violate the equipotential spacecraft requirement and create a potential electrostatic discharge (ESD) situation. Secondly, if the outer layer of the thermal blanket material (a black polyester coating deposited over Kapton) is removed down to the substrate, the Kapton could prove to be a glint source to the sensitive science instruments. Finally, there is concern that the material which is eroded away could

*AIAA Paper 85-7020, presented at the AIAA Shuttle Environment and Operations II Conference, 1985.

become another source of contamination. The advent of the Space Station will provide another situation.

Although the Earth's upper atmosphere is not a simple function of altitude, but varies in composition, density, and temperature with (among other things) solar activity, latitude, local time and season, Figure 1 represents the average composition[1]. At altitudes between 200 and 700 km, the predominant species is atomic oxygen, and at altitudes above this, it remains a significant constituent. The atomic oxygen density in LEO is not particularly high even at SS altitudes; the 10^9 atoms/cm^3 corresponds to the density of residual gas in a vacuum of 10^{-7} torr. However, due to the high orbital velocity (approximately 8 km/sec at SS altitude), the flux is indeed high, being of the order of 10^{15} atoms/cm^2-sec. In addition, this high orbital velocity corresponds to collisions with highly energetic (5.3 eV) oxygen atoms. The result has been

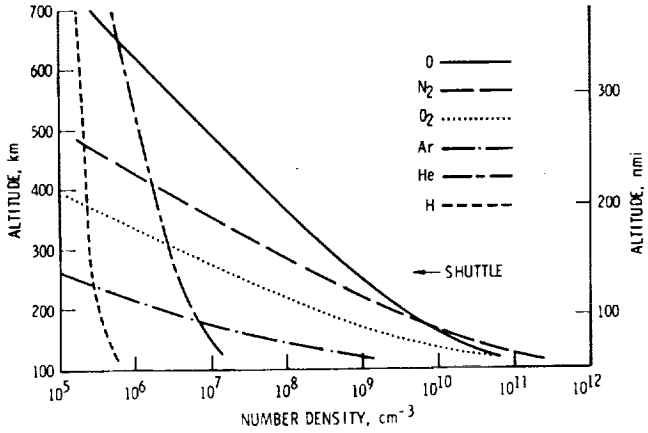

Figure 1. Atmospheric composition in low Earth orbit (Ref. 1)

observed to be surface erosion and mass loss for exposed materials.[2]

If atomic oxygen incompatibilities are discovered to be extensive and difficult to remedy for Galileo, the option exists to raise the SS orbit altitude. The Galileo design fluence [2.2 × 10^{20} atoms/cm^2, (7 orbits) to 6.9 × 10^{20} atoms/cm^2 (22-orbit contingency)] allows for SS orbits as low as 196 km. Raising the altitude by 40 km will reduce the total fluence to the spacecraft by one-half. A marginal design may become acceptable in this manner, but, of course, there are mission impacts with this approach that affect the mission trajectory and flight time. Another option to reduce extensive atmosphere interactions with the Galileo materials is to either overcoat the existing materials with a protective layer and/or include an additive in the bulk coating which would reduce the effective erosion. STS-41G provided the platform and the fluence to understand the effectiveness of this option.

10.2 Description of Experiment

The Advanced Composite Materials Exposure to Space Experiment (ACOMEX) on STS-41G was designed to investigate the above phenomenon on selected polymeric materials and to assess the effectiveness of a thin fluorocarbon coating to act as a protective barrier to the attack. Of particular interest were high performance advanced composite materials of carbon-epoxy and Kevlar-epoxy and thermal control coatings. The advanced composite materials were in the form of thin, four-ply strips (nominally 15 cm × 2.25 cm × .05 cm) and included three aerospace grade materials (2 carbon fiber-based: Fiberite T300/934 and Narmco T300/5208; and one Kevlar fiber-based: 3M SP 328) in typical ply orientation configurations. The thermal coatings were selected from possible materials to be used on the Galileo spacecraft. These included carbon-filled polyester (Sheldahl black) coated Kapton film (.003 cm) with a thin-spluttered and vapor-deposited overcoat (275 A) of indium tin oxide; and three thermal coatings: carbon-filled epoxy (BOSTIC 463-14), carbon-filled polyurethane (Chemglaze Z004) and a carbon-filled silicone (GE-PD-224) all modified with a siloxane additive (10 percent by weight). These materials were applied to round disks (2.5-cm diameter) and mounted in an aluminum boat together with a carbon-coated atomic oxygen fluence

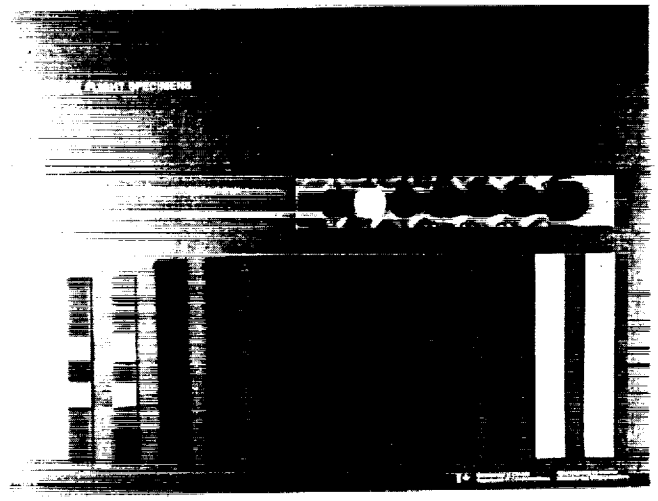

Figure 2. ACOMEX flight specimens

monitor. Finally, two thin films of Kapton 20 cm × 10 cm × 0.00125 cm, and 2.5 cm dia. × .0075 cm completed the material complement. The material specimens prior to flight are shown in Figure 2.

The specimens were mounted directly to the thermal blankets of the lower arm boom of the Canadarm, as shown in Figure 3, by means of both transfer adhesive on the back of each and circumferential bands of Kapton tape. During the mission, the Canadarm was positioned over the port wing to expose the specimens normal to the direction of the flight velocity vector in order to achieve the greatest effect. The arm was to remain in this position for up to 30 hours to accumulate a total fluence of approximately 2×10^{20} atoms/cm^2. Unfortunately, an equipment malfunction of the flash evaporator system required periodic water dumps from the side water dump nozzle. Because of past problems on STS-41D with ice buildup after this procedure, the RMS was repositioned for each water dump (approximately every 12 hours) to inspect the side water dump nozzle. This procedure, along with other RMS maneuvers, had the disadvantage of providing off-normal exposure of the specimens, but it was beneficial in that it allowed close inspection of the specimens by the Canadian payload specialist Cmdr. Garneau. During the mission, Cmdr. Garneau was scheduled to provide photographic record of the material specimens in order to monitor the rate of change with time and accumulated fluence as recorded by the carbon-coated fluence monitor and the Kapton film.

The carbon-coated fluence monitor[3] consisted of a ground KG-1 glass plate with three parallel bands of gold of different thickness, 2500 A, 5000 A, and 7500 A deposited on the surface. This was then overcoated with vapor-deposited amorphous carbon to a total thickness of 10 000 A resulting in carbon bands of thickness 2500 A, 5000 A, and 7500 A, plus the base. The carbon was expected to erode due to the attack of the oxygen at a predetermined rate and accordingly provide visual indication of the accumulated fluence as each band of gold appeared from beneath the carbon layer. In addition, the erosion rate of Kapton which has been measured on previous flights was designed to provide an end-of-flight fluence measurement and a calibrated sample of the surface morphology after erosion.

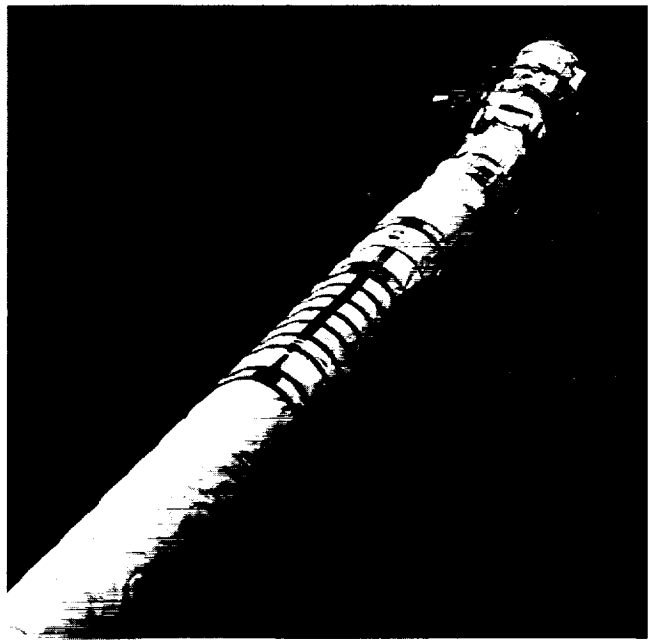

Figure 3. ACOMEX specimens mounted on Canadarm

10.3 Observations

10.3.1 Surface Analysis

Visual inspection with only the unaided eye after the flight confirmed material changes which manifested themselves in the form of loss of surface gloss or color changes as compared to laboratory reference samples. In addition, sharp shadow effects on areas unexposed to the flight direction but exposed to other influences of vacuum, thermal excursions, or radiation gave support to the cause of the observed change being atomic oxygen impingement.

As noted earlier, the specimens experienced exposure in both the designed manner as well as in a somewhat uncontrolled and undefined fashion during such mission events as water dump inspection and Earth Radiation Budget Satellite deployment. Consequently, the exposure time and orientation can only be estimated from records taken by the Canadian payload specialist on board and ground-based observation of telemetered ephemeris data taken during the mission. Fortunately, most of the exposure time was logged with the specimens in the

desired normal position which reduced the error in calculating fluence. Based on an exposure estimated to be the equivalent to 38 hours of normal exposure at an altitude of 225 km, the total fluence of atomic oxygen on the specimens was approximately 3×10^{20} atoms/cm^2.

Detailed analysis of the material specimens confirmed the magnitude of the changes observed visually. The surface of carbon-epoxy specimens prior to exposure was smooth and glossy with only superficial scratches as shown in the scanning electron microscope (SEM) photomicrograph in Figure 4. Although it is possible to identify the fiber direction of the upper layer in this figure, the fiber features are not distinct because they are covered by a layer of epoxy matrix. After exposure in space, the surface resembled the pattern of corduroy as shown in the SEM photomicrograph in Figure 5. The depth of this erosion is approximately 5 μm which corresponds to a reactivity of 2×10^{-24} cm^3/atom for the epoxy matrix.

Figure 4. Control carbon-epoxy specimen (500X)

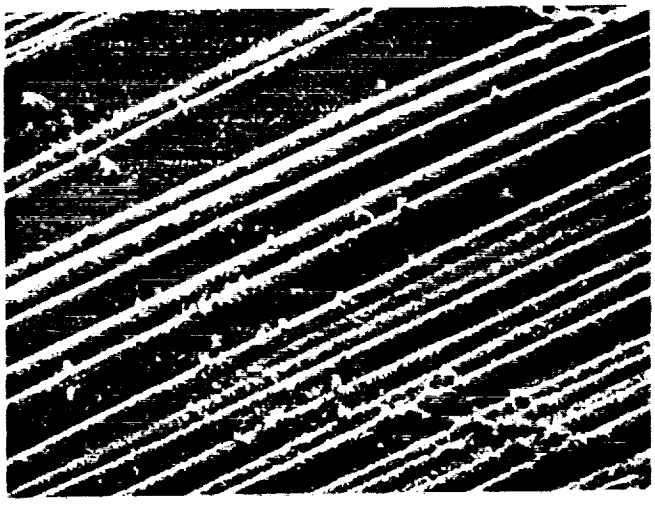

Figure 5. Exposed carbon-epoxy specimen (1000X)

Of particular interest, as shown in Figure 5, is the fact that the fibers themselves have been attacked and appear only as porous ridges with little residual strength or stiffness. This porous nature is in direct contrast to nonexposed fibers from the control specimens from the same material lot as shown in Figure 6. Similar fiber erosion was observed for Kevlar specimens. The initially smooth specimen surfaces were eroded to expose a similar corduroy-like surface which exhibited a comparable reaction rate for the epoxy matrix.

Kapton specimens exposed on ACOMEX were originally included in order to provide a standard of comparison to other flight data in this field. However, the two specimens chosen represented material of differing manufacturing times (circa 1984 and circa 1969) which exhibited very different resistance to the environment. The more recently manufactured specimen reacted as expected, experiencing visibly apparent changes whereas changes were much more subtle for the other as noted below.

Initially, the newer Kapton surface was typically smooth with small pits suspected to be due

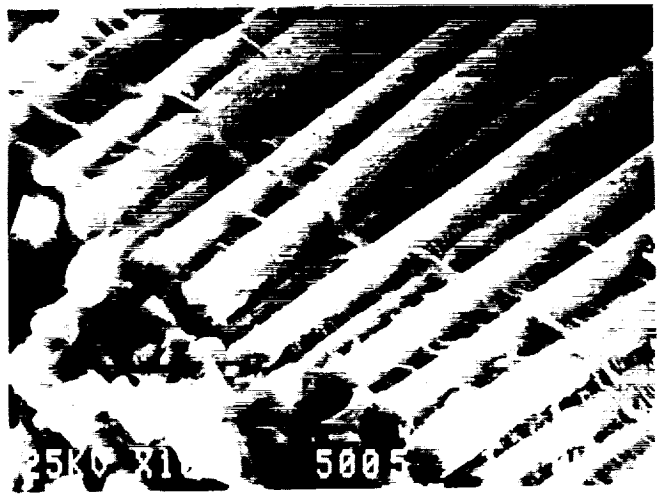

Figure 6. Control carbon-epoxy specimen internal surface (1000X)

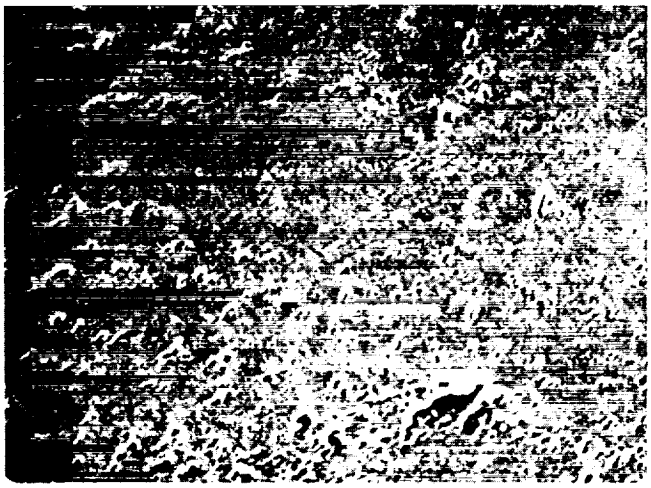

Figure 7. Control Kapton (circa 1984) specimen (5000X)

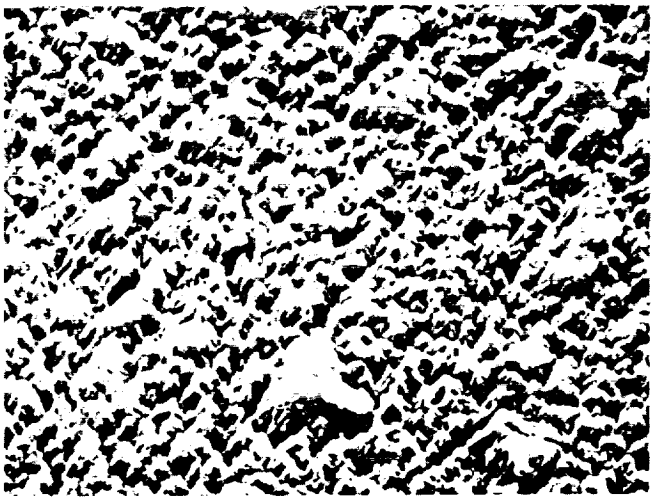

Figure 8. Exposed Kapton (circa 1984) specimen (5000X)

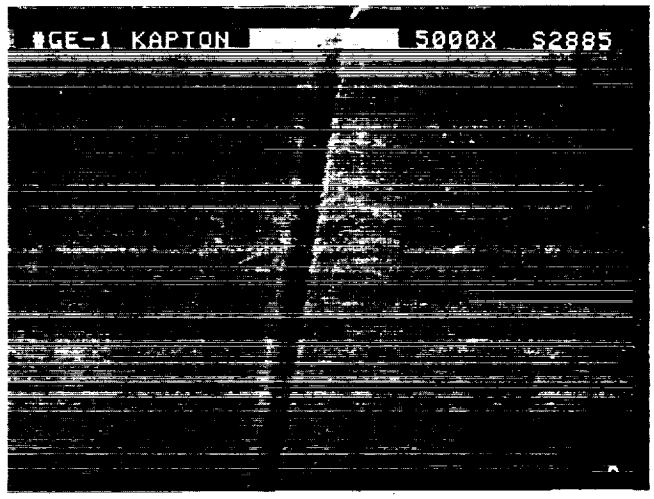

Figure 9. Control Kapton (circa 1969) specimen (5000X)

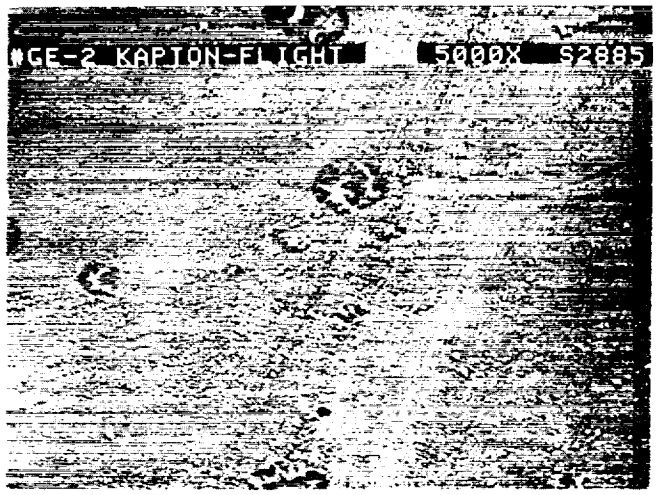

Figure 10. Exposed Kapton (circa 1969) specimen (5000X)

to processing as shown in the (SEM) photomicrograph in Figure 7. After exposure, the surface was uniformly irregular with a rug-like surface appearance as shown in Fig. 8. Mass loss measurements indicate a reduction of 60 pecent due to the erosion effect. For the 12.7-μm-thick Kapton film, this corresponds to a reactivity of approximately 2.5×10^{-24} cm^3/atom.

Although the older Kapton exhibited a similar preflight appearance to the newer Kapton as shown in Figure 9, the flight specimen showed a marked decrease in surface roughness as shown in Figure 10. In addition, draw lines from the manufacturing process are still visible indicating that the depth of erosion was small. Subsequent investigation[4] with the manufacturer suggested that a manufacturing process change incorporated in the late 1960's may be the cause of the different resistance. The previous manufacturing process included a heat treatment to passivate the surfaces and alter surface tension properties. This treatment was later eliminated because the market for Kapton had changed from electronics to aerospace. The possibility of using the formerly-used heat treatment in the manufacture of Kapton for spacecraft applications warrants further investigation as a method of increasing the erosion resistance of this important thermal control material.

10.4 Protective Coatings for Composite Materials

Duplicate specimens of carbon-epoxy were overcoated with a thin (1000 A) coating of plasma-sprayed fluorinated ethylene propylene copolymer to act as a protective barrier to the erosion.[6] Although the results of this coating are not uniformly successful, some of the specimens exhibited little if any change after flight while others exhibited increased resistance over areas where the coating remained intact. Successful application of the protective coating is exhibited in the photomicrograph of Figure 11 taken after flight which shows little change from the control specimen in Figure 12. However, the specimen in Figure 13 shows areas of protected material interspersed with eroded areas similar to those seen for the unexposed specimens. It is thought that the variation in protection is a result of the application procedure which allowed the coating to be removed exposing the surface. Investigation of the source of this problem is necessary to confirm the effectiveness of this technique. The location of the problem whether it be at the substrate interface or outer surface could have an important effect on the practicality of the concept. However, the results observed showed promise that the use of a thin overcoat that would not measurably alter the base properties of the material could provide an effective barrier to the environment.

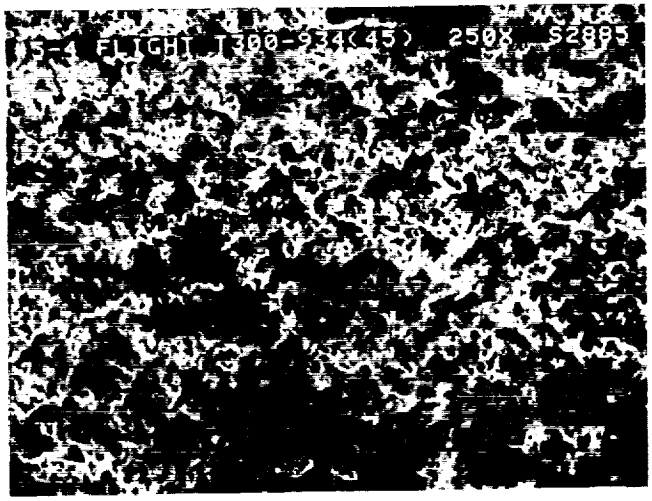

Figure 11. Exposed fluorocarbon protected carbon-epoxy specimen (250X)

Figure 12. Control fluorocarbon protected carbon-epoxy speciment (1000X)

Figure 13. Exposed incompletely protected carbon-epoxy specimen (1000X)

10.5 Thermal Properties Analysis

Thermal radiative properties of solar absorptance and emittance were measured for carbon-epoxy specimens before and after exposure to the environment. The solar absorptance was measured with a Gierdunkle solar reflectometer model #MS-251 and thermal emittance measured with a Gierdunkle infrared reflectometer model #DB100. Unprotected

specimens exhibited an increase in absorptance (α) of 7 percent and a decrease in emittance (ε) of 11 percent for a combined α/ε ratio change of approximately 20 percent.

For thin Kapton film (circa 1984), transmittance over the near ultraviolet to infrared wavelengths was compared to a laboratory control specimen. The change in absorbance is shown in Figure 14, which clearly verifies the increased opacity of the exposed film after exposure to the environment. Although the change is more pronounced on a percentage basis in the far infrared region, the change over the visible and near infrared is approximately 30 to 40 percent increasing to 60 percent at longer wavelengths.

The Galileo thermal control coating specimens that were exposed on ACOMEX represented the few remaining Galileo materials which needed to be "qualified" for atomic oxygen exposure particular to that mission. The SEM appearance of the pre-exposed sample of sputtered ITO/Sheldahl black polyester/Kapton is shown in Figure 15. The effects of flight exposure on that sample are shown in Figure 16. Although microcracking had apparently been induced by the exposure to the ambient environment, postflight testing indicated that the material had remained intact, i.e., did not create particulates from sloughing, and had retained its surface conductivity. It is interesting to note that the vacuum-deposited ITO-coated specimens reacted in exactly the same manner as the specimen with the sputtered coating even though the stoichiometry was different. The before and after condition of the remaining Galileo materials exposed in ACOMEX are shown in Figures 17 through 22. Of particular interest is the complete lack of attack on the GE-PD-224 coating. This was of great importance because of the fact that this coating is the primary thermal control coating used on the radioisotope thermoelectric generators (RTG). If these surfaces become more diffuse with time, the result would increase the operating temperature of these critical power sources. Both the modified Bostic and the Chemglaze coatings reacted as expected and pose no threat to the Galileo mission. Results of thermal properties analysis for the Galileo thermal control coatings before and after exposure are shown in Table 1.

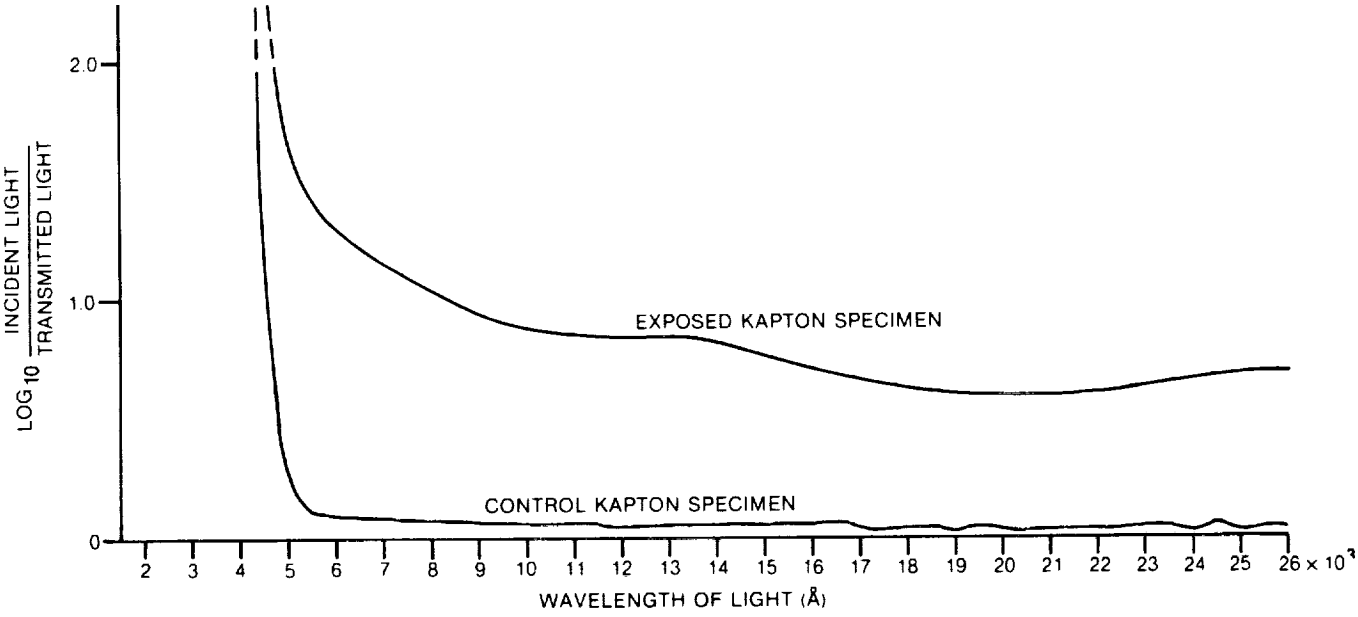

Figure 14. Transmittance of Kapton (circa 1984)

Figure 15. Control sputtered ITO/polyester/Kapton

Figure 16. Exposed sputtered ITO/polyester/Kapton

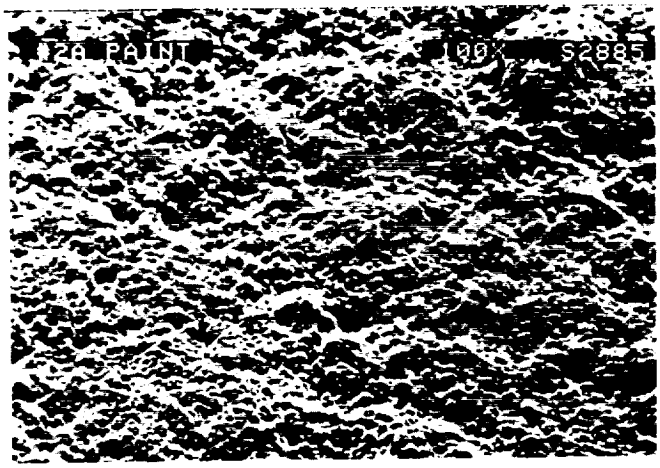

Figure 17. Control Chemglaze 2004/9832 paint

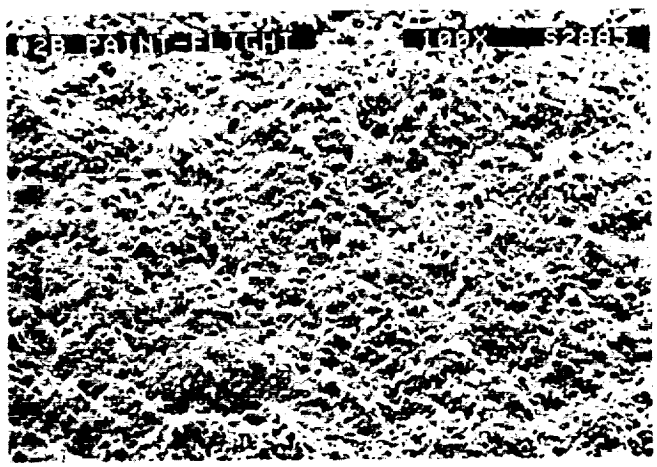

Figure 18. Exposed Chemglaze Z004/9832 paint

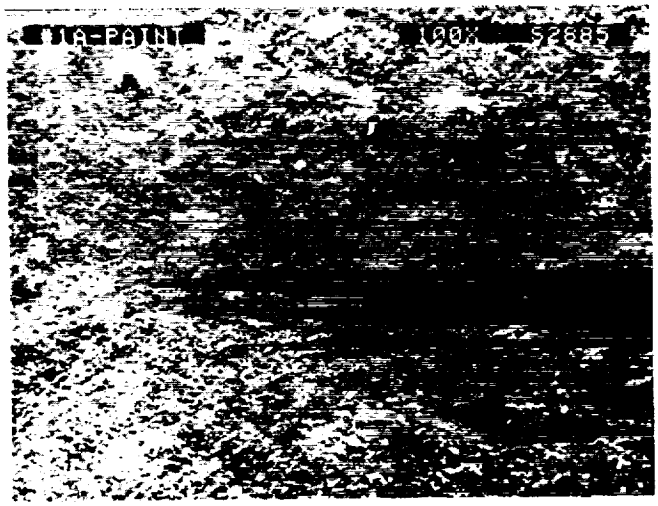

Figure 19. Control Bostic 463-14 paint

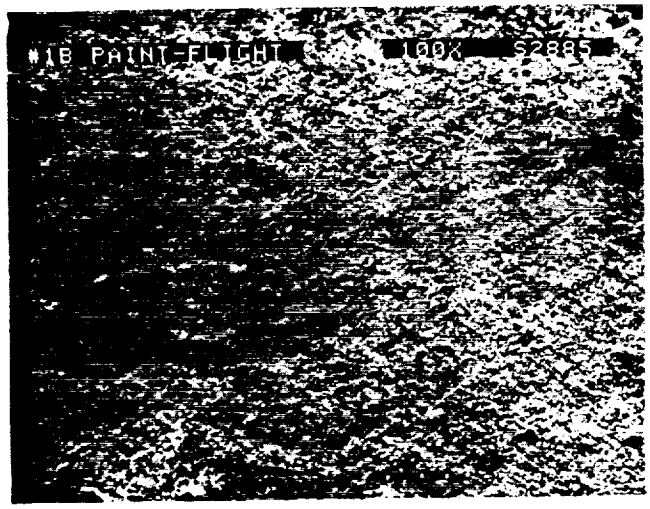

Figure 20. Exposed Bostic 463-14 paint

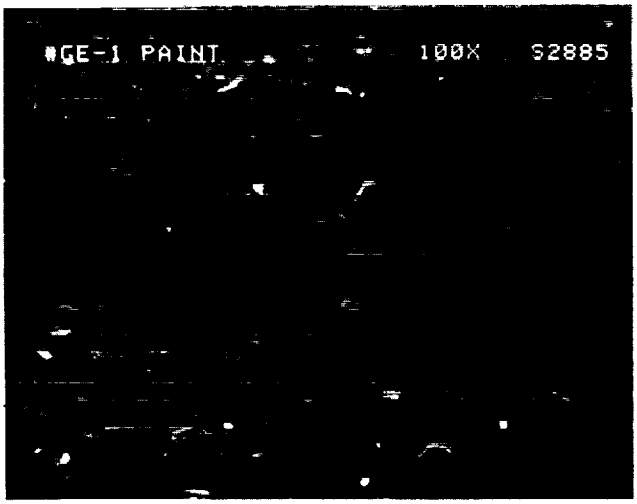

Figure 21. Control GE-PD-224 paint

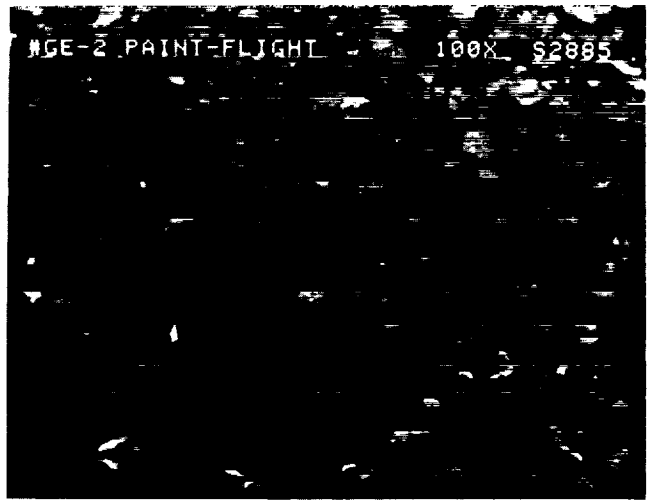

Figure 22. Exposed GE-PD-224 paint

Table 1.- Galileo Thermal Control Coating Properties

Material	Solar Absorptance (α_s)		Thermal Emittance (ε_T)	
	Before	After	Before	After
ITO (S)* Sheldahl Black/Kapton	0.88	0.89	0.83	0.83
ITO (VD) + /Sheldahl Black/Kapton	0.90	0.90	0.86	0.86
Bostic 463 – 14	0.93	0.94	0.86	0.86
Chemglaze Z004	0.94	0.95	0.87	0.87
GE-PD-224	0.94	0.94	0.88	0.88

* Sputtered
\+ Vacuum Deposited

10.6 Conclusions

The Advanced Composite Materials Exposure to Space Experiment (ACOMEX) flown on Space Shuttle mission STS-41G has provided a valuable data set for selected spacecraft polymeric material specimens. Unprotected exposed surfaces exhibit severe erosion and mass loss with the possibility of seriously degrading structural and thermal performance. However, the use of a thin fluorocarbon overcoat (although not conclusive) showed promise of providing a protective barrier to the attack without altering the base properties of the material. This and other possible protective measures previously discussed deserve additional evaluation to confirm their performance.

Acknowledgement

Part of the work described in this paper was carried out by the Jet Propulsion Laboratory, California Institute of Technology, under contract with the National Aeronautics and Space Administration.

References

1. Peplinski, D. R., Arnold, G. S. and Borson, E. N., "Satellite Exposure to Atomic Oxygen in Low Earth Orbit" Proc. 13th NASA/AIAA/ASTM Space Simulation Conference, Orlando, Fla., NASA Conf. Publication 2340, Oct. 1984.

2. Leger, L. J., Visentine, J. T., and Kuminecz, J. F., "Low Earth Orbit Oxygen Effects on Surfaces," Proc. AIAA 22nd Aerospace Sciences Meeting, Paper No. 84-0548, Reno, Nevada, Jan. 1984.

3. Maag, C. R., "Atomic Oxygen Fluence Monitor," NASA New Technology Report, December 1984.

4. Maag, C. R., personal conversation, with Dupont Engineering Technology, February, 1985.

5. Liang, R. H., "Evaluation of Surface Modification Procedures Leading to Atom Resistant Thermal Control Coating," JPL Quarterly Report UPN 482-53-25-28-00, Feb, 1985.

1. Report No.	2. Government Accession No.	3. Recipient's Catalog No.
NASA TM 100459		

4. Title and Subtitle	5. Report Date
Atomic Oxygen Effects Measurements for Shuttle Missions STS-8 and 41-G (3 volumes)	September 1988
	6. Performing Organization Code

7. Author(s)	8. Performing Organization Report No.
James T. Visentine, Compiler	10. Work Unit No. 992-15-00-00-72
9. Performing Organization Name and Address	11. Contract or Grant No.
Lyndon B. Johnson Space Center Houston, Texas 77058	13. Type of Report and Period Covered
12. Sponsoring Agency Name and Address	Technical Memorandum
National Aeronautics and Space Administration Washington, D. C. 20546	14. Sponsoring Agency Code

15. Supplementary Notes

16. Abstract

This technical memorandum represents a compilation of 15 technical papers and is organized by subject matter into three separate volumes. Volume 1 of this document summarizes the effects of atomic oxygen exposure upon typical spacecraft materials, such as polyimide films, thermal control paints, epoxies, silicones, and fluorocarbons. Volume 2 summarizes the effects of these interactions upon optical coatings, thin metallized films, and advanced spacecraft materials, such as high-temperature coatings and new coatings for infrared optical systems. In addition to these results, Volume 2 includes a description of a generic model proposed by the NASA Jet Propulsion Laboratory, which may explain the atomic oxygen interaction mechanisms that lead to surface recession and weight loss. Volume 3 presents a futuristic look into the atomic oxygen program and outlines requirements for follow-on studies to produce an accurate reaction rate data base for Space Station design. It also identifies Shuttle flight experiments and ongoing activities underway at research laboratories in the United States to evaluate materials in a neutral, 5 eV O-atom environment and to develop a more thorough understanding of the chemical mechanisms leading to surface recession and space glow. This volume, entitled Atomic Oxygen Effects Experiments: Current Status and Future Directions includes a detailed discussion of atomic oxygen simulation techniques now under development in the United States. In light of these discussions, it is limited in its distribution to U. S. Government agencies and contractors only.

17. Key Words (Suggested by Author(s))	18. Distribution Statement
Atomic oxygen Environmental exposure Space environmental effects Space durable materials STS material exposure studies	Volume I: Unlimited Volume II: Unlimited Volume III: U.S. Government agencies and contractors only Subject category: 27

19. Security Classif. (of this report)	20. Security Classif. (of this page)	21. No. of pages	22. Price*
Unclassified	Unclassified	Volume I: 92 pages	

*For sale by the National Technical Information Service, Springfield, Virginia 22161